Slab-derived metasomatism in the Carpathian-Pannonian mantle revealed by investigations of mantle xenoliths from the Bakony-Balaton Highland Volcanic Field

Laura Créon, Guillaume Delpech, Virgile Rouchon, François Guyot

Slab-derived adakitic metasomatism in the Carpathian-Pannonian mantle revealed by mantle xenolith investigations from the Bakony-Balaton Highland Volcanic Field

Laura Créon [a], *Guillaume Delpech* [b], *Virgile Rouchon* [a] *and François Guyot* [c]

[a] *IFP Energies nouvelles, 1 & 4 avenue Bois Préau, 92852 Rueil-Malmaison Cedex, France ;* [B] *Geosciences Paris Sud department, Paris Sud University, Bâtiment 504, 91405 Orsay Cedex, France ;* [C] *IMPMC, Museum National d'histoire Naturelle, Sorbonne Universités, CNRS, UPMC, IRD, 61 Rue Buffon, 75005 Paris, France ;*

Corresponding Author: Laura Créon, lauracreon@gmail.com; Present address: Universidad Nacional Autónoma de México, Centro de Geociencias, Campus Juriquilla, A.P. 1-742, Boulevard Juriquila No. 3001, Juriquilla. Qro., C.P. 76230

Abstract

We report new major and trace element data on minerals and glass from fifteen xenoliths from four different locations (Szentbékkálla, Szigliget, Füzes-tó and Mindszentkálla) in the Bakony-Balaton Highland Volcanic Field (Pannonian Basin, Central Europe). We show evidences for different stages of partial melting and metasomatism in the lithospheric mantle. The relict mantle minerals show compositions related to previous lithospheric mantle conditions, resulting from (1) an important early stage partial melting (~10-15 %) event indicated by a low modal content of clinopyroxene (cpx) 4-9 vol. % and low HREE contents in cpx ($(La/Yb)_N$ = 0.2 to 0.8), and (2) a metasomatic event associated to the crystallization of pargasite amphiboles and enrichment of cpx trace element patterns ($(La/Yb)_N$ = 0.7 to 15.7). A more recent metasomatic event is widespread and associated to the breakdown of

amphibole and to the formation of silicate melt pockets, forming a network of melt veins and pockets associated with large CO_2 vesicles at grain boundaries. The melt in veins is trachy-andesitic and displays trace element patterns very distinct from the andesitic melt in pockets, the latter resulting from *in situ* amphibole breakdown. The melt in veins records the extraction and onset of migration of a silicic melt with high-Nb and adakitic affinities (high SiO_2 = 54.2 to 62.7 wt. % and high LREE contents $(La/Yb)_N$ = 2.6 to 68.5). Adakite-like melts are believed to have been produced at conditions of 1000-1200°C and 2-3 GPa from a subducting slab, and injected in the lithospheric mantle where they triggered widespread pargasite melting at 1200°C and pressures above 0.7-1.1 GPa, below Moho depths. We suggest that this late stage metasomatic event is associated to the calc-alkaline volcanic suite that was active throughout most of the Miocene during the formation of the Pannonian Basin. This late stage event is also believed to have injected large amounts of CO_2 in the lithosphere mantle.

1 Introduction

Quenched melts in the form of glasses have been extensively reported in mantle xenoliths from many locations worldwide; they commonly occur in veins as intergranular films and/or as pockets between the primary minerals, or as inclusions in primary mantle minerals (e.g., Coltorti et al., 1999; Yaxley and Kamenetsky, 1999; Beccaluva et al., 2001; Shaw et al., 2006; Lu et al., 2015). The occurrence of glass provides important information on chemical and physical processes occurring in the lithospheric mantle, such as partial melting and metasomatism. Glasses in mantle xenoliths show a very wide range of compositions, from carbonate-rich melts (Coltorti et al., 1999; Delpech et al., 2004; Moine et al., 2004), to highly silicic melts (e.g., Wulff-Pederson et al. 1999).

Different origins for glasses in mantle xenoliths have been proposed on the basis of mineralogical observations, geochemical datasets and experimental results. Such melts have been interpreted either as agents or products of mantle metasomatism (e.g., Coltorti et al., 1999; Beccaluva et al., 2001; Neumann et al., 2002; Ionov et al., 2005), or the products of in situ incongruent melting of pre-existing minerals (e.g., Laurora et al., 2001) prior to or during entrainment of the xenoliths. There are also compelling evidence for the circulation of volatile-rich fluids that play a significant role as efficient metasomatic agents (e.g Szabó et al. 1996; Dawson 1984). Another alternative explanation is that the melts are the products of reaction between xenoliths and their host magma due to chemical disequilibrium (e.g., Shaw et al., 2006; Shaw and Dingwell, 2008; Miller et al., 2012) during their transport to the Earth's surface.

Embey-Isztin & Scharbert (2001) and Bali et al. (2002) suggested that melt pockets in ultramafic xenoliths from the Bakony–Balaton Highland Volcanic Field (BBHVF, Western Hungary) formed by reactions between pre-existing mantle phases (clinopyroxene ± amphibole) and metasomatic agents that were compositionally distinct from the host alkali basalts. The infiltrating melts were inferred to have originated from melting of previously metasomatized upper mantle during the Middle Miocene mantle upwelling (Huismans et al., 2002). Bali et al. (2002; 2008a; 2008b) and Szabó et al. (2009) also showed that migrating melts within the lithospheric mantle beneath the BBHVF have strong affinities with subduction-related melts/fluids or slab melts.

In this contribution, we present new major and trace element data on minerals and glass from fifteen xenoliths from four different BBHVF locations (Szentbékkálla, Szigliget, Füzes-tó and Mindszentkálla), two of which having never been published before in the literature for mantle xenoliths (Füzes-tó and Mindszentkálla). This new dataset, together with textural features, allows further constraining the origin of the metasomatic agents migrating through the

lithospheric mantle beneath the Pannonian Basin and their chemical reactions with the host lithospheric mantle. Based on the results, two metasomatic and partial melting events are recognized. The source of the last metasomatic event is also constrained.

2 Geological background

2.1 Geodynamic context

The Pannonian Basin (PB) is located in Central Europe and is part of the Carpathian–Pannonian region (CPR). The PB is surrounded by the Carpathian fold and thrust belt to the east and north, and by the Alps to the west and Dinarides to the south (Fig.1).

The CPR is composed of the ALCAPA (ALpian–CArpathian PAnnonian) and the Tisza–Dacia tectonic units that are separated by a major shear zone, the Middle Hungarian Zone.

The PB is a typical inter-arc basin (Embey-Isztin et al., 2001); nevertheless, it shows a number of features characteristic of rift zones, such as high heat flow, recent alkali basaltic volcanism, a thin crust and lithospheric mantle, and a doming asthenosphere (Spakman, 1990; Falus et al., 2007). The major driving forces that led to the formation of the Pannonian Basin (~20 Ma) were the continuous subduction and roll-back on its eastern boundaries and the synchronous eastward extrusion of ALCAPA blocks (Kazmer and Kovacs, 1985) from the Alpine compressional belt (Csontos et al., 1992; Horvath, 1993; Fodor et al., 1999).

The Pannonian Basin has experienced several geodynamic events during Miocene to Pleistocene times (Bali et al. 2008): (1) an early extensional phase during Miocene, related to the roll-back of the subducting European plate (Csontos et al., 1992; Horvath, 1993), resulting in a lithospheric thinning over the entire basin; (2) a short-lived compressional event during late Miocene to Pleistocene (Fodor et al., 1999); and (3) a late extensional phase during the

Plio-Pleistocene that affected the central part of the Carpathian–Pannonian region (Bada et al., 1999; Huismans et al., 2002). An extensive volcanic activity followed this second rifting phase (7.96 ± 0.03 to 2.61 ± 0.03 Ma, Wijbrans et al. 2007) during which formed the Bakony–Balaton Highland Volcanic Field (BBHVF).

2.2 The Bakony–Balaton Highland Volcanic Field (BBHVF)

The Bakony–Balaton Highland Volcanic Field (BBHVF) is situated in the northern part of the Lake Balaton (western Hungary, Fig.1). It is a well-studied young volcanic area on the southern margin of the ALCAPA microplate, which is located in the center of the Carpathian–Pannonian region and in the central southeastern part of the ALCAPA mega unit (Bali et al. 2008). The BBHVF itself has more than 50 basaltic volcanoes in a relatively small (around 3500 km^2) area (Martin et al., 2003; Kereszturi et al., 2011). The volcanic centers of the BBHVF were active between 7.96 Ma and 2.61 Ma (Balogh and Pécskay, 2001; Balogh and Németh, 2005; Wijbrans et al., 2007; Szabó et al., 2010) and produced mostly alkali basaltic volcanics (Szabó et al., 1992; Embey-Isztin et al., 1993). The Szigliget, Mindszentkálla and Füzes-tó volcanic events are respectively dated at 4.2-3.9 Ma, 2.8-2.6 Ma and 2.6 Ma. The age of the Szentbékkálla volcanic event is not known.

Ultramafic xenoliths can be found in basanitic lava flows and pyroclastic products at six locations (Tihany, Bondoró Hill, Füzes-tó, Szentbékkálla, Mindszentkálla, and Szigliget). Most xenoliths are spinel-bearing lherzolites; however, spinel-bearing harzburgites, clinopyroxenites, orthopyroxenites, wehrlites, websterites and more rarely, composite xenoliths were also found. The lithospheric mantle beneath the BBHVF is more deformed than the known mantle portions on the edges of the Carpathian–Pannonian region (Downes et al., 1992; Szabó et al., 1995). The most common textural type in peridotites is equigranular

(e.g. Downes et al., 1992; Szabó et al., 2004; Embey-Isztin et al., 2014), whereas xenoliths with protogranular, porphyroclastic and poikilitic are rarer. The peridotite xenoliths contain olivine (ol), orthopyroxene (opx), clinopyroxene (cpx) and spinel (sp) as primary minerals. The equilibrium temperatures of BBHVF mantle xenoliths vary between 880 and 1090 °C (Downes et al., 1992; Szabó et al., 1995; Bali et al., 2002; Kovacs et al., 2012). Using the geotherm of Kovacs et al. (2012), the sampling depths represent a mantle column of about 33 to 56 km and correspond to pressures between 0.95 and 1.60 GPa.

The occurrence of middle and lower crustal xenoliths in the BBHVF are also described by Szabó et al. (2010) and references therein. These crustal xenoliths were brought to the surface by the BBHVF alkali volcanism. These granulites are composed of clinopyroxenes, plagioclases, garnets ± orthopyroxenes ± amphiboles (Török et al., 2005).

3 Petrography

3.1 Petrography of the mantle xenoliths

More than 150 ultramafic xenoliths from the BBHVF (Szentbékkálla, Szigliget, Füzes-tó and Mindszentkálla) were collected. After observation by optical microscopy, six ultramafic xenoliths from Szentbékkálla, four from Szigliget, three from Füzes-tó and two from Mindszentkálla were selected for geochemical analyses (Table 1).

Selected samples are 7 to 18 cm in diameter, except one smaller sample from Mindszentkálla (2.5 cm in diameter). Xenoliths are composed of ol, opx, cpx and sp as primary minerals. Point-counting analyses (400 points) indicate that most xenoliths are spinel-bearing peridotites (n = 13), ten of which are lherzolites and three are harzburgites (Fig. 2). The Cpx modal composition varies from 1.8 to 4 wt. % in harzburgites and from 6 to 18.5 wt. % in

lherzolites. Two samples (SZB51 and SZB66) were classified as cpx-poor lherzolites (<10% cpx).

Based on the classification of Mercier & Nicolas (1975), the xenoliths show either protogranular or equigranular microstructures. Samples with a protogranular microstructure display coarse grain sizes (2-6 mm), whereas those with equigranular microstructure are fine-grained (1-2 mm). Protogranular samples have grains of olivine and orthopyroxene with heterogeneous sizes (<1 to 5 mm) and show curvilinear grain boundaries and vermicular spinels. Most samples with an equigranular microstructure refer to the mosaic subtype variety (SZB44, SZB50, SZG30, FT12) and one has a tabular texture (FT08P). In these xenoliths, grains have straight grain boundaries and they very often show triple junctions with angles at 120°. Spinel (and amphibole in FT08P) may be abundant in these samples (up to 12 vol. %) and it occurs as an interstitial (frequently) sub-euhedral mineral forming alignments of spinel aggregates. Two samples (SZG14, SZG44) display an intermediate microstructure grading from a protogranular to an equigranular texture. Some also display poikilitic features marked by poikilitic olivine enclosing opx or poikilitic opx enclosing olivine (Fig. 3b). There is no relationship between microstructures and the cpx modal contents of the peridotites.

Amphibole also occurs in some xenoliths (Szigliget, Füzes-tó and Mindszentkálla), regardless of the microstructure, as a secondary mineral disseminated between primary minerals (up to 7 vol. %).

3.2 Petrography of melt pockets and veins

All the xenoliths in this study bear mineralogical evidence of melt and fluid circulation in both lherzolites and harzburgites such as fluid and silicate melt inclusions in primary minerals (opx, cpx, ol) and silicate glass in veins or melt pockets (Fig. 3). Clinopyroxenes sometimes

displays spongy rims when in contact with melt veins or melt pockets (Fig.3a). Spinel can also display spongy rims but in lower abundance. Melt pockets (Fig. 3d, e, g, h) were observed in seven samples in SZB44, SZB50, SZB51, SZG23, SZG44 and FT12 lherzolites and in FT08P harzburgite. The size of silicate melt pockets is variable and ranges from few hundred microns up to few millimeters in diameter (similar to those described by Bali et al., 2002). In most cases, they are connected to each other by a network of thin silicate melt veins occurring at the contacts or cross cutting primary minerals. The shape of melt pockets is mostly irregular or it may have the shape of ghost minerals that have entirely broken down (e.g. amphibole).

Melt pockets are composed of brownish glass (gl), in which euhedral to sub-hedral secondary minerals crystallized such as olivine (ol-II), clinopyroxene (cpx-II) and spinel (sp-II), all smaller than 0.3 mm in diameter. Most melt pockets also contain large vesicles (up to 0.5 mm) (Fig. 3d, g, h). In xenoliths SZG23, FT12 and FT08P, melt pockets are associated with resorbed amphibole (amp-I). In this case, a resorbed amphibole crystal is often observed in the center of the pockets, surrounded by silicate glass and secondary minerals mentioned above. Some melt pockets are entirely composed of glass.

Melt veins (Fig. 3c) are observed in all samples and are mainly located at grain boundaries between primary minerals or cross-cut the primary mineralogy. The size of melt veins is variable (few tens of microns to 0.4 mm) and they are mainly composed of brownish glass and large vesicles (Fig. 3c), where ol-II, cpx-II, sp-II are present in lower abundance compared to melt pockets.

3.3 Petrography of silicate melt and fluid inclusions

Silicate melt inclusions (SMI) were only observed in the SZG14 lherzolite. They occur as primary inclusions (Roedder, 1984) in the rim of a clinopyroxene (Fig. 3a). The size of the primary SMI are 40, 60 and 100 µm in diameter and their shape is spherical. The SMIs consist of brownish glass (50-70 vol. %), one CO_2-rich retraction bubble (10-25 vol. %) and tiny not identified mineral phases (10-40 vol. %).

Fluid inclusions are present by order of abundance (i.e. number of inclusions per unit volume of hosting mineral) in Opx, Cpx and Ol. They occur along healed fractures that crosscut the entire host crystal (Fig. 3f) as already described in the BBHVF by Bali, et al., (2008).The fluid inclusions display negative crystal shapes or have rounded shapes with sizes varying between 5 and 60 µm. At room temperature, the fluid inclusions contain one (liquid) or two (liquid + vapor) phases. Using the definition of Roedder (1984), the inclusions can be classified as secondary fluid inclusions.

4 Geochemistry

4.1 Analytical methods

4.1.1 Major and volatile element analyses

Electron microprobe analyses (EMPA) of mantle minerals, melt pockets and veins were carried out on a CAMECA SX FIVE at CAMPARIS (Jussieu, Paris, France). Minerals were analyzed with a focused beam (1-2 µm), a beam current of 20 nA and a counting time of 10 s for each element on peak and 10 s on background. Vanadium was determined with a beam current of 300 nA in all minerals. Glass was analyzed with a 10 nA defocused beam (10 µm) and a counting of 10 s on the peak and 10 s on the background. The concentrations of S, Cl

and F were determined with a 45 nA defocused beam and a counting time of 100 s on peak. Accuracy was checked against standards (albr, phn9, ortr, apat, mnti, baso, sca2 and Fe_2O_3). Detection limits are <50 ppm for S, <60 ppm for F, <100 ppm for Cl, <300 ppm for P and <1000 ppm for other major elements.

4.1.2 Trace element analyses

Clinopyroxene, amphibole, and glass in melt pockets and veins were analyzed for trace elements by laser ablation LA-ICP-MS, using a 193 nm ArF laser ablation system (Photon Machine Analyte G2) coupled to an ICP-QMS (Varian 800-MS) at the Laboratoire de Planétologie et de Géodynamique (LPGN, Nantes, France). Cpx and amphibole were analyzed using a laser repetition rate of 5 Hz, a pulse energy of 6 mJ, a 65 to 85 µm laser spot diameter, corresponding to a fluence between 4.08 and 7.26 J/cm². Glass in melt pockets and veins was analyzed using identical pulse frequency and energy, but with a 20 to 50 µm laser spot diameter (fluence of 5.45 J/cm²). The background was measured for 30 s before ablation and each analysis lasted for about 90 s. Measurements were calibrated against NIST 612 glass standard (Gagnon et al., 2008), using CaO for Cpx and amphibole, and Al_2O_3 for glass as internal standards (measured by EMPA). Reproducibility and accuracy were characterized using the BCR-2G international standard, which was analyzed at the beginning and end of each run as well as every series of 10-15 unknown analyses. The analytical reproducibility is better than 5% except for Cr, Th and U, which are better than 10%. Data reduction was performed using the Glitter software (Achterberg et al., 2001).

4.2 Chemistry of the primary mantle minerals

4.2.1 Major element analyses

No significant major element zonation was observed between cores and rims in the rock-forming minerals of peridotites from Szentbékkálla, Szigliget, Füzes-tó and Mindszentkálla (Table 2).

4.2.1.1 Olivine

Primary olivines in lherzolites have homogeneous compositions and relatively low Mg-number (88.8-90.6). Their Mg-numbers are slightly higher in the spinel harzburgites (90.2–90.4) than in the other xenoliths. NiO contents in olivines from harzburgites and cpx-poor lherzolites vary from 0.33 to 0.41 wt. % and from 0.28 to 0.42 wt. % in the lherzolites. The Mg-numbers of secondary olivines (Ol II) in melt pockets are higher than those of primary olivines (89.7–92.7). Concentration of CaO (0.1–1.9 wt. %), Cr_2O_3 (0.0– 0.3 wt. %) and Al_2O_3 (0.0– 0.22 wt. %) in secondary olivines are higher than those in the primary olivines (Table 3).

4.2.1.2 Orthopyroxene

The composition of orthopyroxene ranges from $En_{90.2}$ to $En_{91.3}$ in harzburgites and from $En_{89.0}$ to $En_{90.9}$ in the lherzolites. The Al_2O_3 contents (2.5–3.6 wt. %) of orthopyroxenes in the harzburgites and in the lherzolites (3.8-5.8 wt. %) are variable; the Cr_2O_3 content is in the range of 0.0–0.1 wt. % in harzburgites and lherzolites orthopyroxenes (Table 2).

4.2.1.3 Clinopyroxene

Primary clinopyroxenes (Cpx I) are augites ($En_{36.8-37.6}$ $Wo_{35.5-36.8}$ $Fs_{26.0-27.2}$). Their Mg-number ranges from 88.0 to 91.0 in the lherzolite and from 90.7 to 92.5 in the harzburgites. Major element contents of Cpx I in lherzolites are highly heterogeneous (Fig. 4) with higher Al_2O_3 and Na_2O and lower CaO content (Al_2O_3 5.3-8.0 wt. %, Na_2O 0.7-1.9 wt. % and CaO 17-8-21.6 wt. %, respectively) than in harzburgites (Al_2O_3 2.2-4.1 wt. %; Na_2O 0.3-1.2 wt. % and CaO 19.0-23.7 wt. %, respectively). Concentrations of TiO_2 in Cpx I are < 0.94 wt. % in lherzolites and between 0.1-0.2 in harzburgites (Table 2). The CaO (18.3-21.7 wt. %), Al_2O_3 (6.2-10.5 wt. %) and TiO_2 (0.2-2.8 wt. %) contents of secondary cpx (Cpx II, augites, $En_{40.7-41.2}$ $Wo_{28.8-29.2}$ $Fs_{29.7-30.1}$) in melt pockets are higher than those of the primary clinopyroxenes for similar Mg-number (Fig.5, Table 3).

4.2.1.4 Spinel

The primary spinel displays large variations in composition ranging from magnesian and aluminous chromite (SZB16, SZB44, SZB50, SZB52, SZG14, SZG30, SZG44, FT12, MSZK1308) to chromite (SZB51, SZB66, SZG23, FT01P, FT08P, MSZK1306A). The Mg-numbers and Cr-numbers range from 59.6 to 78.1 and from 7.7 to 43.9, respectively (Table 2, Fig. 4). The spinels in harzburgites are more chromiferous than in the lherzolites; the Mg-number versus Cr-number diagram (Fig. 4) shows a linear distribution from low Cr-number–high Mg-number in spinels from the lherzolite to high Cr-number–low Mg-number in spinels from harzburgites. Secondary spinels in reaction zones commonly have higher Mg-number (65.9-82.4) and Cr-number (9.7–45.8) compared with primary spinel, corresponding to the most chromiferous spinels of the harzburgites (Fig.5, Table 3).

4.2.1.5 Amphibole

Amphiboles occur in four xenoliths (SZG30, FT12, FT08P, MSZK1306A, Table 3) and are pargasites according to the classification of Locock, (2014). Their Mg-numbers range from 88.2 to 89.0 and are similar to those described by Bali et al. (2002) and Szabó et al. (2004). They are variable in TiO_2 (0.3-2.7 wt. %) and rather rich in Cr_2O_3 (1.0-1.8 wt. %) and Na_2O (2.1-3.7 wt. %). Amphiboles in MSZK1306A have lower TiO_2, Al_2O_3 and Na_2O contents and higher CaO, SiO_2 and K_2O contents than resorbed amphiboles in reaction zones (SZG30, FT12, FT08P).

4.2.1.6 Carbonates

Carbonates were analyzed in veins in lherzolite SZG30. They have compositions typical of Mg-calcites (CaO between 50.7 and 52.6 wt. %) with low FeO (1.61 to 1.99 wt. %), MgO (4.36 to 5.02 wt. %), MnO (0.31 to 0.51 wt. %) and SiO_2 (0.02 to 0.07 wt. %).

In summary, primary minerals (Ol, Opx, Cpx, Sp) show the same range of major element compositions as those published in previous studies for xenoliths from Szentbékkálla and Szigliget (Downes et al., 1992; Bali et al., 2002; Falus et al., 2004; Demény et al., 2004; Bali et al., 2007; Szabó et al., 2009) (Fig.4). However, some samples display more fertile compositions than those from previous studies, as shown by the lower Mg-numbers (e.g. samples SZB44, SZB50, SZG30, SZG44 and FT12) in olivine (88.8-89.3), orthopyroxene (89.2-90.0) and clinopyroxene (88.8-90.4). Similar major element compositions of secondary minerals were previously reported by Bali et al. (2008) in melt pockets from mantle xenoliths form Szentbékkálla (Fig. 5).

325

326 4.2.2 Trace element analyses

327

328 The rare-earth elements (REE) concentrations of mineral phases (clinopyroxene, amphibole)
329 are given in Table 4 and REE and trace element patterns are presented in Figure 6. Trace
330 element contents of clinopyroxenes correspond to cores of primary clinopyroxenes (Cpx I) to
331 avoid potential metasomatic modification.
332 The lherzolites have clinopyroxenes with very variable trace element contents and were
333 subdivided into three groups on the basis of the shape of their REE patterns and on the light
334 REE (LREE)/Heavy REE (HREE) ratios, as follows.
335 Group I. Clinopyroxenes are characterized by low abundances of LREE compared with
336 MREE and HREE (SZB16, SZG14, SZG30, SZG44, MSZK1308, Fig. 6). The lherzolites in
337 which they occur have a protogranular texture (except SZG30). The $(La/Yb)_N$ (where N
338 indicates primitive mantle normalized) ratios are low and range from 0.2 to 0.8. The
339 multielement patterns display low contents in highly incompatible elements. A slight
340 enrichment in Nb is observed on MSZK1308. There are negative anomalies in Ba, Zr and Ti
341 and a slight Pb negative anomaly in SZB16, SZG30, MSZK1308. The concentration of Sr in
342 this group ranges from 56.9 to 90.0 ppm (Table 4).
343 Group II. Clinopyroxenes from group II are characterized by flat or nearly flat REE patterns
344 (SZB44, SZB50, SZB52). They are found in lherzolites with equigranular mosaic textures
345 (except SZB52). These clinopyroxenes have (La/Yb)N = 0.6–1.3, (La/Sm)N = 0.8–1.0 and
346 (Sm/ Yb)N = 0.6-1.5 with weak negative anomalies in Nb, Zr and Ti and no enrichment in the
347 most incompatible elements (Th and U). The concentration of Sr in this group ranges from
348 21.4 to 71.9 ppm.

Group III. Clinopyroxenes from group III are characterized by REE or trace element patterns showing enrichments in the most incompatible trace elements (SZB51, SZB66, SZG23, FT12, FT01P, FT08P, MSZK1306A), and therefore high $(La/Yb)_N$ ratios ranging from 0.7 to 15.7. Their trace element patterns show enrichments in large ion lithophile elements (LILE Th and U) and negative anomalies in Ba and high field strength elements (HFSE; Ta, Zr and Ti) except Nb. The concentration of Sr in group III ranges from 36.9 to 182 ppm. Finally, the microstructure in group III lherzolites range from protogranular to equigranular mosaic. The harzburgites have clinopyroxenes with very variable trace element contents and are characterized by low abundances of HREE and variable MREE and LREE abundances. All the HREE depleted clinopyroxenes are in the group III (SZB51, SZB66, FT01P, FT08P, MSZK1306A).

REE and other trace element patterns of the amphibole in harzburgite MSZK1306A and FT08P (Fig. 6) are similar to those of clinopyroxene from the same sample (group I). However, amphiboles in sample MSZK1306A have a higher concentration in most trace elements such as U, Th and Sr (U 0.1 ppm, Th 0.6 ppm and Sr 107.1-115.6 ppm; in MSZK1306A and U 3.0-3.4 ppm, Th 13.9-15.3 ppm and Sr 472.9-513.2 ppm in FT08P) than in the coexisting clinopyroxene (U 0.0 ppm, Th 0.2 ppm and Sr 36.9-39.4 ppm; in MSZK1306A and U 1.5-2.0 ppm, Th 5.3-7.5 ppm and Sr 121-144 ppm in FT08P), in agreement with observations in amphibole-bearing xenoliths from Antarctica (Coltorti et al., 2004) and Kapfenstein (Coltorti et al., 2007).

4.3 Chemistry of the melt phases

4.3.1 Major element analyses

Glasses show very variable compositions (Table 5, Fig.7) and will be subdivided into three groups on the basis of their petrographic textures and of their major element contents, as follows.

Group I. The glasses in melt veins. The major element compositions of glass in melt veins are highly variable both between and within single xenoliths. Overall, they are characterized by relatively high SiO_2 (55.8-62.7 wt. %) and K_2O (1.6-5.9 wt. %) and low Na_2O (3.9–5.7 wt. %), Al_2O_3 (17.0-20.4 wt. %), MgO (2.4-4.2 wt. %) and FeO_T (2.5-4.3 wt. %) contents (Fig. 7).

Group II. The glasses in silicate melt inclusions. The major element compositions of glass in silicate melt inclusions are characterized by relatively high SiO_2 (55.0 wt. %), Na_2O (7.31 wt. %), Al_2O_3 (22.9 wt. %), and low FeO_T (3.3 wt. %), MgO (2.3 wt. %) and K_2O (<1.8 wt. %) contents (Fig. 7).

Group III. The glass in melt pockets. The major element compositions of glass in melt pockets are highly variable both between and within single samples. Overall, they are characterized by relatively low SiO_2 (50.8-57.2 wt. %), Na_2O (4.0-5.5 wt. %), high Al_2O_3 (19.5-23.8 wt. %) and FeO_T (3.0-4.9 wt. %) contents (Fig. 7) compared with group I and II.

4.3.2 Trace element analyses

The trace element concentrations of glass phases are given in Table 6 and REE and their patterns are shown in Figure 8. The glasses present very variable trace element contents and were subdivided into two groups on the basis of their location and their trace element contents, as follows.

Group I. The glass in melt veins and silicate melt inclusions. Glasses are characterized by REE or other trace element patterns showing enrichments in the most incompatible trace elements (SZB16, SZB51, SZB52, SZB66, SZG14, FT01P, Fig. 8a) and therefore high (La/Yb)N ratios ranging from 2.6 to 68.5. Glass in melt veins have trace element patterns similar to glass analyzed by Szabó et al. (2009) in silicate melt inclusions.

Group II. The glasses in melt pockets present very variable trace element contents and were subdivided into two sub-groups on the basis of their trace element contents, as follows.

Group IIa. Glasses from group IIa are characterized by flat or nearly flat REE patterns (SZB44, SZB50, SZG44). These glasses have $(La/Yb)_N$ = 0.1-1.6, $(La/Sm)_N$ = 0.1-1.2 and $(Sm/ Yb)_N$ = 1.0-1.4 with positive anomalies in Nb, Sr and Ti and a negative anomaly in Zr, Hf.

Group IIb. Glasses from group IIb are characterized by REE or trace element patterns showing enrichments in the most incompatible trace elements (SZG23, FT12, FT08P), and therefore high $(La/Yb)_N$ ratios ranging from 6.2-53.0. Their trace element patterns show enrichments in LILE (Th and U) and negative anomalies in HFSE (Nb, Ta, Zr and Ti). The MREE–HREE pattern is almost flat and resembles that of group I or group IIa glasses.

Glasses in melt pockets (Group IIa, IIb, Fig.3) present incompatible element enrichments that parallel those of the associated amphiboles, and those described in the Pannonian Basin (Demény et al. 2004; Demény et al. 2005; Bali et al., 2008).

4.4 Bulk melt pocket compositions

Bulk compositions of melt pockets have been reconstructed from modal composition and from the chemistry of the glasses and the secondary mineral phases that compose them. The results are presented in Table 7 for one sample of Szentbékkálla, one of Szigliget and one of

Mindszentkálla. The reconstructed bulk compositions of the silicate melt pockets are very similar to pargasitic amphibole compositions and to the analyzed amphiboles in the respective locations.

4.5 Thermobarometry

Equilibrium temperatures of the studied xenoliths were determined using the 'Ca-in-opx' and 'opx-cpx' thermometers of Brey et al. (1990), using a pressure of 1.5 GPa. All xenoliths show moderate equilibrium temperatures (Szentbékkálla: 960-1080°C; Szigliget: 990-1010°C; Füzes-tó: 960-1090°C; and Mindszentkálla: 930-1030°C). These results are similar to those of mantle xenoliths published from the same volcanic field (BBHVF) (Szabó et al., 1995; Bali et al., 2002; Szabó et al., 2009). The equilibrium temperatures vary with the microstructure of the xenoliths. Xenoliths with coarse-grained protogranular microstructure record high equilibrium temperatures (930-1090°C) whereas xenoliths with a mosaic microstructure record lower equilibrium temperatures (930-993°C), consistent with the recent study of Embey-Isztin et al. (2014). According to the geotherm of Kovacs et al. (2012), the mantle section sampled represents depths of 35 to 50 km.

5 Discussion

The peridotite xenoliths from the BBVHF record a complex multi-stage partial melting and metasomatic history, such as demonstrated by Bali et al. (2002, 2008) and Downes et al. (1992). The following discussion will mostly focus on the origin of the latest metasomatic imprint in the four xenolith suites. The mineralogical and geochemical evidences for earlier processes are briefly described below.

448

449 5.1 Processes recorded before the late stage metasomatism

450

451 5.1.1 Partial melting of the peridotite

452

453 The major element compositions of the primary mineral phases in six protogranular samples
454 of the suite show high Mg# or Cr# (Ol, Opx, Cpx Sp) associated to a low modal content of
455 clinopyroxene (4-9 vol.%), low contents of basaltic components in the primary clinopyroxene
456 and low HREE contents in clinopyroxenes. These mineralogical and geochemical
457 characteristics indicate that some samples have recorded variable, yet high partial melting
458 degrees in the lithospheric mantle beneath the Pannonian Basin. Some xenoliths (SZB66,
459 MSZK1306A, FT01P and FT08P) have low Dy, Er, Yb and Lu contents compared with the
460 CI-chondrite and primitive mantle estimates (Fig. 6) and have preserved the trace element
461 signature of partial melting residues. To assess the extent of partial melting, we used the non-
462 modal fractional partial melting model of Johnson et al. (1990) and Hellebrand et al. (2002) in
463 the spinel stability field (see supplementary material). Two harzburgites (MSZK1306A and
464 FT08P) and two lherzolites from Szentbékkálla (SZB52 and SZB66) indicate moderate to
465 high melting degrees of ≈10-15%, in accordance with their low cpx modal contents (1.75-9
466 vol.%) and the low basaltic components of their cpx. The occurrence of peridotites showing
467 evidence of moderate to high partial melting degree (until 25 %) has been already described in
468 the BBHVF (Bali et al. 2002, 2008 for Szentbékkálla and Downes et al., 1992 for Szigliget
469 and other locations in the BBHVF).
470 However, there is a discrepancy between mineralogical and geochemical indicators in some
471 cases. One of the lherzolites (SZB52) and one of the harzbugites (FT08P) show lower melting
472 degrees of ≈5-10% and have low Cr# in spinel (16.7-18.5 wt. %). In case of FT08P this is

incompatible with the low cpx modal content of the harzburgite (2.3 vol.%; ≈20% melting). In the SZB52 lherzolite the cpx modal content is very high (18.5 vol.%). Since these samples show enrichments in the most incompatible elements, their HREE contents may not simply represent melting residues, but were also likely re-enriched due to metasomatic overprint. Some protogranular lherzolites (SZB16, SZG14, SZG44, MSZK1308) from Szentbékkálla, Mindszentkálla and Szigliget have fertile compositions with minerals with low Mg# and Cr#, high modal contents of cpx (12-18 vol.%), high amounts of basaltic components in their cpx as well as slightly LREE depleted REE patterns. Major and trace element compositions for these samples are very similar to Primitive Mantle values (McDonough and Sun, 1995). These mineralogical and geochemical characteristics suggest that these samples suffered from very low degrees of melting. Most of these samples also have high HREE compared to those of the primitive cpx used in the trace element modeling (taken from Johnson et al., 1990), which suggest that if these samples melted, the melting degree was low enough (<1%) not to affect the HREE contents but only the most incompatible LREE.

5.1.2 Metasomatism

Metasomatic processes have also affected the xenoliths prior to the formation of melt pockets and veins. The occurrence of amphibole is widespread in the lithospheric mantle below the BBHVF (Bali et al. 2002, 2008) and has been interpreted as a crystallization from volatile-bearing silicate melt possibly linked to the percolation of subduction zone melts during the Miocene. The trace element patterns in primary clinopyroxenes from most xenoliths (lherzolites and harburgites) also show enrichments in the most incompatible elements (Th, U, Ba, LREE) that were acquired during metasomatism. Lherzolites SZB51, SZG23, FT12, FT08P have clinopyroxenes with selective enrichments in Th, U, LREE and depletions in

HFSE. The gradual enrichments in the most incompatible elements can result from metasomatic imprint during chromatographic-like effects produced during interaction between the host peridotite and small melt fractions of a silicate melt enriched in trace elements (Bodinier et al., 1990). These trace elements characteristics in clinopyroxenes have also been interpreted as resulting from metasomatism by carbonate-rich melts below the BBHVF (Embey-Isztin et al., 2014). These enrichments are mostly seen in lherzolites with a mosaic microstructure that equilibrated at shallow depth below the MOHO (~30 km, Posgay et al. 1995). The metasomatic overprint is also more pronounced in clinopyroxenes from harzburgites with enrichments in MREE and HREE, a characteristic feature of SZB51, SZB66, MSZK1306A and FT01P.

5.2 Late stage metasomatism

Textural observations in the studied BBHVF xenoliths indicate that trails of secondary fluid inclusions, glass veins and glass pockets form a common network of melt circulation (Fig. 3d, Creon et al., this volume). Moreover, as shown by Creon et al. (this volume), vesicles trapped in melt veins and melt pockets and FIs are composed almost exclusively of CO_2. The CO_2-rich character of percolating melts has previously been highlighted by the observation of carbonates in veins and melt pockets in some xenoliths of the BBHVF (Embey-Isztin and Scharbert, 2001; Bali et al., 2002; Demény et al., 2004; Demény et al., 2010). However, only few carbonates were recognized in this study (SZG30). Seven xenoliths from three locations (SZB44, SZB50, SZB51, SZG23, SZG44, FT12, FT08P; Table 1) display the development of reaction zones at the expense of amphibole (Fig. 3g, h). Theothers (SZB16,SZB52, SZB66, SZG14, SZG30, FT01P, MSZK 1306A, MSZK1308, Table 1) display glass in veins between

primary minerals, commonly associated with newly formed minerals (olivine, clinopyroxene and spinel) that have higher Mg# than the primary minerals (Fig. 9).

The amphibole-bearing harzburgite FT08P probably illustrates a primordial stage for melt pocket formation. The textural features in FT08P (Fig. 9) indicate that a melt was formed by incongruent breakdown of amphibole, due to heating or infiltration of a melt/fluid in the xenolith, according to the following reaction (Ban et al., 2005):

amphibole + $melt_1$ + CO_2 → olivine + clinopyroxene + spinel + $melt_2$ + CO_2

In other xenoliths (SZB44, SZB50, SZB51, SZG23, SZG44), the melt pockets only displays gl+ol+cpx+sp+CO_2 but no relict amphibole. This observation suggests that amphibole may locally have fully reacted and broken down. These melt pockets are similar to those described by Bali et al. (2008) for lherzolites and websterites from Szentbékkálla and Szigliget or by Embey-Isztin & Scharbert (2001). The occurrence of large empty vesicles also indicates that a gas phase formed at some stage during in-situ partial melting of the amphibole or was rather inherited from a CO_2-supersaturated metasomatic agent. This idea is in agreement with the measured high abundance of dissolved volatiles in the trapped glass (veins and melt pockets) which are up to 4.25 ± 0.27 wt. % H_2O and 0.96 ± 0.02 wt. % CO_2 (Creon et al., this volume), corresponding to CO_2-saturated melt at lithospheric conditions (0.69 to 1.78 GPa).

The glass in the melt pockets has variable major element compositions and vary from basaltic andesitic or basaltic trachy-andesitic to andesitic-trachyte in composition (53.7-58.4 wt. % SiO_2). The glass in veins has a comparably more silicic composition and is typically trachy-andesitic (57.1-62.1 wt. % SiO_2). The glass in veins are also more homogeneous at the scale of the sample than the glass in melt pockets. Such variable major element compositions are frequent in glass from mantle xenoliths worldwide (e.g. Wulff-Pedersen et al., 1999; Coltorti

et al., 2000). Wulff-Pedersen et al. (1999) interpreted silicic glasses as cogenetic melts derived by infiltration-reaction-crystallization (IRC) processes (Vannucci et al., 1998), with the (highly) silicic melts being derived by percolation-reaction-crystallization mechanisms during metasomatism by an infiltrating silicate melt (host basalt) and preferential reaction with orthopyroxene. However, similar melt compositions in the BBHVF xenoliths have been attributed by several authors (e.g. Bali et al., 2007; Bali et al., 2008a,b) to metasomatic imprints unrelated to the alkali host basalts. These authors proposed that melt pockets have formed by the breakdown of former amphibole due to the introduction of a metasomatic melt (Bali et al., 2007). In the following sections, the origin of melt veins and pockets will be addressed based on geochemical and petrographic grounds.

5.2.1 Glass in the melt pockets

Compared with the literature data on glass from xenoliths from the BBHVF, the glass in the melt pockets analyzed in this study resembles the compositional spectrum of glasses documented in Bali et al. (2002) for similar melt pockets in peridotites and pyroxenites from Szentbékkálla (samples from SZB group, Fig.7). The SMI in pyroxenes from spinel-lherzolites from Szigliget (Szabó et al., 2009) have comparable SiO_2 (54.2 wt. %) and other major elements (Al, Ca, Na) than in the glass analyzed in the melt pockets but have lower MgO, FeO and higher K_2O contents (5.3 wt. %). The glass in melt pockets is very different in composition from the SMI reported by Bali et al. (2008) from Szigliget since the latter is Si-rich (57.3-74.0 wt. %) and has always low MgO (0-0.88 wt. %), FeO (0.44-3.57 wt. %) and CaO (0.69-3.06 wt. %). Most of the glass in melt pockets has lower contents of the most incompatible elements than alkali basalts (Embey-isztin et al., 1993) and also than calc-alkali volcanics (Harangi and Lenkey, 2007) in the area for similar SiO_2 contents (50.5-77.9 wt. %).

572 Some of the major element variations in glasses in veins and melt pockets could be consistent
573 with a fractional crystallization process (e.g. SiO_2, MgO, CaO, FeO; Fig.7). The possible
574 cogenetic relationship between glass in veins and less silicic melt pockets was tested using
575 crystal fractionation modeling of olivine, clinopyroxene and spinel from a parental melt in the
576 reaction zones using the rhyolite-MELTS software (Gualda et al., 2012; Ghiorso and Gualda,
577 2015) including the H_2O and CO_2 contents of the melts. The starting compositions were taken
578 from the most primitive composition measured for SZG44 glass. The crystal fractionation
579 (CF) calculations for a crystallizing assemblage of 0.1% ol + 84.4% cpx + 15.6% sp at 970°C
580 and 1.2 GPa fit well some major elements in glass from veins (CaO, MgO, FeO) for about
581 30% FC (Fig. 7). However, the model fails to explain the high K_2O and the low Na_2O and
582 Al_2O_3 concentrations of the glass in veins. Trace elements contents of the Si-rich glass in
583 veins also argue against a cogenetic relationship with melt pockets by crystal fractionation
584 (Fig. 8). For example, the glass in the melt pockets and in the veins that have similar SiO_2%
585 display contrasting trace element patterns, one being smoothly enriched in the most
586 incompatible elements (veins) and one displaying a rather flat distribution of trace elements
587 with some pronounced "negative" anomalies in HFSE (Fig. 8). The absence of negative HFSE
588 anomalies in the glass from veins is difficult to reconcile with an origin by simple crystal
589 fractionation process of an assemblage of ol+cpx+sp from a glass in melt pockets that display
590 negative/positive anomalies of these elements (Nb, Ta, Zr, Hf, Sr, Pb). We conclude that the
591 glass in veins does not in most cases evolve from the glass in melt pockets due to simple
592 fractional crystallization of secondary ol+cpx+sp.
593 We suggest that the glass in veins represents a CO_2 (-H_2O) rich Si-rich melt, that infiltrated
594 the xenoliths and triggered melting of interstitial amphibole to form the secondary melt
595 pockets. This interpretation is supported by the very similar trace element patterns in some
596 glasses from melt pockets and coexisting resorbing amphibole (Fig. 10). The compositional

spectrum of hybrid melts resulting from assimilation of amphibole into Si- and trace element-rich melt such as that occurring in some veins is shown in Figure 10. The close resemblance of hybrid melts with the glass in melt pockets suggests that the incongruent melting of amphibole buffered most of the trace element contents of the glass in melt pockets, except the HREE budget. For instance, sample FT08P has glasses with trace element compositions very similar to the resorbed amphibole (Fig. 10). Furthermore, the calculated bulk major element compositions of the melt pockets by inverting the fractional crystallization of OlII+CpxII+SpII in the pockets are fairly similar to that of the amphibole in the xenoliths (this study, Table 7; Bali et al., 2008). Therefore, the glass in melt pockets is believed to result from incongruent melting of amphibole, triggered by the influx of a hot CO_2-rich silica-rich melt into the peridotites (similar to the glass in veins), and subsequent CF of newly formed OlII, CpxII and SpII. This metasomatic agent was defined as a CO_2 or aqueous-rich fluid enriched in LILE or as a LREE-enriched silicate melt. The Sr-Nd-Pb isotopic data on glass in similar melt pockets from other SZB xenoliths (Bali et al., 2002) are not consistent with those of the host Pliocene and Quaternary alkali basalts but rather support a melt source containing a slab-derived component, that may have reacted with the upper lithospheric mantle during percolation. This study further demonstrates that the metasomatic agent was likely Si-rich, and enriched in LILE, HFSE, LREE, and had high volatile contents such as H_2O and CO_2 (Creon et al., this volume).

The geothermometer of Putirka (2008) has been used on clinopyroxeneII-glass pairs that show evidence for chemical equilibrium to estimate the temperature of clinopyroxene-melt equilibration in the melt pockets. Calculated temperatures (Szentbékkálla: 1,210-1,250°C; Szigliget: 1,230-1,270°C; Füzes-tó: 1,220°C; Table 8) represent minimum temperatures for the formation of melt pockets. Similar calculations for clinopyroxenes in melt pocket in other xenoliths from the Szentbékkálla locality yield similar temperatures (1110 to 1200°C from

622 Demény et al. (2004) and Bali et al. (2008)). This range is 150–350°C higher than the
623 estimated equilibrium temperatures of the host peridotites and pyroxenites (Table 8). These
624 temperature estimates suggest that the studied melt pockets formed at higher temperatures
625 than equilibrium temperatures recorded by the primary mantle minerals, likely induced by hot
626 Si-rich magma injection. Pressure estimates based on Putirka (2008) indicate a minimum
627 pressure for melt pocket formation of 0.7-0.8 GPa for Szentbékkálla, 1.0-1.1 GPa for
628 Szigliget and 0.8-1.0 GPa for Füzes-tó, corresponding to depths of 28–38 km (Fig. 11). Figure
629 11 shows the comparison of the pressures determined from primary mineral chemical
630 equilibrium (M-I), fluid inclusions trapping pressures (FI), vesicles pressure at the last melt-
631 fluid equilibrium (CO_2-melt; Creon et al., this volume) and newly formed minerals chemical
632 equilibrium in melt pockets (M-II). The figure 11 illustrates in Szentbékkálla samples that
633 vesicles, fluid inclusions and secondary crystallization of melt pockets happened almost at the
634 same pressure, at about ~0.8 GPa. In Szigliget samples, vesiculation and secondary
635 crystallization of melt pockets took place at the same pressure close to the MOHO (~1.0
636 GPa). However fluid inclusions trapping seems to have happened at shallower depths (~0.5
637 GPa), a result likely biased by fluid inclusions decrepitation (Creon et al., this volume). In
638 Füzes-tó samples, secondary crystallization of melt pockets and fluid inclusions show the
639 same pressure close to the MOHO (~0.9 GPa), whereas vesicles have lower pressure (~0.6
640 GPa), which can be the result of a late melt-fluid equilibrium before the melt quenching. The
641 P-T conditions estimated for mineral-melt equilibrium in the melt pockets show that the melt
642 pockets formed in the upper part of the lithosphere, close to the MOHO, and that this occurred
643 outside the stability field of amphibole-bearing peridotite due to an increase in temperature
644 after melt injection (Olafsson and Eggler, 1983; Niida and Green, 1999).
645
646 5.2.2 Glass in veins

The glass in the veins has variable but high SiO_2 contents (54.2 to 62.7 wt. %). The lowest silica-rich glass in veins (SZB16, SZB52) has a composition similar to the richest silica glass in melt pockets (55.8-59.0 wt. %). According to petrographic observations, there is only little evidence for reaction between primary minerals (CpxI and SpI) and the interstitial glass in veins. Figure 12 evidences that the melt in veins cannot be associated to in-situ melting of peridotites (Draper and Green, 1997). This observation suggests that the Si-rich glass was in close equilibrium with the host spinel peridotites in which they are found.

The glass in veins has high SiO_2, MgO and K_2O contents and has trace element contents enriched in the most incompatible elements, showing variable Pb negative/positive and Sr positive anomalies but no relative depletion in HFSE (Fig. 13). The Si-rich glass in veins has different major element compositions compared to the Pliocene alkali basalts and calc-alkali volcanics (Fig. 12) and show differentiated compositions in terms of major elements. The glass in veins also display different trace element abundances or ratios than the more mafic alkali basalts and calc-alkali volcanics from the Pannonian Basin (Fig. 13).

They also do not display the typical geochemical characteristics of worldwide calc-alkali magmas as seen in most pannonian calc-alkali volcanics (ie. high Ba/Nb, negative anomalies in HFSE) but it resembles some of the calc-alkali volcanics of the Pannonian Basin (Fig. 13 and 15), especially from the Northern Pannonian Basin (NPB, 17-10 Ma, Harangi and Lenkey, 2007). They are however distinctive given their higher Nb and Ti and lower HREE contents (Fig. 13) but also their higher SiO_2 and Na_2O and lower FeO, CaO than the NPB (Fig. 12).

The occurrence of Si-rich melts as efficient metasomatic agents and their interaction with the lithospheric mantle beneath the BBHVF has already been documented by Bali et al. (2007, 2008a, 2008b) for xenoliths from Szentbékkálla and Szigliget (samples SZB and SZG) and

672 was also documented by Coltorti et al. (2007) for mantle xenoliths from the Kapfenstein
673 (Austria). In the BBHVF, there are mineralogical and geochemical evidences that the
674 lithospheric mantle was modified by percolation of Si-saturated melts. The occurrence of opx-
675 rich lithologies in peridotites as well as of Qz-bearing websterite veins/bands were interpreted
676 as resulting from the interaction between melts/fluids derived from subducted slab (Bali et al.,
677 2008) and the lithospheric mantle beneath the BBHVF. In the BBHVF, the silica richest glass
678 (54.2-62.7 wt. % SiO_2) occurs as primary silicate melt inclusions in pyroxenes (opx, cpx) as
679 well as interstitial glass in veins in pyroxenes-rich xenoliths (Qz-bearing websterite,
680 clinopyroxenite) or in peridotites (lherzolites, harzburgites) from Szigliget (Bali et al., 2008).
681 However, these primary SMI have lower MgO, CaO and much higher K_2O for 57.3-80.2 wt.
682 % SiO_2 compared to the glass in veins (54.2-62.7 wt. % SiO_2). Of particular interest, the
683 interstitial glass in veins reported by Bali et al. (2008) in the Qz-bearing websterite is much
684 more silicic (63.8-80.5 wt. % SiO_2) and more depleted in terms of most major elements
685 except K_2O. In terms of trace elements, the SMI in opx and cpx from Bali et al. (2008) have
686 quite similar LREE, MREE (±HREE) but they have higher Th, U contents and pronounced
687 negatives anomalies in Nb, Ta, Sr.
688 Bali et al., (2008) described several features of the trace element composition which resemble
689 those of adakites in silicate melt inclusions of Szentbékkálla and Szigliget. Oppositely, the
690 low Sr content of the silicate melt inclusions (74-116 ppm) and high K/Na ratios, and large
691 ion lithophile element (LILE) and LREE concentrations are not typical for adakites (4400
692 ppm Sr). These features were interpreted as resulting from (1) the presence of a mineral phase
693 that retains Sr in the source during slab melt generation, (2) incompatible trace elements of
694 the source and (3) small degrees of partial melting. In this study, several characteristics of the
695 major and trace element compositions of the glass in veins also resemble those of adakites,
696 especially the low-Si adakites as illustrated in Figures 12 and 14. For instance, the Si-rich

697 glasses have high MgO and CaO, high La/Yb at low Yb contents, high Sr/Y at low Y contents
698 (Fig. 14). However, as demonstrated for the lithospheric mantle beneath the BBHVF (Bali et
699 al. 2008), the silicic melts derived from subduction zones have probably reacted within the
700 lithospheric mantle before being trapped as SMI or silicate melt pockets in the host peridotites
701 so it is unlikely that they have preserved their original geochemical signature.
702 Rapp et al. (1999) showed in their experiments a range of melts produced by assimilation of
703 peridotite by adakitic melts in order to understand the geochemical changes during migration
704 of melts in the mantle wedge. Some of the vein glasses have major element compositions
705 close to the composition obtained by assimilation experiments in Rapp et al. (1999) (MgO,
706 Na_2O, K_2O). However CaO and Al_2O_3 are much higher in the glass in veins than in the
707 experiments (Fig. 12). The trace elements of the glass in veins are also comparable in terms of
708 REE+Y, U, Rb, Ba from the assimilation experiments, but have higher Th, Nb and do not
709 display a relative enrichment in Sr. The high HFSE contents observed in the glass in veins
710 could be a geochemical characteristic of high-Nb basalts that are found associated with
711 adakites in subduction zones (Defant and Kepezhinskas, 2001), such as the in Northern
712 Pannonian Basin found in the area (Harangi and Lenkey, 2007). The experiments of Xiong et
713 al. (2005) and those of Foley et al. (2000) show that rutile dominates Nb and Ta budgets
714 during the partial melting of subducted oceanic crust and only rutile is able to cause strong
715 fractionation of Nb and Ta from other trace elements to produce a negative Nb–Ta anomaly in
716 the derived liquid (see next section). The absence of negative anomaly in Nb-Ta imply
717 therefore the absence of rutile as a stable phase during melting in the source region of these
718 melts and during interaction with the lithospheric mantle.
719 The trace elements in the glass in veins could allow to place some constraints on the P-T
720 conditions of the formation of the adakitic melts. The low HREE contents (La/Yb > 20) and Y
721 (< 18 ppm) suggests the presence of garnet in the source region (Castillo et al., 1999; Defant

and Kepezhinskas, 2001). The high abundance of K_2O in the melts also suggests a substantial contribution of phlogopite. In figure 15, the postulated melt source is located below the lithosphere-asthenosphere boundary (LAB, ~2.2GPa, Tašárová et al., 2009) above the Pannonian Basin (1000-1200°C and 2.2-3 GPa, Fig. 15). These estimations are higher than those of Bali et al., (2008) for the melt source (950-1050°C and 1.5-2 GPa), which were determined using silicate melt pockets modified by amphibole assimilation. Our estimation is based on melt compositions unmodified by amphibole assimilation, and are thus more representative of the source of the metasomatic agent.

5.3 Melt generation and migration in the Carpathian-Pannonian mantle

In the Figure 15a, the different P-T conditions determined using geochemical thermo-barometers of the different magma genesis events are shown together with mineral phase stability fields. The metasomatic agent was generated along a subduction geotherm, in contact with hotter asthenospheric mantle between 2-3 GPa. The metasomatic agent migrated from its source region to the primary lithospheric mantle mineral equilibrium area (M_I), which we locate on the geotherm postulated by Kovacs et al. (2012) to react with the amphiboles and form SMPs. Melt-mineral equilibrium compositions in SMPs (M_{II}) recorded minimum pressure/temperature conditions near present day Moho depths. The M_{II} P-T region is located in the plagioclase equilibrium field, which is contradiction with our observations. We suggest that the minimum pressures estimated with the method of Putirka are underestimating true melt generation pressures which were more likely in the spinel stability field, at above 1.2-1.3 GPa, within the pressure range of primary mineral equilibrium (M_I). The M_{II} area is located within the carbonate equilibrium field; which does not satisfy our observations and those of the literature (Bali et al., 2002; Demény et al., 2004; Demény et al., 2010) which illustrate the

747 presence of free CO_2 and potentially carbonates in the mantle xenoliths. We do not explain
748 this discrepancy between known thermodynamic phase equilibrium and our observations. The
749 determination of carbon phase stability is beyond the scope of this work and will not be
750 discussed further here.
751 The Si-rich melts percolating the lithospheric mantle of the BBHVF have strong affinities
752 with high-Nb adakites and are associated with subduction zone fluids. The high CO_2 and H_2O
753 contents of Si-rich melts (Creon et al., this volume) are in favor of a hydrated and carbonated
754 pyrolith. Altered oceanic lithosphere and/or sediment melting are best candidates for
755 providing a significant carbon and hydrogen budget (Staudigel et al., 1989; Plank and
756 Langmuir, 1998) to subduction melts. Dehydration and decarbonation of eclogites and
757 metasediments on the subduction geotherm at pressures above 3 GPa liberated volatile and
758 incompatible element-rich fluids that migrated towards the metasomatized mantle wedge (Fig.
759 15). The percolation of these primary fluids destabilized phlogopite and amphibole rich
760 peridotites to generate CO_2-supersaturated Nb-rich silicic melts that rapidly reached
761 asthenospheric temperatures. The injection of such hot Si-rich melts in the lithospheric mantle
762 in turn triggered the fusion of pargasite due to increased temperatures within the spinel
763 stability field. Amphibole melts of initial basaltic compositions fractionated into olivine,
764 clinopyroxene, spinel and andesitic melts before the system quenched on its way up to the
765 surface.
766
767 6 Conclusion
768
769 Compositional and textural features of fifteen ultramafic mantle xenoliths from four different
770 localities (Szentbékkálla, Szigliget, Füzes-tó and Mindszentkálla) have been studied. They
771 contain trails of secondary fluid inclusions, primary silicate melt inclusions, veins and pockets

of melts which allow reconstructing different stages of partial melting and metasomatism in the lithospheric mantle:

1. The lithospheric mantle below the Pannonian Basin is highly heterogeneous and has recorded a history of high to low partial fusion events overprinted by cryptic and modal metasomatism involving the formation of widespread pargasitic amphiboles.
2. The melting of a CO_2-rich subducting slab derived source produced high-Nb silicic melts of adakitic affinity. Melting conditions were comprised at temperatures between 1000-1200°C and pressures between 2 and 3 GPa, near the lithosphere-asthenosphere boundary. This silicic melt is found in mantle xenoliths as a network of glass veins enclosing large CO_2 vesicles.
3. The silicic melt migrated into the lithospheric mantle and interacted with pargasitic amphiboles. The melting of amphiboles was triggered by temperature increase due to magma injection and the high CO_2 abundances in melts. The P-T conditions for melting and crystal fractionation of amphibole melt pockets were of 0.7-1.1 GPa and 1200 °C, near the Moho transition. The melt pockets are found in mantle peridotites as an assemblages of andesitic glass, CO_2-vesicles and secondary olivine, clinopyroxene and spinel. Pargasite melts could be the parental magmas of the calc-alkaline suite of the Pannonian Basin.

7 Acknowledgements

This project was funded by IFP Energies nouvelles. Thank you to Csaba Szabó for his kindness help in the field and in the study of these mantle xenoliths. Herman Ravalojaona is acknowledged for his assistance during sample and thin section preparation. We are grateful to Carole La for her efficient help in LA-ICP-MS analyses of trace elements at LPG Nantes.

Michel Fialin and Nicolas Rividi of the centre CAMPARIS at UPMC assisted for EPMA.

8 References

Achterberg V., E., Ryan C. G., Jackson S. E. and Griffin W. (2001) Data reduction software for LA-ICP-MS. In: Sylvester, P. (ed.) Laser Ablation ICPMS in Earth Science: Principles and Applications. *Mineral. Assoc. Canada* **29**, 239–243.

Bada G., Hovath F., Gerner P. and Fejes I. (1999) Review of the present day geodynamics of the Pannonian Basin progress and problems. *Geodynamics* **27**, 501–527.

Bali E., Falus G., Szabó C., Peate D. W., Hidas K., Török K. and Ntaflos T. (2007) Remnants of boninitic melts in the upper mantle beneath the central Pannonian Basin? *Mineral. Petrol.* **90**, 51–72. Available at: http://link.springer.com/10.1007/s00710-006-0167-z [Accessed January 25, 2014].

Bali E., Szabó C., Vaselli O. and Torok K. (2002) Significance of silicate melt pockets in upper mantle xenoliths from the Bakony – Balaton Highland Volcanic Field , Western Hungary. *Lithos* **61**, 79–102.

Bali E., Zajacs Z., Kovacs I., Szabó C., Halter W., Vaselli O., Torok K. and Bodnar R. J. (2008) A Quartz-bearing Orthopyroxene-rich Websterite Xenolith from the Pannonian Basin , Western Hungary : Evidence for Release of Quartz-saturated Melts from a Subducted Slab. *J. Petrol.* **49**, 421–439.

Bali E., Zanetti A., Szabó C., Peate D. W. and Waight T. E. (2008) A micro-scale investigation of melt production and extraction in the upper mantle based on silicate melt pockets in ultramafic xenoliths from the Bakony–Balaton Highland Volcanic Field (Western Hungary). *Contrib. to Mineral. Petrol.* **155**, 165–179. Available at: http://link.springer.com/10.1007/s00410-007-0234-4 [Accessed January 25, 2014].

822 Balogh K. and Németh K. (2005) Evidence for the Neogene small-volume intracontinental
823 volcanism in Western Hungary: K/Ar geochronology of the Tihany Maar Volcanic
824 Complex. *Geol. Carpathica* **56**, 91–99.
825 Balogh K. and Pécskay Z. (2001) K/Ar and Ar/Ar geochronological studies in the Pannonian-
826 Carpathians-Dinarides (PANCARDI) region. *Acta Geol. Hung.* **44**, 281–299.
827 Ban M., Witt-Eickschen G., Klein M. and Seck H. a. (2005) The origin of glasses in hydrous
828 mantle xenoliths from the West Eifel, Germany: Incongruent break down of amphibole.
829 *Contrib. to Mineral. Petrol.* **148**, 511–523.
830 Beccaluva L., Bondadiman C., Coltorti M., Salvini L. and Siena F. (2001) Depletion Events,
831 Nature of Metasomatizing Agent and Timing of Enrichment Processes in Lithospheric
832 Mantle Xenoliths from the Veneto Volcanic Province. *J. Petrol.* **42**, 173–187.
833 Bodinier J. ., Vasseur G., Vernieres J. and Dupuy C. F. (1990) Mechanisms of mantle
834 metasomatism: geochemical evidence from the Lherz orogenic peridotite. *J. Petrol.* **31**,
835 597–628.
836 Brey G. P., Kohler T. and Nickel K. G. (1990) Geothermobarometry in Four-phase
837 Lherzolites I . Experimental Results from 10 to 60 kb. *J. Petrol.* **31**, 1313–1352.
838 Castillo P. R., Janney P. E. and Solidum R. U. (1999) Petrology and geochemistry of
839 Camiguin Island, southern Philippines: insights to the source of adakites and other lavas
840 in a complex arc setting. *Contrib. to Mineral. Petrol.* **134**, 33–51.
841 Coltorti M., Beccaluva L., Bonadiman C., Faccini B., Ntaflos T. and Siena F. (2004)
842 Amphibole genesis via metasomatic reaction with clinopyroxene in mantle xenoliths
843 from Victoria Land, Antarctica. *Lithos* **75**, 115–139.
844 Coltorti M., Beccaluva L., Bonadiman C., Salvini L. and Siena F. (2000) Glasses in mantle
845 xenoliths as geochemical indicators of metasomatic agents. *Earth Planet. Sci. Lett.* **183**,
846 303–320. Available at: http://linkinghub.elsevier.com/retrieve/pii/S0012821X00002740.

Coltorti M., Bonadiman C., Faccini B., Ntaflos T. and Siena F. (2007) Slab melt and intraplate metasomatism in Kapfenstein mantle xenoliths (Styrian Basin, Austria). *Lithos* **94**, 66–89.

Coltorti M., Bonadiman C., Hinton R. W., Siena F. and Upton B. G. J. (1999) Carbonatite Metasomatism of the Oceanic Upper Mantle : Evidence from Clinopyroxenes and Glasses in Ultramafic Xenoliths of Grande Comore , Indian Ocean. *J. Petrol.* **40**, 133–165.

Creon L., Rouchon V., Youssef S., Rosenberg E., Delpech G., Guyot F., Szabó C., Tafforeau P., Boller E., Asimow P. D., Antoshechkina P. M. and Ghiorso M. S. Highly CO2-supersaturated melts in the Pannonian lithospheric mantle – A transient carbon reservoir? *this Vol.*

Csontos L., Nagymarosy A., Horváth F. and Kovác M. (1992) Tertiary evolution of the Intra-Carpathian area: a model. *Teconophysics* **208**, 221–241.

Dawson J. (1984) Contrasting types of upper-mantle metasomatism? In: Kornprobst J (ed) Kimberlites II: The mantle and crust– mantle relationships. *Holland*, 289.

Defant M. J. and Kepezhinskas P. (2001) Evidence suggests slab melting in arc magmas. *Eos, Trans. Am. Geophys. Union* **83**, 256.

Delpech G., Grégoire M., O'Reilly S. Y., Cottin J. Y., Moine B., Michon G. and Giret a. (2004) Feldspar from carbonate-rich silicate metasomatism in the shallow oceanic mantle under Kerguelen Islands (South Indian Ocean). *Lithos* **75**, 209–237.

Demény A., Dallai L., Frezzotti M.-L., Vennemann T. W., Embey-Isztin A., Dobosi G. and Nagy G. (2010) Origin of CO2 and carbonate veins in mantle-derived xenoliths in the Pannonian Basin. *Lithos* **117**, 172–182. Available at: http://linkinghub.elsevier.com/retrieve/pii/S0024493710000575 [Accessed December 7, 2012].

Demény A., Vennemann T. ., Hegner E., Nagy G., Milton J. ., Embey-Isztin A., Homonnay Z. and Dobosi G. (2004) Trace element and C–O–Sr–Nd isotope evidence for subduction-related carbonate–silicate melts in mantle xenoliths (Pannonian Basin, Hungary). *Lithos* **75**, 89–113. Available at: http://www.sciencedirect.com/science/article/pii/S0024493704000209 [Accessed March 16, 2015].

Demény A., Vennemann T. W., Homonnay Z. and Milton A. (2005) Origin of amphibole megacrysts in the Pliocene-Pleistocene basalts of the Carpathian-Pannonian region. *Geol. Carpathica* **56**, 179–189.

Downes H., Embey-Isztin A. and Thirlwall M. F. F. . (1992) Petrology and geochemistry of spinel peridotite xenoliths from the western Pannonian Basin (Hungary): evidence for an association between enrichment and texture in the upper mantle. *Contrib. Mineral. Petrol.* **109**, 340–354.

Draper D. S. and Green T. H. (1997) P – T Phase Relations of Silicic , Alkaline , Aluminous Mantle-Xenolith Glasses Under Anhydrous and C – O – H Fluid-saturated Conditions. *J. Petrol.* **38**, 1187–1224.

Embey-Isztin a, Dobosi G., Altherr R. and Meyer H.-P. (2001) Thermal evolution of the lithosphere beneath the western Pannonian Basin: evidence from deep-seated xenoliths. *Tectonophysics* **331**, 285–306. Available at: http://linkinghub.elsevier.com/retrieve/pii/S0040195100002870.

Embey-Isztin A., Dobosi G., Bodinier J.-L., Bosch D., Jenner G. a., Pourtales S. and Bruguier O. (2014) Origin and significance of poikilitic and mosaic peridotite xenoliths in the western Pannonian Basin: geochemical and petrological evidences. *Contrib. to Mineral. Petrol.* **168**, 1054. Available at: http://link.springer.com/10.1007/s00410-014-1054-y.

Embey-Isztin A., Dobosi G., James D., Downes H., Poultidis C. and Scharbert H. G. (1993) A

compilation of new major, trace element and isotope geochemical analyses of the young alkali basalts from the Pannonian Basin. *Fragm. Mineral. Palaeontol.* **16**, 5–26.

Embey-isztin A., Downes H., James D. E. E., Upton B. G. J. G. J., Dobosi G., Ingram G. A. a., Harmon R. S. S. and Scharbert H. G. G. (1993) The petrogenesis of Pliocene alkaline volcanic rocks from the Pannonian Basin, Eastern central Europe. *J. Petrol.* **34**, 317–343.

Embey-Isztin A. and Scharbert H. G. (2001) Glasses in peridotite xenoliths from the western Pannonian Basin. *Per. Mineral.* **70**, 359–376.

Embey-Isztin A., Scharbert H. G., Dietrich H. and Poultidis H. (1989) Petrology and geochemistry of peridotite xenoliths in alkali basalts from the Transdanubian volcanic region. *J. Petrol.* **30**, 79–106.

Falus G., Drury M. R., van Roermund H. L. M. and Szabó C. (2004) Magmatism-related localized deformation in the mantle: a case study. *Contrib. to Mineral. Petrol.* **146**, 493–505. Available at: http://link.springer.com/10.1007/s00410-003-0513-7 [Accessed February 8, 2014].

Falus G., Szabó C., Kovács I., Zajacz Z. and Halter W. (2007) Symplectite in spinel lherzolite xenoliths from the Little Hungarian Plain, Western Hungary: A key for understanding the complex history of the upper mantle of the Pannonian Basin. *Lithos* **94**, 230–247. Available at: http://linkinghub.elsevier.com/retrieve/pii/S0024493706001848 [Accessed December 7, 2012].

Fodor L., Csontos L., Bada G., Györfi I. and Benkovics L. (1999) Tertiary tectonic evolution of the Pannonian basin and neighbouring orogenes: a new synthesis of palaeostress data. In: Durand, B., Jolivet, L., Horváth, F., Séranne, M. (Eds.), The Mediterranean Basins: Tertiary Extension with Alpine Orogen. *Geol. Soc.* **156**, 295–334.

Foley S. F., Barth M. G. and Jenner G. a. (2000) Rutile/melt partition coefficients for trace elements and an assessment of the influence of rutile on the trace element characteristics

of subduction zone magmas. *Geochim. Cosmochim. Acta* **64**, 933–938.

Gagnon J. E., Fryer B. J., Samson I. M. and Williams-Jones A. E. (2008) Quantitative analysis of silicate certified reference materials by LA-ICPMS with and without an internal standard. *J. Anal. At. Spectrom.* **23**, 1529.

Ghiorso M. S. and Gualda G. A. R. (2015) An H2O-CO2 mixed fluid saturation model compatible with rhyolite-MELTS. *Contrib. to Mineral. Petrol.*

Gualda G. A. R., Ghiorso M. S., Lemons R. V. and Carley T. L. (2012) Rhyolite-MELTS: a Modified Calibration of MELTS Optimized for Silica-rich, Fluid-bearing Magmatic Systems. *J. Petrol.* **53**, 875–890. Available at: http://www.petrology.oxfordjournals.org/cgi/doi/10.1093/petrology/egr080.

Harangi S. and Lenkey L. (2007) Genesis of the Neogene to Quaternary volcanism in the Carpatian Pannonian region : Role of subduction , extension , and mantle plume. *Geol. Soc. Am.* **Special Pa**, 67–92.

Hellebrand E., Snow J. E., Hoppe P. and Hofmann A. W. (2002) Garnet-field Melting and Late-stage Refertilization in " Residual " Abyssal Peridotites from the Central Indian Ridge. *J. Petrol.* **43**, 2305–2338.

Horvath F. (1993) Towards a mechanical model for the formation of the Pannonian Basin. *Tectonophysics* **226**, 333–357.

Huismans R. S., Podladchikov Y. Y. and Cloetingh S. a. P. L. (2002) The Pannonian basin: Dynamic modelling of the transition from passive to active rifting. In *EGU Special publication Series* pp. 41–63. Available at: http://www.stephan-mueller-spec-publ-ser.net/3/41/2002/.

Ionov D. a., Chanefo I. and Bodinier J. L. (2005) Origin of Fe-rich lherzolites and wehrlites from Tok, SE Siberia by reactive melt percolation in refractory mantle peridotites. *Contrib. to Mineral. Petrol.* **150**, 335–353.

947 Johnson K. T. M., Dick H. J. B. and Shimizu N. (1990) Melting in the oceanic upper mantle:
948 An ion microprobe study of diopsides in abyssal peridotites. *J. Geophys. Res.* **95**, 2661.
949 Kazmer M. and Kovacs S. (1985) ermian–Paleogene paleogeography along the Eastern part
950 of the Insubric–Periadriatic Lineament system: evidence for continental escape of the
951 Bakony- Drauzug unit. *Acta Geol. Hung.* **1-2**, 71–84.
952 Kereszturi G., Németh K., Csillag G., Balogh K. and Kovács J. (2011) The role of external
953 environmental factors in changing eruption styles of monogenetic volcanoes in a
954 Mio/Pleistocene continental volcanic field in western Hungary. *J. Volcanol. Geotherm.*
955 *Res.* **201**, 227–240. Available at:
956 http://www.sciencedirect.com/science/article/pii/S0377027310002647 [Accessed
957 January 19, 2015].
958 Kovacs I., Falus G., Stuart G., Hidas K., Szabó C., Flower M. F. J., Hegedűs E., Posgay K.
959 and Zilahi-Sebess L. (2012) Seismic anisotropy and deformation patterns in upper
960 mantle xenoliths from the central Carpathian–Pannonian region: Asthenospheric flow as
961 a driving force for Cenozoic extension and extrusion? *Tectonophysics* **514-517**, 168–179.
962 Available at: http://linkinghub.elsevier.com/retrieve/pii/S0040195111004562 [Accessed
963 November 14, 2014].
964 Laurora a, Mazzucchelli M., Rivalenti G., Vannucci R., Zanetti A., Barbieri M. a and
965 Cingolani C. a (2001) Metasomatism and melting in carbonated peridotite xenoliths from
966 the mantle wedge: The Gobernador Gregores case (southern Patagonia). *J. Petrol.* **42**,
967 69–87.
968 Locock A. J. (2014) An Excel spreadsheet to classify chemical analyses of amphiboles
969 following the IMA 2012 recommendations. *Comput. Geosci.* **62**, 1–11. Available at:
970 http://dx.doi.org/10.1016/j.cageo.2013.09.011.
971 Lu J., Zheng J., Grif W. L., Reilly S. Y. O. and Pearson N. J. (2015) Lithos Microscale effects

of melt in filtration into the lithospheric mantle : Peridotite xenoliths from Xilong , South China. *Lithos* **232**, 111–123.

Martin U., Auer A., Németh K. and Breitkreuz C. (2003) Mio-pliocene phreatomagmatic volcanism in a Fluvio–Lacustrine basin in Western Hungary. *GeoLines* **15**, 93–97.

McDonough W. F. F. and Sun S. -s. S. . (1995) The composition of the Earth. *Chem. Geol.* **120**, 223–253. Available at: http://www.sciencedirect.com/science/article/pii/0009254194001404 [Accessed January 15, 2015].

Mercier J. C. and Nicolas A. (1975) Textures and Fabrics of Upper-Mantle Peridotites as Illustrated by Xenoliths from Basalts. *J. Petrol.* **16**.

Miller C., Zanetti a., Thöni M., Konzett J. and Klötzli U. (2012) Mafic and silica-rich glasses in mantle xenoliths from Wau-en-Namus, Libya: Textural and geochemical evidence for peridotite-melt reactions. *Lithos* **128-131**, 11–26. Available at: http://dx.doi.org/10.1016/j.lithos.2011.11.004.

Moine B. N., Grégoire M., O'Reilly S. Y., Delpech G., Sheppard S. M. F., Lorand J. P., Renac C., Giret a. and Cottin J. Y. (2004) Carbonatite melt in oceanic upper mantle beneath the Kerguelen Archipelago. *Lithos* **75**, 239–252.

Neumann E.-R., Wulff-Pedersen E., Pearson N. J. and Spenser E. a (2002) Mantle xenoliths from Tenerife (Canary Islands): evidence for reactions between mantle peridotites and silicic carbonatite melts inducing Ca metasomatism. *J. Petrol.* **43**, 825–857. Available at: http://petrology.oupjournals.org/cgi/content/abstract/43/5/825.

Niida K. and Green D. H. (1999) Stability and chemical composition of pargasitic amphibole in MORB pyrolite under upper mantle conditions. *Contrib. to Mineral. Petrol.* **135**, 18–40.

Olafsson M. and Eggler D. H. (1983) Phase relations of amphibole, amphibole-carbonate, and

997 phlogopite-carbonate peridotite: petrologic constraints on the asthenosphere. *Earth*
998 *Planet. Sci. Lett.* **64**, 305–315. Available at:
999 http://linkinghub.elsevier.com/retrieve/pii/0012821X83902121.
1000 Posgay K., Bodoky T., Hegedus E., Kovacsvolgyi S., Lenkey L., Szafian P., Takacs E., Tımar
1001 Z. and Varga G. (1995) Asthenospheric structure beneath a Neogene basin in southeast
1002 Hungary. *Tectonophysics* **252**, 467–484.
1003 Putirka K. D. (2008) Thermometers and Barometers for Volcanic Systems. *Mineral.*
1004 *Geochemistry* **69**, 61–120.
1005 Rapp R. ., Shimizu N., Norman M. . and Applegate G. . (1999) Reaction between slab-derived
1006 melts and peridotite in the mantle wedge: experimental constraints at 3.8 GPa. *Chem.*
1007 *Geol.* **160**, 335–356. Available at:
1008 http://www.sciencedirect.com/science/article/pii/S0009254199001060 [Accessed March
1009 16, 2015].
1010 Roedder E. (1984) Fluid inclusions. *Rev. Mineral.* **12**.
1011 Shaw C. S. J. and Dingwell D. B. (2008) Experimental peridotite-melt reaction at one
1012 atmosphere: A textural and chemical study. *Contrib. to Mineral. Petrol.* **155**, 199–214.
1013 Shaw C. S. J., Heidelbach F. and Dingwell D. B. (2006) The origin of reaction textures in
1014 mantle peridotite xenoliths from Sal Island, Cape Verde: the case for "metasomatism" by
1015 the host lava. *Contrib. to Mineral. Petrol.* **151**, 681–697. Available at:
1016 http://link.springer.com/10.1007/s00410-006-0087-2 [Accessed November 14, 2014].
1017 Spakman W. (1990) Tomographic images on the upper mantle below Europe and the
1018 Mediterranean. *Ter. Nov.* **2**, 542–553.
1019 Szabó C., Bodnar R. J. and Sobolev A. V. (1996) Metasomatism associated with subduction-
1020 related, volatile-rich silicate melt in the upper mantle beneath the Nograd-Gomor
1021 Volcanic Field, Northern HungarySouthern Slovakia – Evidence from silicat. *Eur. J.*

Miner. **8**, 881–899.

Szabó C., Falus G., Zajacz Z., Kovács I. and Bali E. (2004) Composition and evolution of lithosphere beneath the Carpathian–Pannonian Region: a review. *Tectonophysics* **393**, 119–137. Available at: http://linkinghub.elsevier.com/retrieve/pii/S0040195104002574 [Accessed December 7, 2012].

Szabó C., Harangi S. and Csontos L. (1992) Review of Neogene and Quaternary volcanism of the Carpathian-Pannonian region. *Tectonophysics* **208**, 243–256.

Szabó C., Harangi S., Vaselli O. and Downes H. (1995) Temperature and oxygen fugacity in peridotite xenoliths from the Carpathian-Pannonian Region. *ACta Vulcanol.* **7**, 231–239.

Szabó C., Hidas K., Bali E., Zajacz Z., Kovács I., Yang K., Guzmics T. and Török K. (2009) Melt-wall rock interaction in the mantle shown by silicate melt inclusions in peridotite xenoliths from the central Pannonian Basin (western Hungary). *Isl. Arc* **18**, 375–400. Available at: http://doi.wiley.com/10.1111/j.1440-1738.2009.00672.x [Accessed December 7, 2012].

Szabó C., Kovacs I., Dégi J., Kothay K., Torok K., Hidas K. K., Konya P., Berkesi M., Degi J., Kothay K., Torok K., Hidas K. K., Konya P. and Berkesi M. (2010) From maars to lava lakes: Ultramafic and granulite xenoliths associated with the alkaline basaltic volcanism of the Pannonian Basin. In *Mineralogica-petrographica field guide series* pp. 1–32.

Tašárová A., Afonso J. C., Bielik M., Götze H.-J. and Hók J. (2009) The lithospheric structure of the Western Carpathian–Pannonian Basin region based on the CELEBRATION 2000 seismic experiment and gravity modelling. *Tectonophysics* **475**, 454–469. Available at: http://linkinghub.elsevier.com/retrieve/pii/S0040195109003229 [Accessed January 22, 2014].

Török K., Dégi J., Szép A. and Marosi G. (2005) Reduced carbonic fluids in mafic granulite

xenoliths from the Bakony–Balaton Highland Volcanic Field, W-Hungary. *Chem. Geol.* **223**, 93–108. Available at: http://linkinghub.elsevier.com/retrieve/pii/S0009254105002913 [Accessed December 7, 2012].

Vannucci R., Bottazzi P., Wulff-Pedersen E. and Neumann E.-R. (1998) Partitioning of REE, Y, Sr, Zr, and Ti between clinopyroxene and silicate melts in the mantle under La Palma (Canary Islands): implications for the nature of the metasomatic agents. *Earth Planet. Sci. Lett.* **158**, 39–51.

Wijbrans J., Németh K., Martin U. and Balogh K. (2007) 40Ar/39Ar geochronology of Neogene phreatomagmatic volcanism in the western Pannonian Basin, Hungary. *J. Volcanol. Geotherm. Res.* **164**, 193–204. Available at: http://www.sciencedirect.com/science/article/pii/S0377027307001357 [Accessed January 14, 2015].

Wulff-Pedersen E., Neumann E.-R., Vannucci R., Bottazzi P. and Ottolini L. (1999) Silicic melts produced by reaction between peridotite and infiltrating basaltic melts : ion probe data on glasses and minerals in veined xenoliths from La Palma , Canary Islands. *Contrib. to Mineral. Petrol.* **137**, 59–82.

Xiong X. L., Adam J. and Green T. H. (2005) Rutile stability and rutile/melt HFSE partitioning during partial melting of hydrous basalt: Implications for TTG genesis. *Chem. Geol.* **218**, 339–359.

Yaxley G. M. and Kamenetsky V. (1999) In situ origin for glass in mantle xenoliths from southeastern Australia : insights from trace element compositions of glasses and metasomatic phases. *Earth Planet. Sci. Lett.* **172**, 97–109. Available at: http://dx.doi.org/10.1016/S0012-821X(99)00196-X.

Figure captions

Figure 1: Location of the Bakony Balaton highland volcanic fied and of the four sampling areas (Szentbékkálla, Szigliget, Füzes-tó, Mindszentkálla). The light grey is area is the Outer Carpathians and the dark grey area represents the Carpathian belt (North, East and South-East), Eastern Alps (West) and Dinarides (South West).

Figure 2: Streckeisen diagram (Streckeisen, 1976) of studied mantle xenoliths. They are all within the fields of lherzolites (diamonds) and harzburgites (triangles). Small circles are literature data from Downes et al. (1992); Falus et al. (2004); Bali et al. (2002). SZB-Szentbékkálla, SZG- Szigliget, FT- Füzes-tó and MSZK- Mindszentkálla. The grey area corresponds to the Sub-continental lithospherique mantle (Downes et al., 1992).

Figure 3: Textural characteristics of the Szentbékkálla, Szigliget, Füzes-tó and Mindszentkálla mantle xenoliths. A- Primary silicate melt inclusions (SMI) in a primary cpx; Some cpx present spongy rim (SZG14). B- Poikilitic opx containing ol and trails of secondary fluid inclusions (SZG14). C- Melt vein crosscutting the peridotite sample and reacting with Cpx (spongy textures); secondary crystallization of SpII, OlII and CpxII in the melt; trails of secondary fluid inclusions are crosscutting the vein (SZB16). D- Interconnected melt pockets in SZG23; The box is a zoom in a melt pocket of SZB16. E- Glass pocket with few cpx secondary crystallization at boundaries (SZG44). F- Numerous trails of secondary fluid inclusions crosscutting together cpx and opx (SZB51); The box is a zoom on fluid inclusions. G-. Pseudomorphic melt pocket after amphibole breakdown (SZB51). H- Pseudomorphic melt pocket after amphibole breakdown (FT08P. Ol- olivine, Opx- Orthopyroxene, Cpx-

Clinopyroxene, Sp- spinel, Amp- amphibole, FI- fluid inclusions, MP- melt pocket, Vs- vesicle, M.I- Primary mineral, M.II- Secondary mineral, SMI- silicate melt inclusion.

Figure 4: Major-element compositions for primary minerals of the mantle xenoliths from the four sampled areas. Literature from Downes et al. (1992); Embey-Isztin et al. (1989); Bali et al. (2002); Falus et al. (2004); Demény et al. (2004, 2005). Blue squares: primitive mantle, triangles: harzburgite-like, diamonds: lherzolites. Black, dark-grey, light grey and white colors are respectively assigned to Szentbékkálla, Szigliget, Füzes-tó and Mindszentkálla. PM – partial melting.

Figure 5: Major element compositions of the newly formed cpx, ol and spinels. The grey area shows the domain for primary mineral compositions for comparison. Black circles: Szentbékkálla, dark-grey circles: Szigliget, light-grey circles: Füzes-tó. Smaller dots are from Bali et al. (2002).

Figure 6: REE and trace-element patterns for primary clinopyroxene and amphibole from the four localities. Grey areas are literature data from Embey-Isztin et al. (2014). Black, dark-grey, light grey and black dashed lines are respectively assigned to Szentbékkálla, Szigliget, Füzes-tó and Mindszentkálla samples. See text for group description.

Figure 7: Major-element compositions for vein (circles) and melt pocket (diamond) glass in samples from SZB (black), SZG (dark-grey) and FT (light grey). The small grey circles are from Bali et al. (2002). Doted lines are assimilation of cpx (black), amp (dark grey) and sp (light grey). The dashed lines represent crystal fractionation (CF) trends calculated using

Rhyolite-MELTS (Gualda et al., 2012; Ghiorso and Gualda, 2015). Black and grey square present respectively the starting compositions for crystal fractionation and assimilation.

Figure 8: Trace-element patterns for glass in melt pockets (SMP) in samples of SZB (dark), SZG (dark-grey) and FT (light-grey).

Figure 9: Textural observations of amphibole breakdown for the FT08P xenoliths. Vs – vesicle, Gl – glass, Amp – amphibole, Cpx – clinopyroxene, Sp – spinel.

Figure 10: Trace element patterns illustrating the assimilation of amphibole in melt. Each doted line corresponds to the addition of 10% amphibole in initial vein type melt.

Figure 11: Pressure comparison between primary mineral chemical equilibrium, secondary crystalized mineral/melt chemical equilibrium, fluid inclusions trapping and vesicles last equilibrium with melt. Primary minerals are formed at deeper pressures and vesicles, silicate melt pockets and fluid inclusions trapping happened at close pressures near to the MOHO.

Figure 12: Major element variations in veins and melt pockets (MP) for Szentbékkálla (SZB), Szigliget (SZG) and Füzes-tó (FT). Comparison is given by adakites, mantle xenolith glasses from Draper & Green (1997), experimental melts from Rapp et al. (1999), calc-alkali magmas of the Pannonian Basin (Harangi and Lenkey, 2007), silicate melt pockets of SZB mantle xenoliths (small circles, Bali et al., 2002; Demény et al., 2004) and silicate melt inclusions of SZG mantle xenoliths (small circles, Szabó et al., 2009).

Figure 13: Trace element patterns comparison between glasses in veins from mantle xenoliths and Northern Panonnian Basalts, calc-alkaline (16.5-2 Ma, Harangi and Lenkey, 2007) and alkaline basalt (11.5 to recently) magmas from BBHVF and assimilation adakite + peridotite experiments.

Figure 14: Glass from melt veins compared with known adakite compositional domains (Grey areas). Small dots are data from Bali et al. (2008).

Figure 15: Phase equilibrium diagram. A- Modified from Stern (2002) and Martin (1999). The blue field represents the assumed P-T source of the Si-rich melts in veins. lhz- lherzolite; gar- garnet; amph- amphibole; sp- spinel; plg- plagioclase. The dry peridotite solidus is from Gudfinnsson & Presnall (2005). B- Pressure–temperature diagram showing the effects of CO_2 on the solidus of carbonated lithologies in the mantle. Two different estimates of the peridotite–CO_2 solidus are reported: CMAS–CO_2 after Dalton & Presnall (1998) and Gudfinnsson & Presnall (2005), and peridotite–CO_2 (2.5 wt.%) from Dasgupta & Hirschmann (2006). The dry peridotite solidus in the CMAS system is from Gudfinnsson & Presnall (2005). Eclogite–CO_2 solidus (dry eclogite+5 wt.% CO_2) from Dasgupta et al. (2004). Asterisks (*) correspond to the KNCFMASH–CO_2 solidus (carbonated pelite+1.1 wt.% H_2O+4.8 wt.% CO_2) from Thomsen & Schmidt (2008). The effect of carbonates on the composition of melts generated at increasing temperature is reported as wt. % CO_2, based on the CMAS–CO_2 system. The solid blue line represents the geotherm from Kovacs et al. (2012)

Supp_data, Fig. a: Trace element modeling of residual clinopyroxene using the non-modal partial melting equations and parameters of Hellebrand et al. (2002) and CI-chondrite

normalization values after McDonough & Sun (1995). The numbers refer to the amount of melting in percentage. Triangles are harzburgite-like rocks and diamonds are lherzolites-like rocks.

Figure 1

Click here to download high resolution image

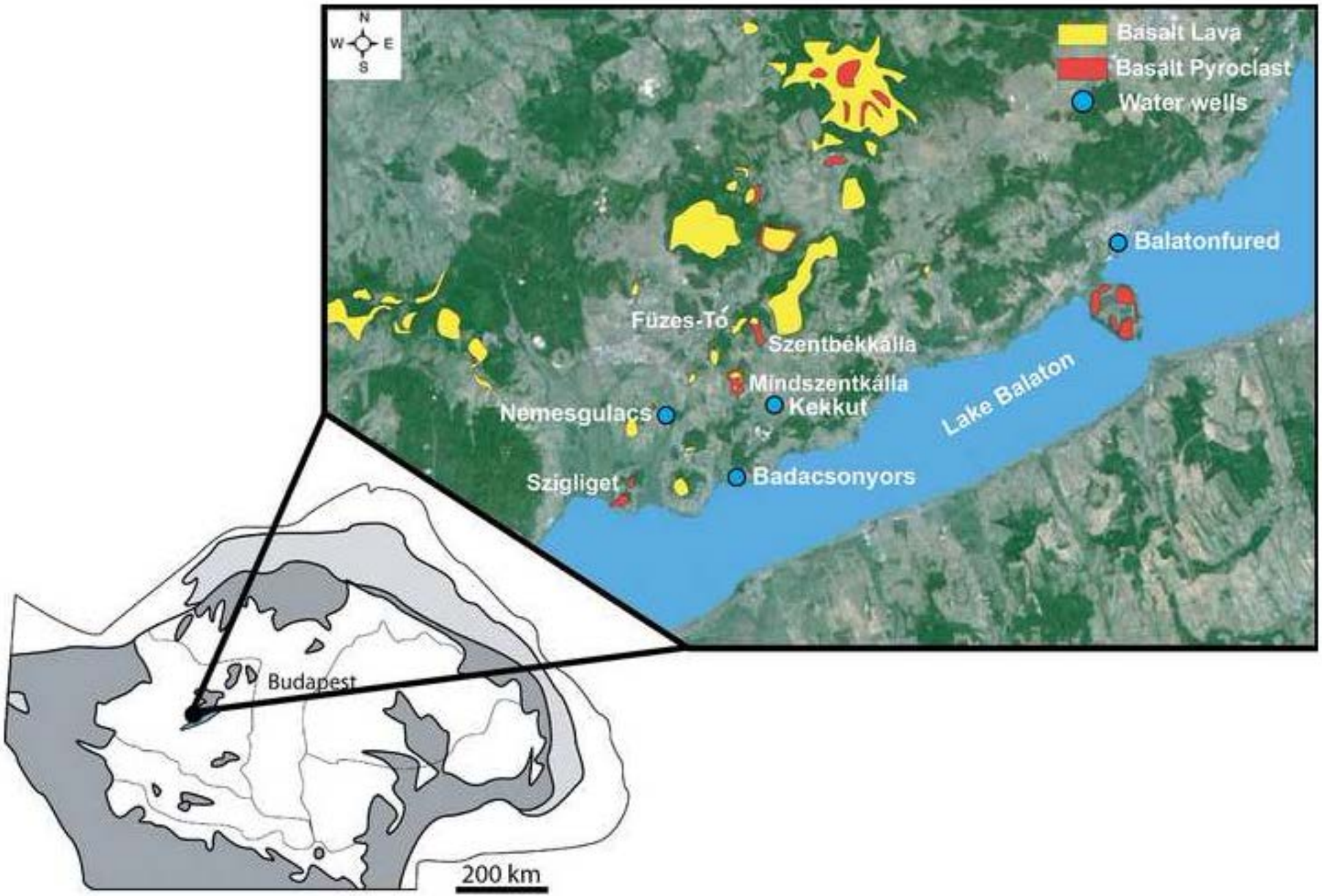

Figure 2

Click here to download high resolution image

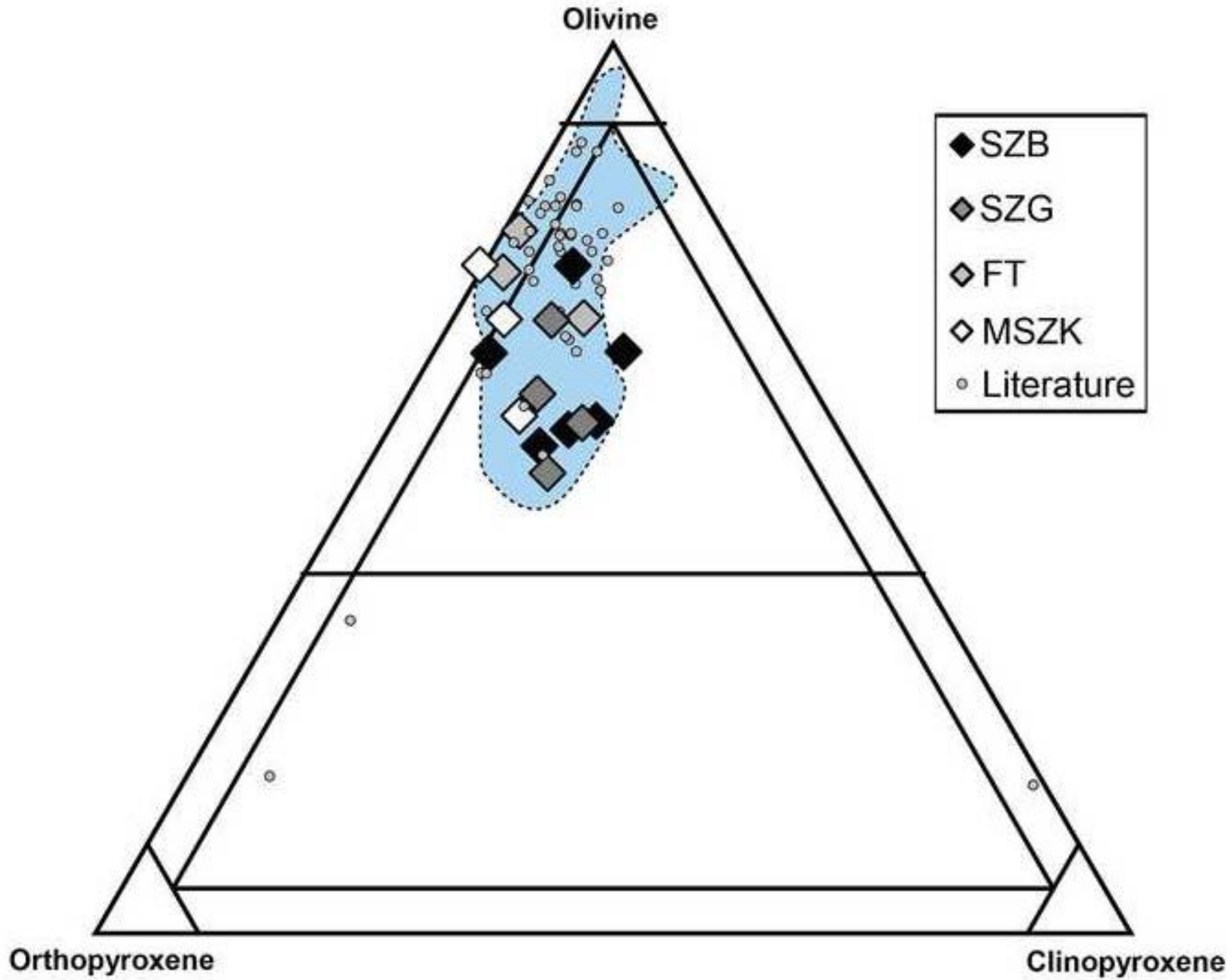

Figure 3

Click here to download high resolution image

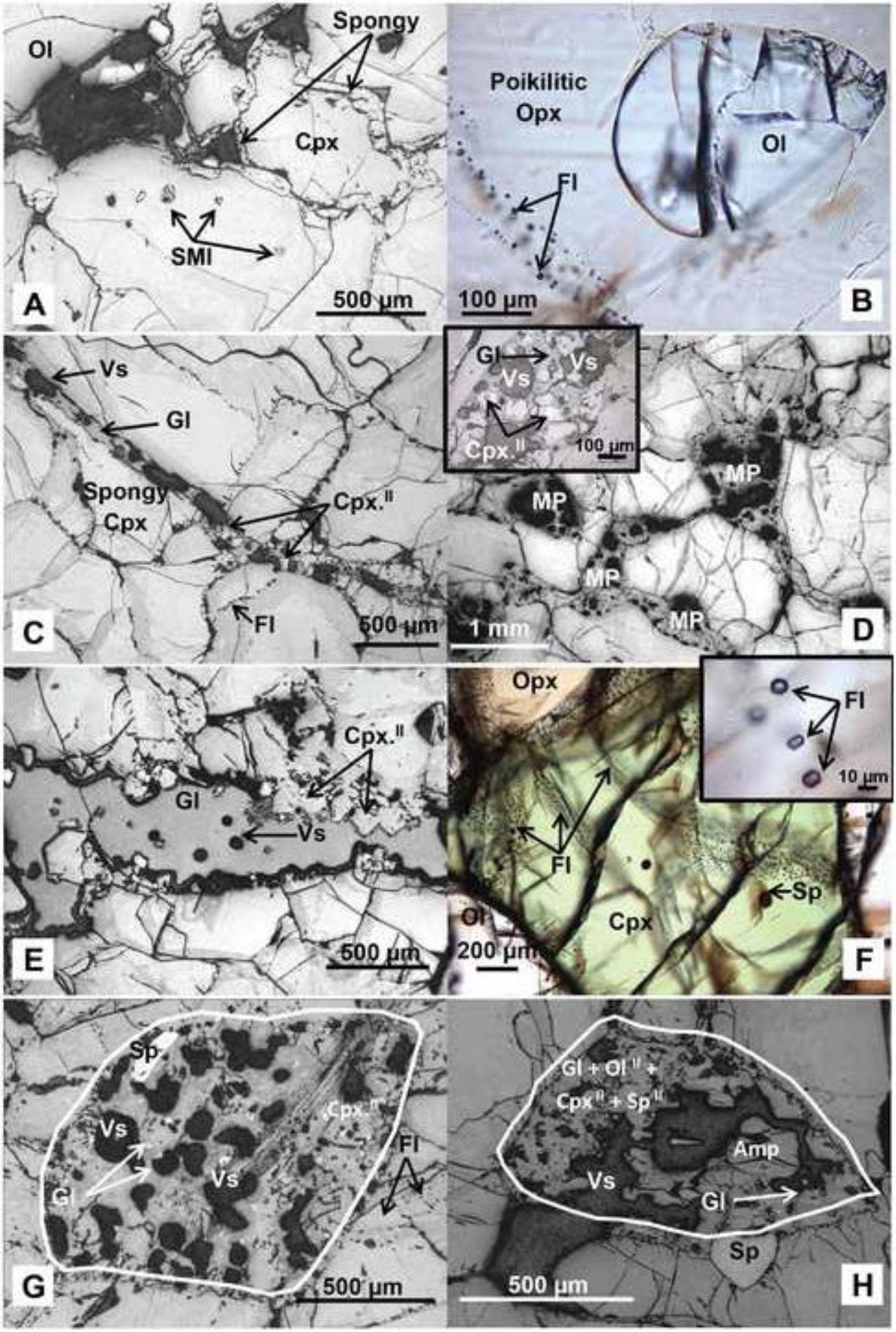

Figure 4

Click here to download high resolution image

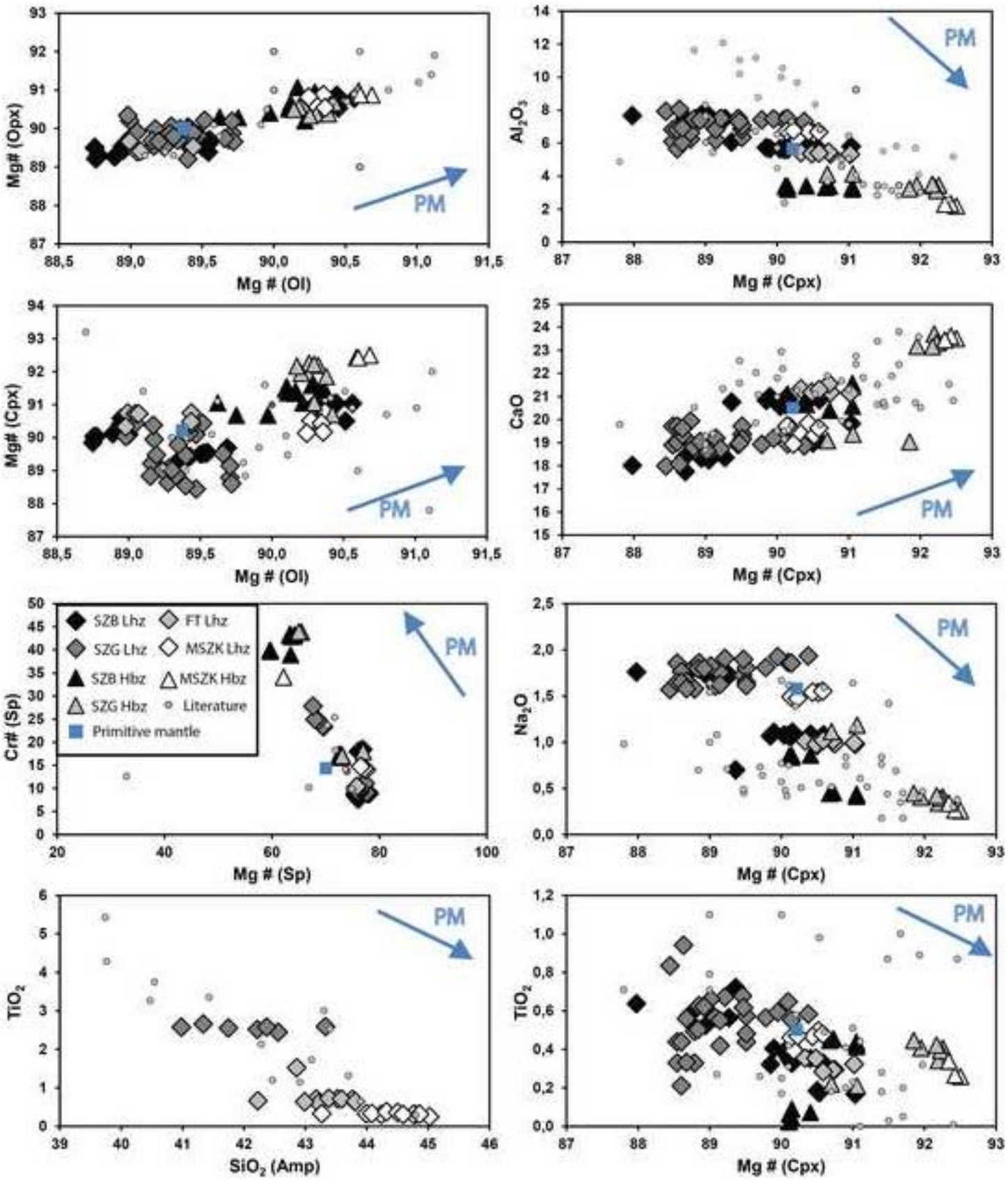

Figure 5

Click here to download high resolution image

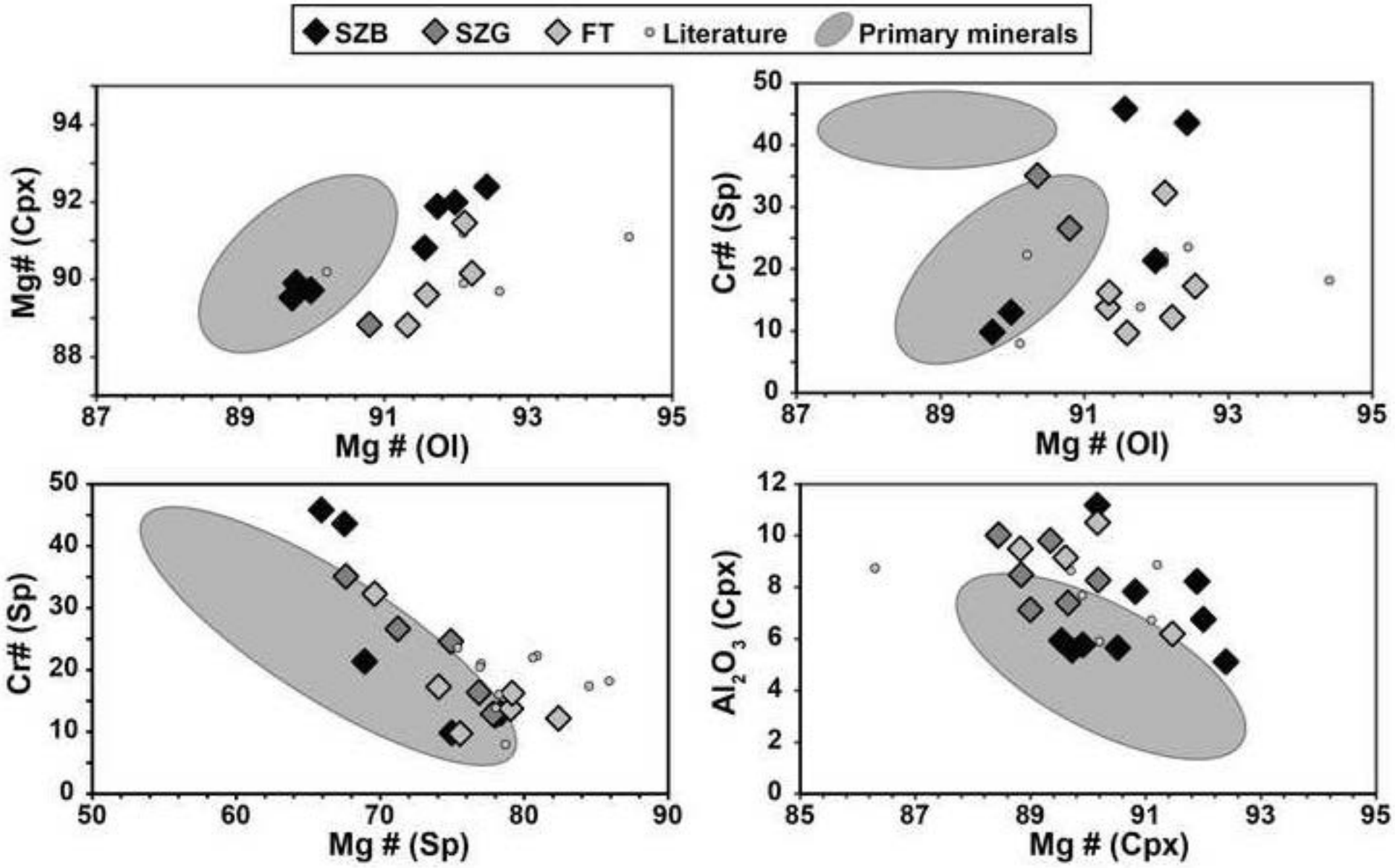

Figure 6

Click here to download high resolution image

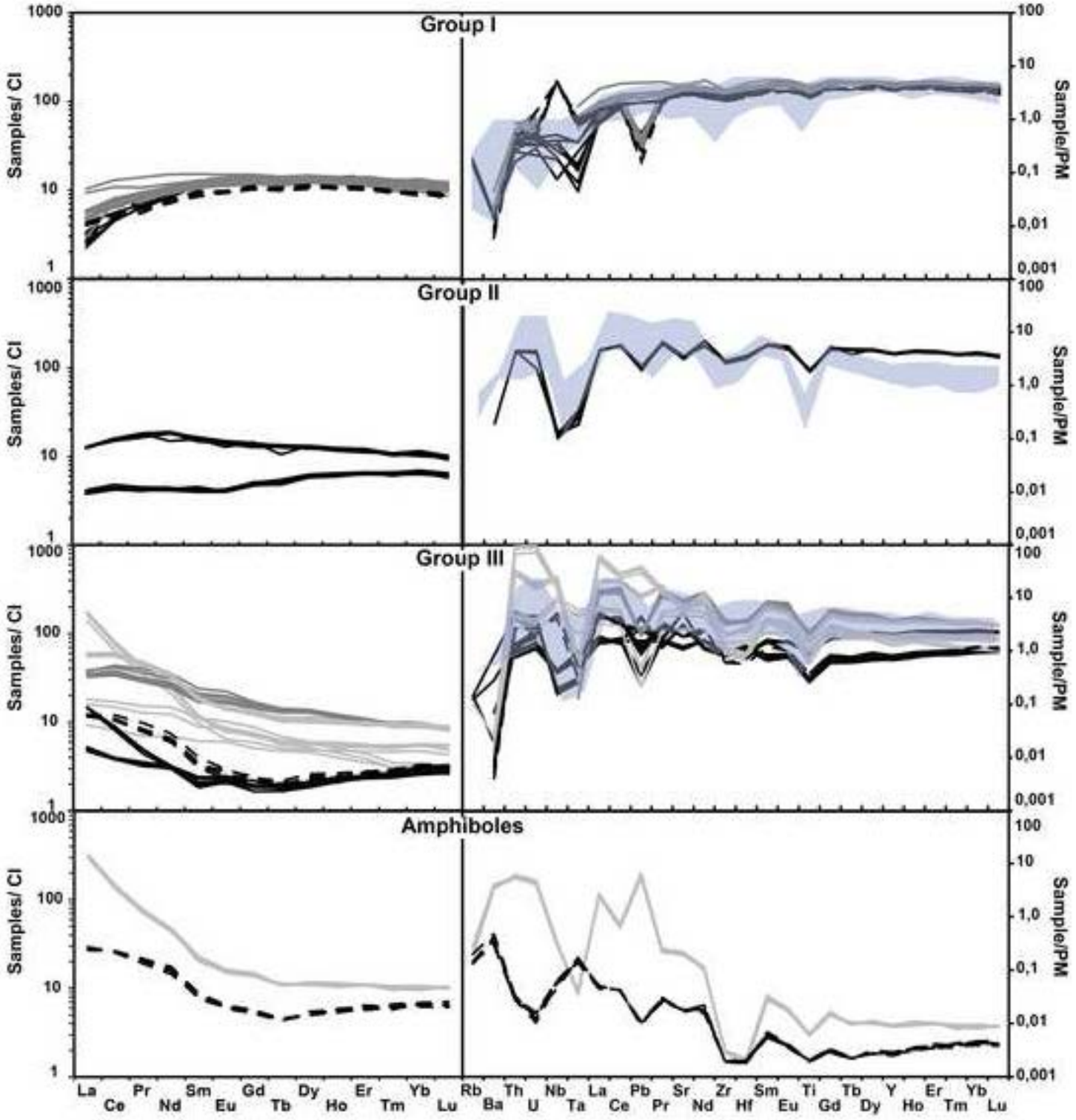

Figure 7

Click here to download high resolution image

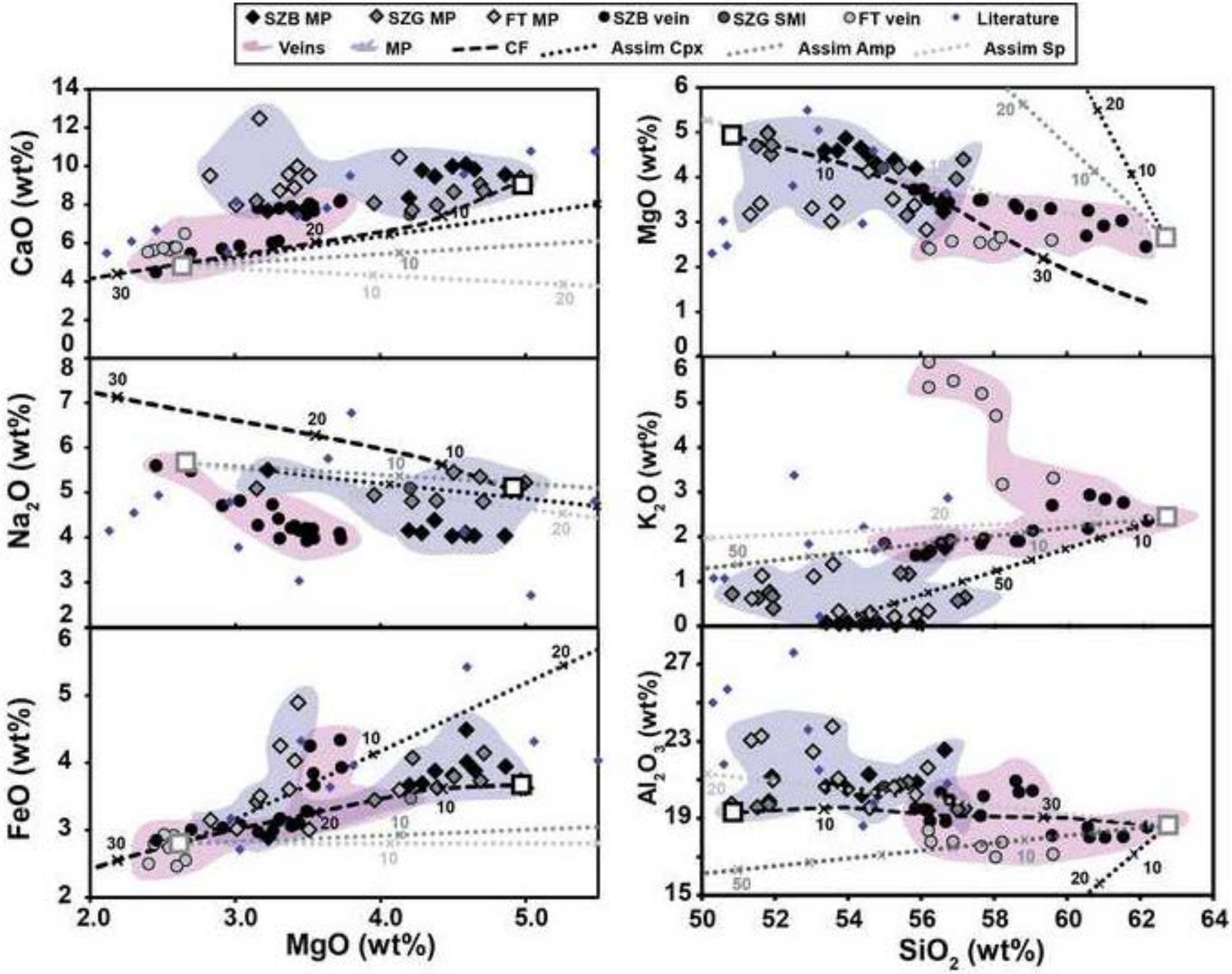

Figure 8

Click here to download high resolution image

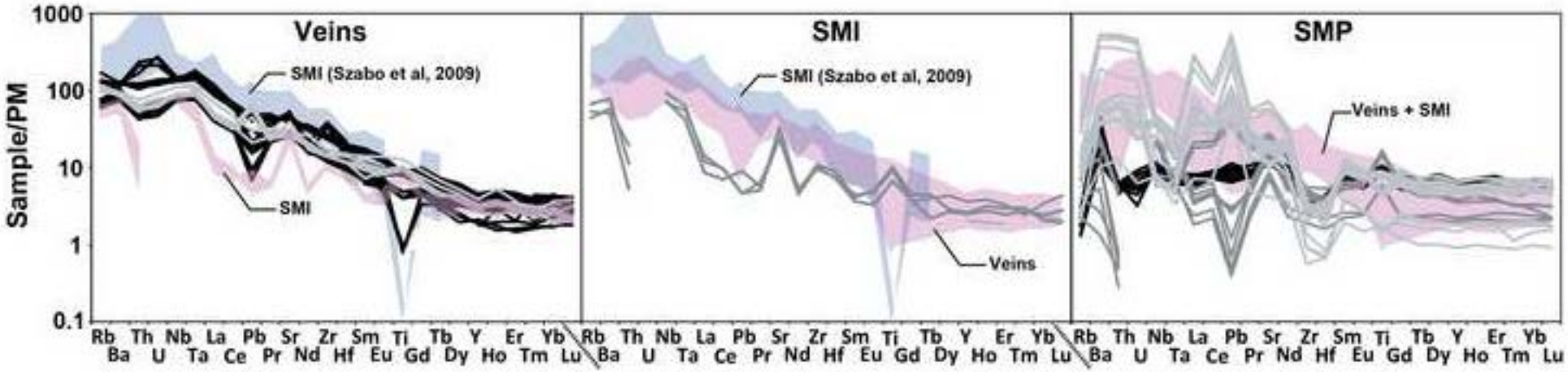

Figure 9

Click here to download high resolution image

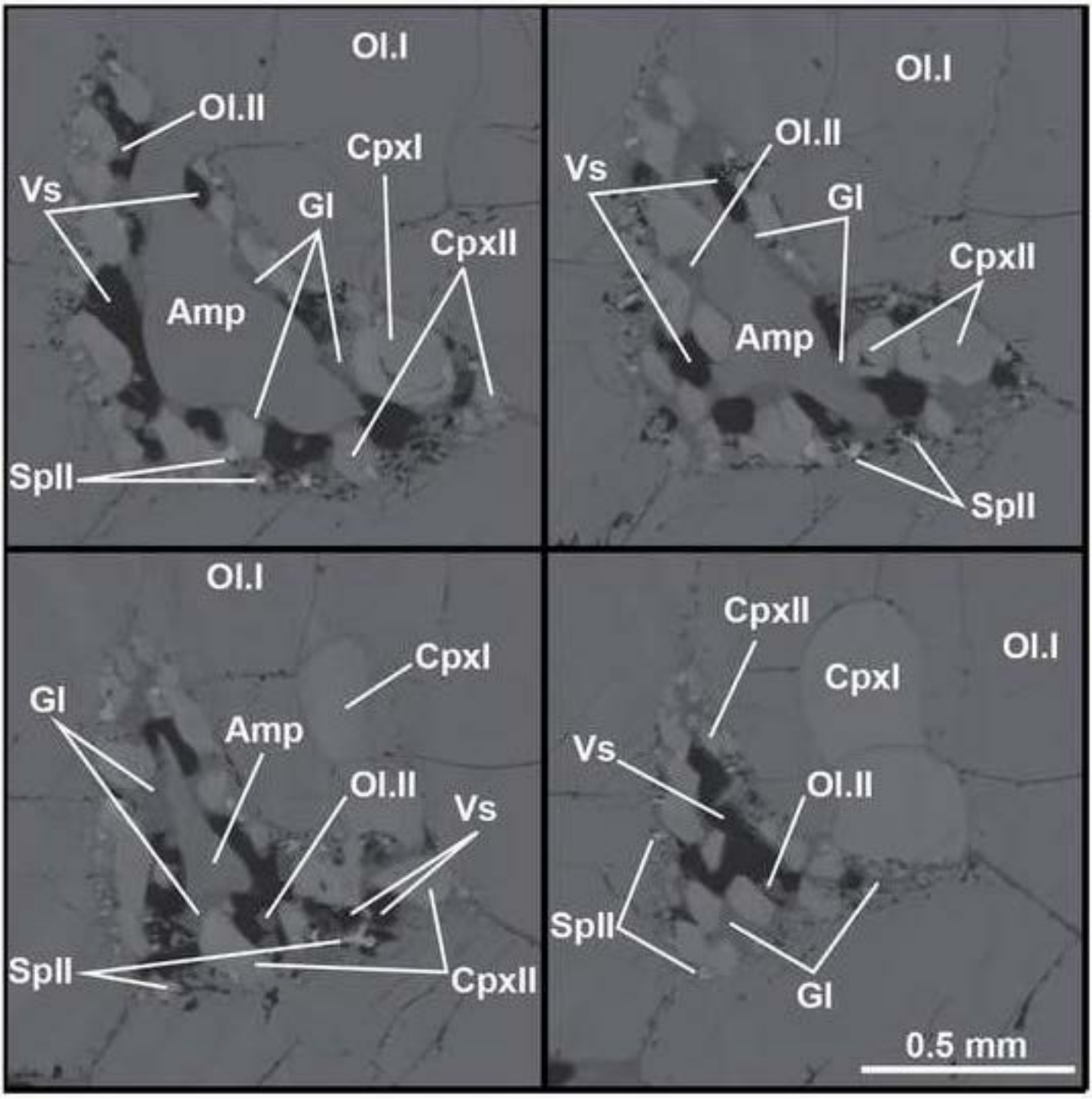

Figure 10

Click here to download high resolution image

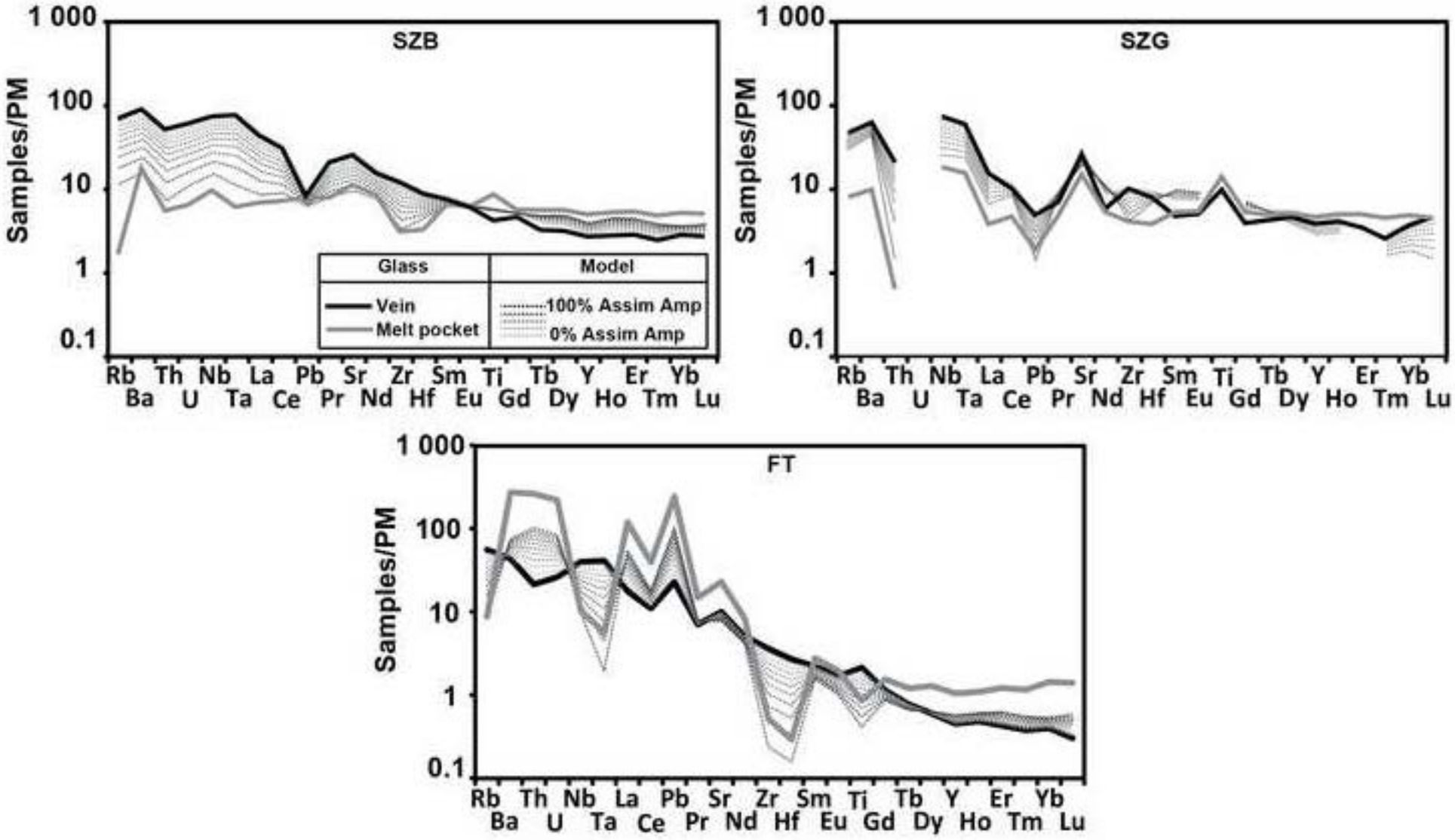

Figure 11

Click here to download high resolution image

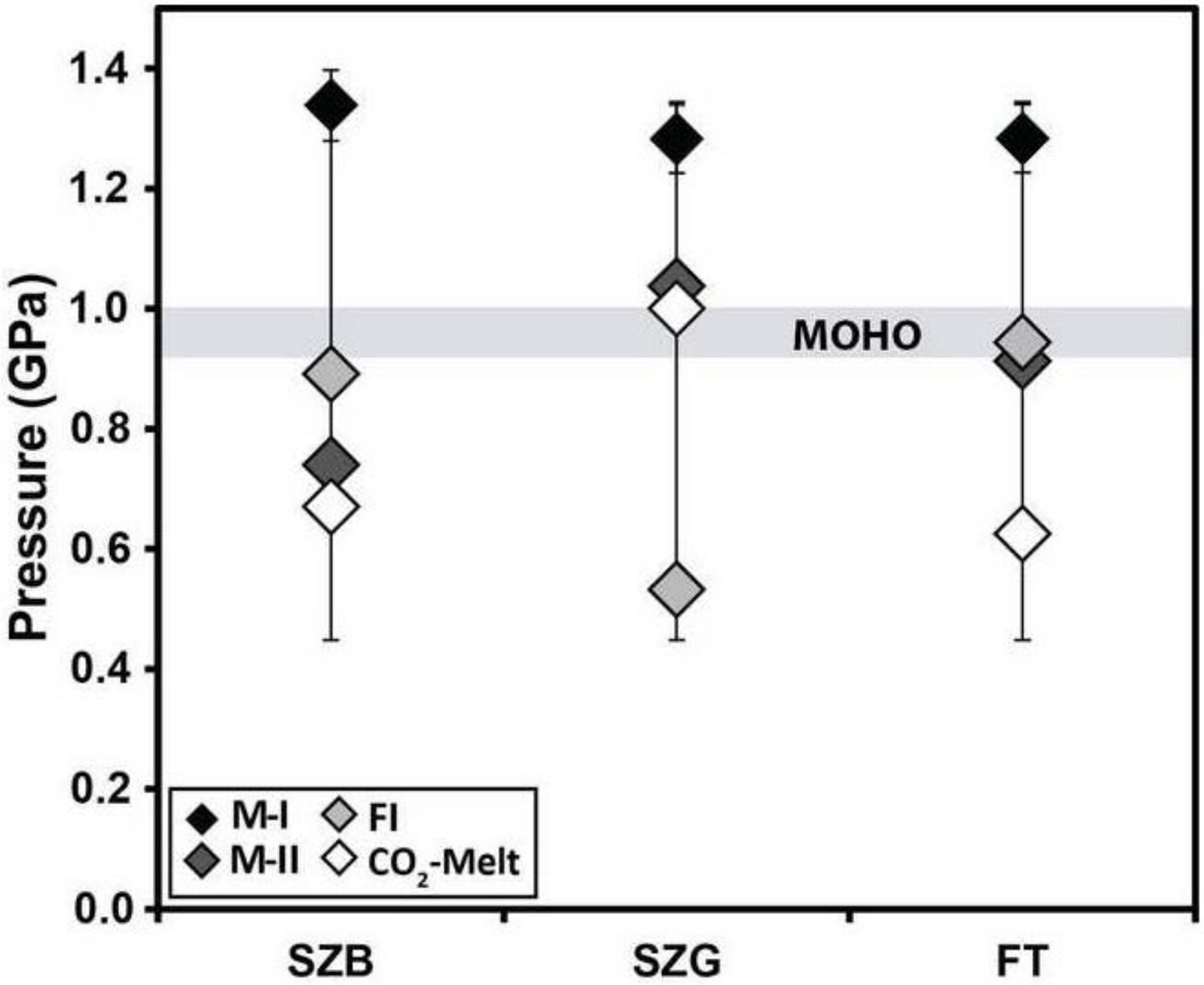

Figure 12

Click here to download high resolution image

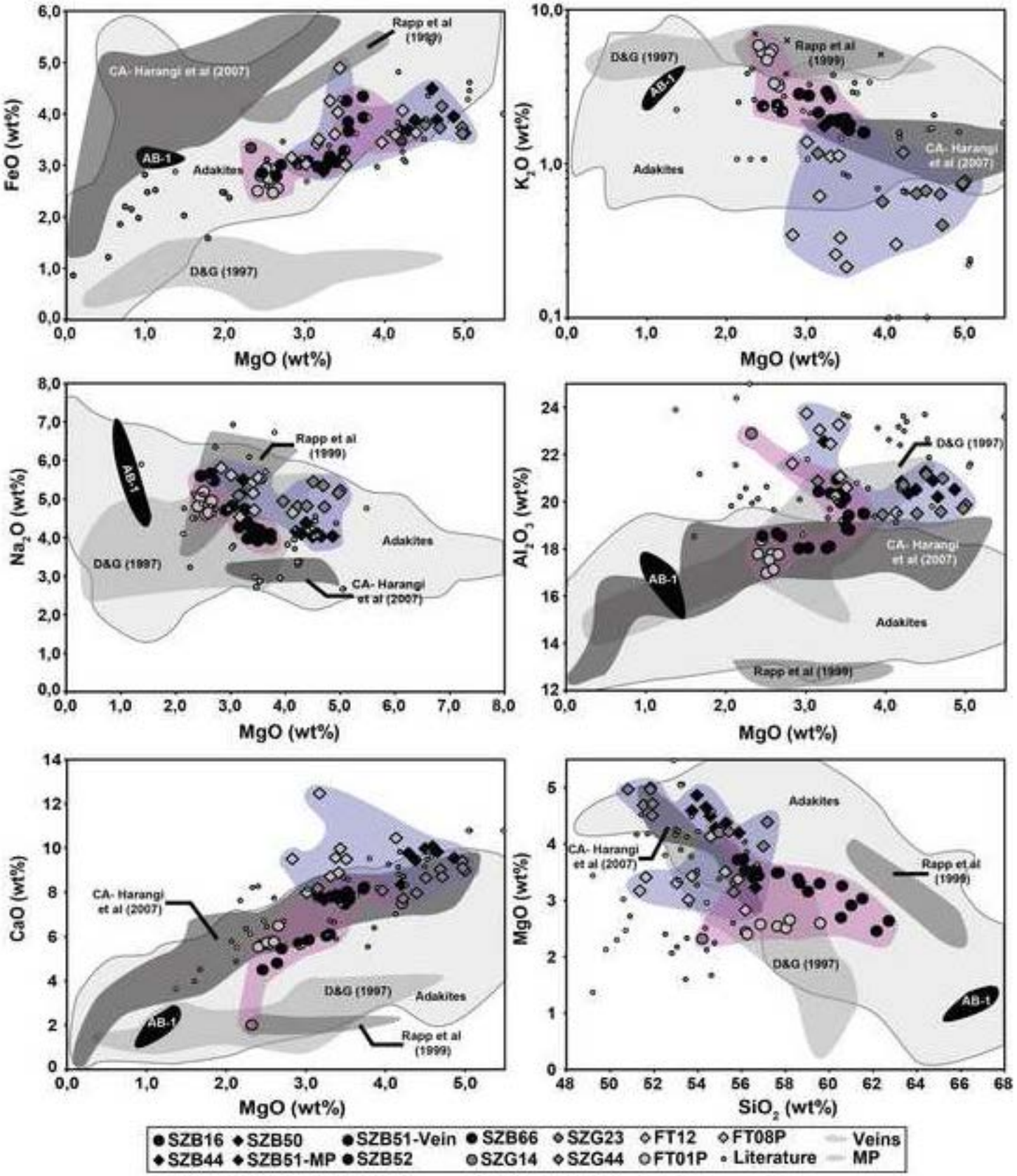

Figure 13

Click here to download high resolution image

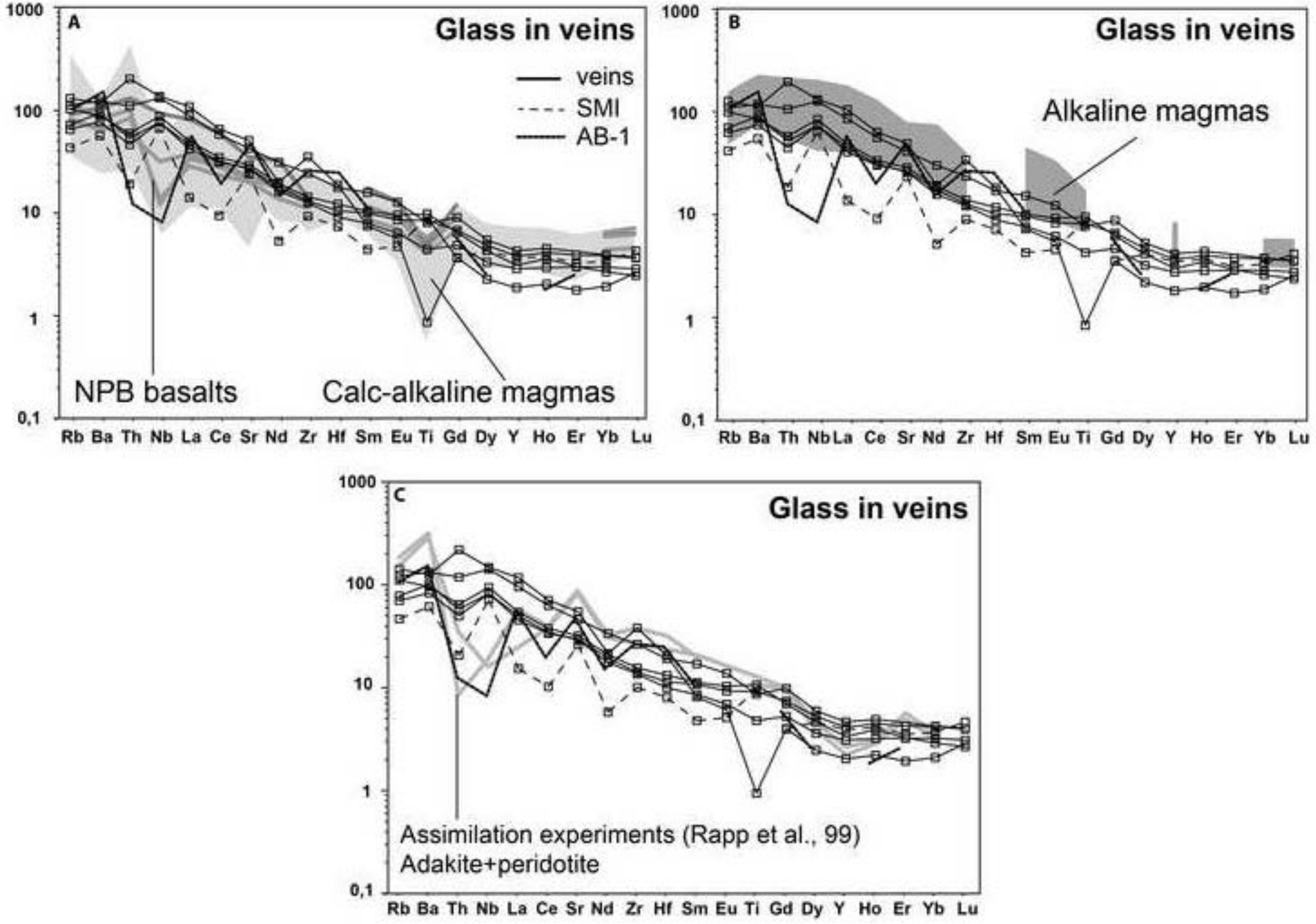

Figure 14

Click here to download high resolution image

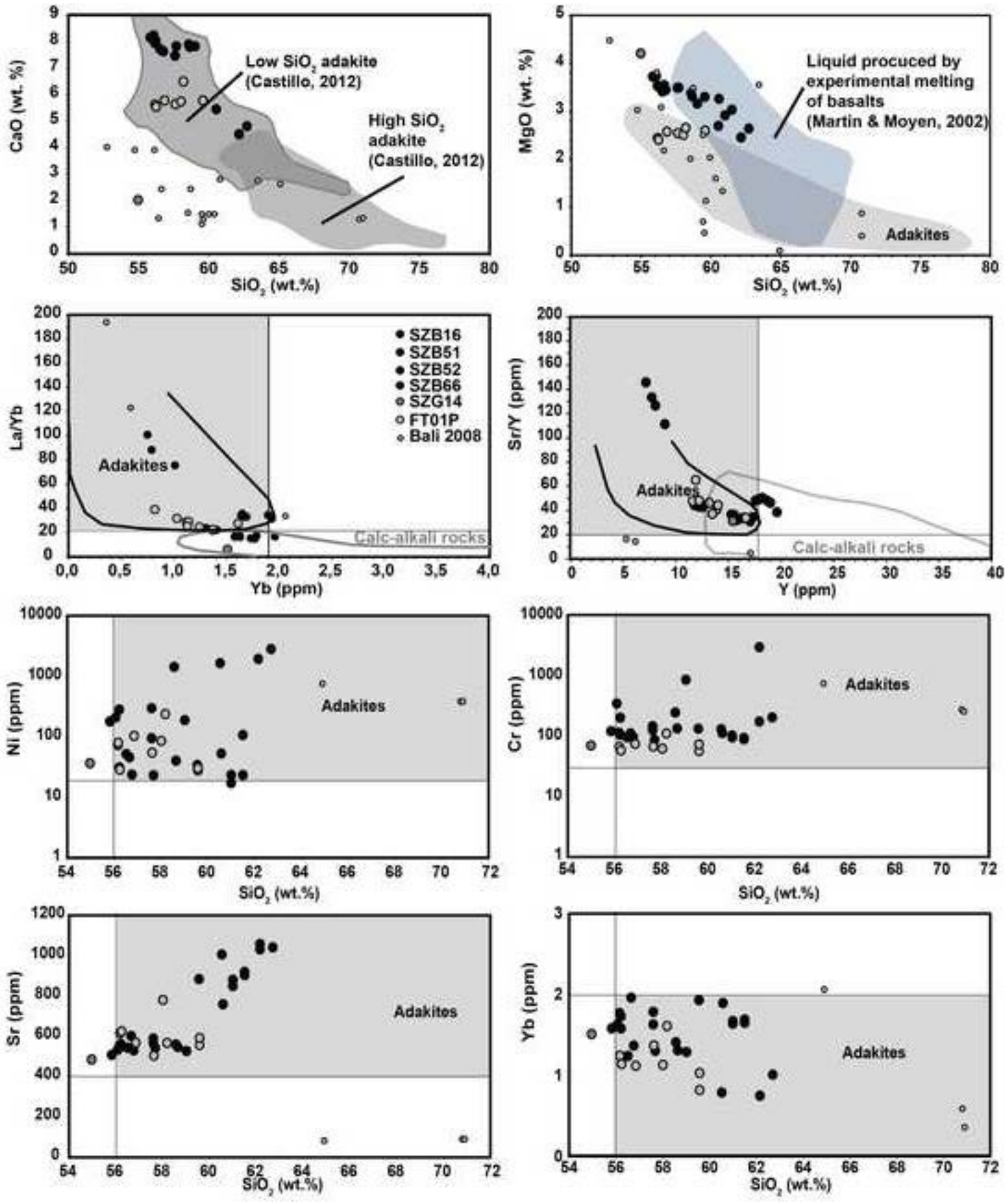

Figure 15

Click here to download high resolution image

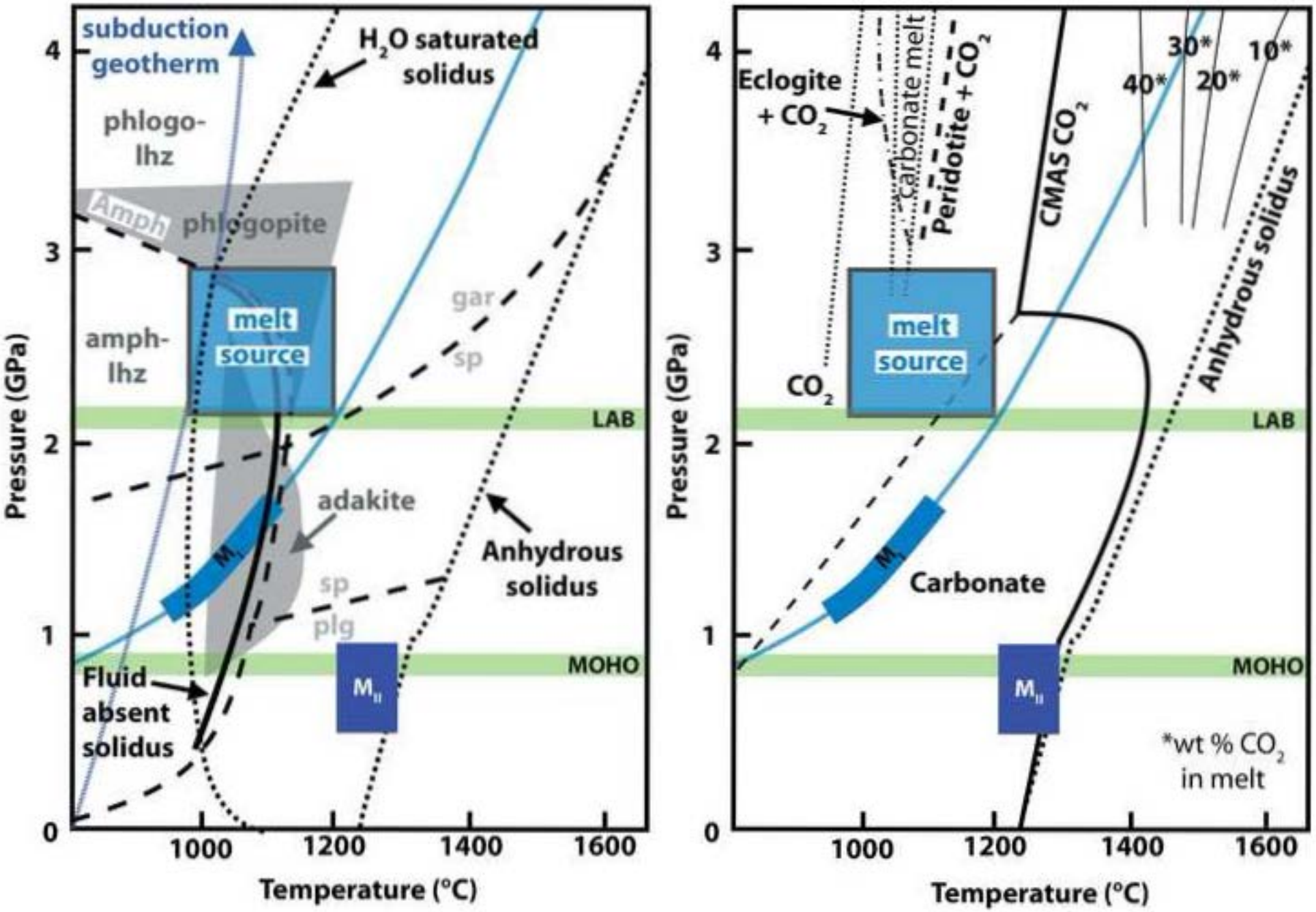

Supplementary material

Click here to download high resolution image

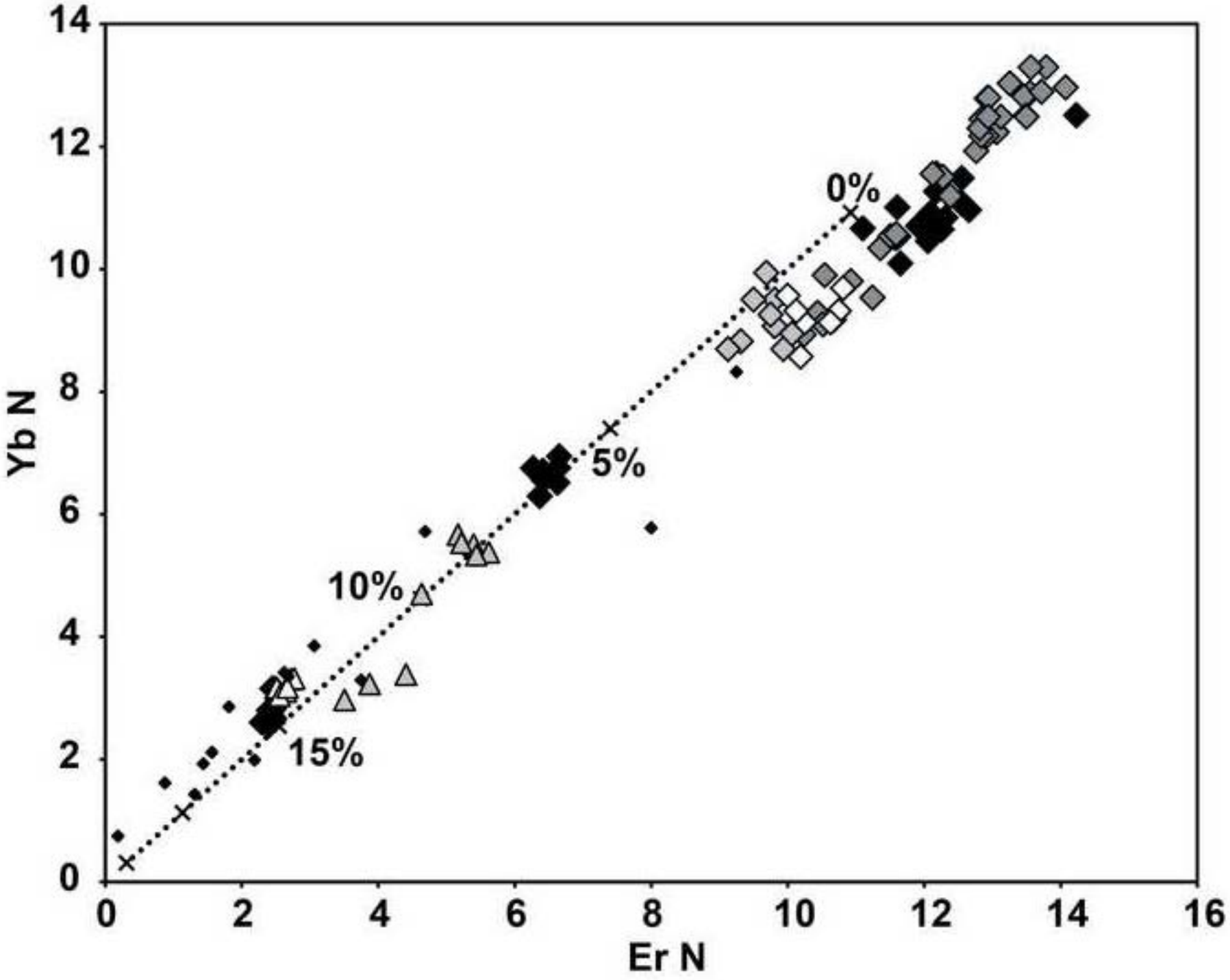

Table1

Click here to download Table: Table 1.doc

Sample	Whole size	Grain size		Texture	Minerals	Rock name	Fluid inclusions	Melt	2nd Minerals	Major petrographic characters
SZB16	9 cm	<1 to >3 mm	H	Protogranular	Ol, Opx, Cpx, Sp	Lz	2^{ndary}	Vein	Ol, Cpx, Sp	Minerals in contact with melt are broken-down. Phyllosilicates observed in vein. Some Gl (S) observed
SZB44	7 cm	<1 mm	E	Mosaic + Poikilitic features	Ol, Opx, Cpx, Sp	Lz	2^{ndary}	MP	Ol, Cpx, Sp	Spongy Sp at melt contact. Some Gl (S) observed
SZB50	7 cm	~1 mm	E	Mosaic	Ol, Opx, Cpx, Sp	Lz	2^{ndary}	Vein + MP	Ol, Cpx, Sp	Spongy Sp. Gl (S) sometimes associated with FI
SZB51	11 cm	1 to 5 mm	H	Protogranular	Ol, Opx, Cpx, Sp	Lz	2^{ndary}	MP	Ol, Cpx, Sp	Spongy Sp. Large Gl (S) in melt. Melt pocket formed from Cpx breakdown
SZB52	9 cm	<1 to 5 mm	H	Protogranular	Ol, Opx, Cpx, Sp	Lz	2^{ndary}	Vein	Ol, Cpx, Sp	Large vein. No mineral breakdown. Gl (S) sometimes associated with FI
SZB66	18 cm	4 to 6 mm	E	Protogranular + Poikilitic features	Ol, Opx, Cpx, Sp	Lz	2^{ndary}	Vein	Ol, Cpx, Sp	Poikilitic Ol (containing Opx). Little reaction between melt and minerals
SZG14	7 cm	~1 mm	E	Protogranular	Ol, Opx, Cpx, Sp	Lz	2^{ndary}	Vein + SMI	Ol, Cpx, Sp	Poikilitic Opx (containing Ol). Spongy Opx
SZG23	7 cm	<1 to 4 mm	H	Protogranular	Ol, Opx, Cpx, Sp	Lz	2^{ndary}	MP + Vein	Ol, Cpx, Sp	Lot of melt and fluid percolation. Lot of oxides in melt pockets
SZG30	5 cm	~1 mm	E	Mosaic	Ol, Opx, Cpx, Sp + Amph	Lz	2^{ndary}	Vein	Ol, Cpx, Sp	Lot of carbonate melts + fluid. Amph are broken-down. Gl (S), carbonate melts veins and FI
SZG44	7 cm	~1-2 mm	E	Protogranular with Mosaic tendency	Ol, Opx, Cpx, Sp	Lz	2^{ndary}	Vein + Pockets	Ol, Cpx, Sp	Ol and Cpx are destabilized at melt contact. Gl (S) observed at melt/minerals boundaries
FT12	9 cm	~1 mm	E	Mosaic	Ol, Opx, Cpx, Sp + Amph	Lz	2^{ndary}	MP + Vein	Ol, Cpx, Sp	Broken-down Amph at melt contact. Some Gl (S) at grain boundaries
FT01P	12 cm	<1 to 5 mm	H	Protogranular	Ol, Opx, Cpx, Sp	Hzb	2^{ndary}	Vein	Ol, Cpx, Sp	Gl (S) sometimes associated with FI. Cryptic metasomatism. Newly formed minerals at grain boundaries
FT08P	8 cm	1 to 2 mm	E	Tabular	Ol, Opx, Cpx, Sp + Amph	Hzb	2^{ndary}	Vein + Mp	Ol, Cpx, Sp	Gl (S) observed. Broken-down Amph with CpxII crystallization. Beginning of Opx break-down
MSZK1306 A	2.5 cm	<1 to 3 mm	H	Protogranular	Ol, Opx, Cpx, Sp + Amph	Hzb	2^{ndary}	Vein	Ol, Cpx, Sp	Broken-down Cpx at melt contact. Sp are enclosed in minerals (Poikilitic features). Little destabilization of Amph
MSZK1308	7 cm	<1 to 5 mm	H	Protogranular + Poikilitic features	Ol, Opx, Cpx, Sp	Lz	2^{ndary}	Vein	Ol, Cpx, Sp	Gl (S) in melt and sometimes associated with FI

Table 1: Petrographic description of BBHVF mantle xenoliths. H- heterogranular, E- equigranular, Lz- Lherzolite, Hzb- Harzburgite, 2ndary- trails of secondary fluid inclusions, Gl (s)- sulfide globule.

Table2

Click here to download Table: Table 2.doc

Olivine																														
Sample	**SZB16**		**SZB44**		**SZB50**		**SZB51**		**SZB52**		**SZB66**		**SZG14**		**SZG23**		**SZG30**		**SZG44**		**FT12**		**FT01P**		**FT08P**		**MSZK1306A**		**MSZK1308**	
n=	**8**	**1σ**	**3**	**1σ**	**2**	**1σ**	**4**	**1σ**	**4**	**1σ**	**3**	**1σ**	**6**	**1σ**	**3**	**1σ**	**4**	**1σ**	**4**	**1σ**	**4**	**1σ**	**2**	**1σ**	**6**	**1σ**	**2**	**1σ**	**4**	**1σ**
SiO_2	40,97	0,21	40,9	0,24	40,43	0,27	41,56	0,15	40,84	0,3	41,04	0,09	41,05	0,22	40,8	0,47	41,47	0,34	41,26	0,3	40,96	0,23	42,09	0,12	41,56	0,17	41,31	0,41	41,39	41,39
TiO_2	0,02	0,02	0,01	0,01	0	0	0,01	0,01	0,02	0,03	0	0	0,01	0,01	0	0,01	0,02	0,02	0,02	0,02	0	0	0,01	0,01	0	0	0	0	0,01	0,01
Al_2O_3	0,05	0,03	0,03	0,02	0,1	0,08	0,03	0,02	0,04	0,01	0,03	0,01	0,06	0,03	0,06	0,04	0,03	0,02	0,03	0,02	0,02	0,02	0,05	0,01	0,02	0,03	0,01	0	0,04	0,04
Cr_2O_3	0,02	0,02	0,03	0,05	0,01	0,01	0,07	0,08	0,07	0,04	0,06	0,04	0,03	0,04	0,05	0,02	0,02	0,04	0,04	0,05	0,02	0,01	0,04	0,01	0,03	0,04	0,02	0,01	0,03	0,03
FeO	10,19	0,1	10,78	0,1	10,68	0,05	9,5	0,13	9,24	0,13	9,74	0,29	10,31	0,12	9,93	0,13	10,04	0,09	10,37	0,1	10,45	0,17	9,28	0,1	9,56	0,09	9,22	0,08	9,43	9,43
MnO	0,13	0,03	0,13	0,04	0,12	0,03	0,12	0,01	0,14	0,01	0,12	0,02	0,15	0,03	0,15	0,04	0,13	0,01	0,15	0,02	0,15	0,02	0,15	0,03	0,14	0,02	0,13	0,02	0,13	0,13
NiO	0,36	0,03	0,35	0,02	0,36	0,02	0,35	0,02	0,36	0,02	0,4	0,02	0	0	0	0	0	0	0	0	0	0	0	0	0	0	0	0	0	0
MgO	48,77	0,13	48,16	0,25	48,06	0,03	49,08	0,12	48,99	0,24	48,59	0,22	48,35	0,12	48,17	0,08	48,37	0,21	48,17	0,15	48,22	0,47	48,78	0,01	49,54	0,29	49,98	0,15	49,31	49,31
CaO	0,09	0,01	0,07	0,01	0,05	0	0,07	0,01	0,12	0,03	0,08	0,01	0,12	0,01	0,11	0,08	0,06	0,01	0,08	0,01	0,05	0,01	0,1	0,02	0,06	0,03	0,04	0,01	0,09	0,09
Na_2O	0,02	0,01	0,01	0,01	0	0	0,01	0,01	0,01	0,01	0,01	0,01	0,02	0,02	0,01	0	0,01	0	0,02	0,01	0	0	0,01	0,01	0,01	0,01	0	0	0,01	0,01
K_2O	0	0	0	0	0	0	0,01	0,01	0	0,01	0	0,01	0	0	0	0	0	0,01	0,01	0,01	0	0	0	0	0	0	0	0	0,01	0,01
V_2O_3	0	0	0	0	0	0	0	0	0	0	0	0	0,35	0,04	0,34	0,03	0,35	0,03	0,34	0,04	0,36	0,03	0,37	0,01	0,38	0,02	0,38	0,02	0,37	0,37
Total	100,62	0,3	100,47	0,21	99,81	0,07	100,81	0,17	99,83	0,44	100,08	0,38	100,45	0,21	99,62	0,37	100,51	0,28	100,48	0,31	100,25	0,27	100,87	0,23	101,3	0,31	101,1	0,64	100,82	100,82
mg#	89,51	0,09	88,85	0,12	88,92	0,04	90,21	0,11	90,43	0,1	89,89	0,26	89,32	0,11	89,64	0,14	89,19	0,26	89,23	0,07	89,16	0,22	90,36	0,09	90,23	0,09	90,63	0,05	90,31	90,31

Opx																														
Sample	**SZB16**		**SZB44**		**SZB50**		**SZB51**		**SZB52**		**SZB66**		**SZG14**		**SZG23**		**SZG30**		**SZG44**		**FT12**		**FT01P**		**FT08P**		**MSZK1306A**		**MSZK1308**	
n=	**7**	**1σ**	**3**	**1σ**	**5**	**1σ**	**4**	**1σ**	**2**	**1σ**	**3**	**1σ**	**7**	**1σ**	**3**	**1σ**	**4**	**1σ**	**3**	**1σ**	**3**	**1σ**	**4**	**1σ**	**5**	**1σ**	**3**	**1σ**	**5**	**1σ**
SiO_2	54,21	0,48	55,41	0,76	55,23	0.19	56,62	33,45	55,45	1,15	56,19	0,2	54,91	0,29	55,25	0,54	55,34	0,45	54,92	0,23	55,17	0,21	56,55	0,23	56,45	0,27	56,82	0,43	55,44	0,23
TiO_2	0,15	0,02	0,09	0,02	0,1	0.03	0,04	33,45	0,06	0,02	0,04	0,02	0,16	0,03	0,09	0,05	0,14	0,04	0,16	0,01	0,08	0,03	0,09	0,03	0,04	0,03	0,03	0,04	0,12	0,03
Al_2O_3	5,7	0,09	4,59	0,14	4,5	0.06	2,8	33,45	5,04	0,19	3,12	0,06	5,18	0,16	3,98	0,22	4,84	0,09	5,12	0,07	4,26	0,07	3,33	0,05	3,48	0,07	2,61	0,07	5,08	0,07
Cr_2O_3	0,44	0,05	0,29	0,02	0,24	0.03	0,61	33,45	0,57	0,01	0,61	0,05	0,34	0,04	0,59	0,03	0,4	0,03	0,37	0,03	0,29	0,04	0,8	0,04	0,34	0,04	0,35	0,05	0,5	0,03
FeO	6,52	0,12	6,76	0,16	6,91	0.13	5,98	3,05	5,81	0,12	6,3	0,05	6,47	0,13	6,49	0,19	6,34	0,14	6,57	0,05	6,79	0,1	5,81	0,12	6,34	0,07	6,08	0,12	5,91	0,1
MnO	0,1	0,03	0,14	0,03	0,13	0.05	0,11	33,45	0,13	0,03	0,14	0,04	0,12	0,03	0,13	0,03	0,13	0,03	0,13	0,03	0,14	0,02	0,09	0,01	0,14	0,03	0,13	0,02	0,11	0,03
NiO	0,09	0,04	0,08	0,01	0,09	0.02	0,08	0,46	0,1	0,02	0,1	0,02	0,01	0	0,01	0	0,02	0,01	0,01	0	0,01	0,01	0,02	0	0,01	0	0,01	0	0,01	0
MgO	31,62	0,41	32,2	0,5	32,35	0.12	33,24	33,45	31,98	0,14	32,77	0,09	31,94	0,22	32,08	0,44	32,29	0,19	31,93	0,16	32,48	0,08	32,38	0,22	33,74	0,16	34,28	0,17	32,51	0,13
CaO	1,03	0,02	0,75	0,08	0,68	0.02	0,81	33,45	1,12	0,01	0,89	0,03	0,88	0,1	0,84	0,03	0,78	0,02	0,83	0,03	0,69	0,03	1,17	0,05	0,6	0,02	0,6	0,01	0,93	0,02
Na_2O	0,18	0,01	0,06	0,01	0,07	0.00	0,06	33,45	0,09	0,01	0,02	0,01	0,15	0,02	0,16	0,01	0,11	0,01	0,15	0,01	0,05	0,01	0,13	0,01	0,02	0,01	0,02	0,03	0,12	0,01
K_2O	0,01	0,01	0,01	0,01	0,01	0.01	0	33,45	0,01	0,01	0	0,01	0,01	0,01	0	0	0	0	0,01	0,01	0	0	0	0	0,01	0,01	0	0,01	0	0
V_2O_3	0,02	0	0,01	0,01	0,02	0.00	0,01	33,45	0,01	0	0,02	0	0,09	0,02	0,08	0,01	0,09	0,01	0,09	0,01	0,09	0	0,1	0,02	0,09	0,02	0,09	0,02	0,1	0,02
Total	100,06	0,84	100,4	0,42	100,33	0.29	100,36	4,96	100,38	1,47	100,19	0,35	100,28	0,35	99,7	0,32	100,48	0,67	100,29	0,21	100,07	0,27	100,47	0,31	101,27	0,25	101,03	0,5	100,84	0,29
mg#	89,62	0,17	89,47	0,19	89,3	0.16	90,83	38,44	90,75	0,15	90,27	0,08	89,8	0,17	89,81	0,37	90,08	0,2	89,65	0,1	89,5	0,12	90,85	0,17	90,46	0,1	90,96	0,17	90,74	0,12

Cpx																														
Sample	**SZB16**		**SZB44**		**SZB50**		**SZB51**		**SZB52**		**SZB66**		**SZG14**		**SZG23**		**SZG30**		**SZG44**		**FT12**		**FT01P**		**FT08P**		**MSZK1306A**		**MSZK1308**	
n=	**9**	**1σ**	**3**	**1σ**	**5**	**1σ**	**4**	**1σ**	**3**	**1σ**	**3**	**1σ**	**7**	**1σ**	**4**	**1σ**	**3**	**1σ**	**3**	**1σ**	**3**	**1σ**	**2**	**1σ**	**4**	**1σ**	**4**	**1σ**	**6**	**1σ**
SiO_2	51,55	0,21	52,10	0,22	52,39	0,33	53,73	0,30	51,99	0,27	53,01	0,46	51,65	0,68	51,88	0,70	52,25	0,34	51,93	0,20	52,32	0,29	53,97	0,36	53,34	0,32	53,83	0,18	52,25	0,23
TiO_2	0,59	0,06	0,37	0,03	0,34	0,01	0,06	0,03	0,17	0,01	0,06	0,02	0,66	0,14	0,40	0,14	0,49	0,05	0,62	0,05	0,32	0,03	0,22	0,01	0,14	0,03	0,05	0,03	0,46	0,03
Al_2O_3	7,38	0,54	5,65	0,07	5,69	0,06	3,36	0,09	5,84	0,05	3,32	0,06	7,54	0,27	6,13	0,24	6,84	0,12	7,40	0,07	5,38	0,05	4,12	0,01	3,36	0,14	2,29	0,05	6,70	0,06
Cr_2O_3	0,81	0,04	0,47	0,02	0,44	0,04	1,07	0,08	1,03	0,04	0,86	0,07	0,70	0,03	1,23	0,07	0,77	0,03	0,71	0,03	0,51	0,06	1,41	0,09	0,40	0,06	0,35	0,05	0,93	0,05
FeO	3,44	0,11	3,08	0,08	3,04	0,05	2,81	0,03	2,96	0,08	3,03	0,09	3,17	0,29	3,31	0,14	2,93	0,05	3,25	0,09	2,87	0,07	3,03	0,05	2,56	0,04	2,57	0,02	2,99	0,06
MnO	0,08	0,02	0,07	0,02	0,07	0,02	0,04	0,02	0,04	0,02	0,04	0,03	0,08	0,03	0,03	0,01	0,05	0,02	0,07	0,01	0,06	0,01	0,04	0,03	0,06	0,02	0,06	0,02	0,07	0,01
NiO	0,05	0,03	0,06	0,02	0,04	0,01	0,04	0,01	0,06	0,01	0,06	0,02	0,04	0,00	0,04	0,01	0,04	0,00	0,04	0,00	0,03	0,00	0,03	0,00	0,03	0,00	0,02	0,00	0,03	0,01
MgO	15,46	0,37	15,71	0,05	15,65	0,15	16,90	0,09	16,41	0,13	16,91	0,32	15,20	0,29	14,96	0,11	15,35	0,10	14,86	0,09	15,70	0,07	16,80	0,16	16,74	0,31	17,51	0,11	15,69	0,06
CaO	18,53	0,93	20,80	0,16	20,71	0,06	20,90	0,19	19,50	0,41	21,17	0,53	18,76	0,44	19,16	0,20	19,59	0,29	18,84	0,17	21,28	0,15	19,19	0,16	22,63	1,77	23,52	0,08	19,58	0,33
Na_2O	1,61	0,37	1,09	0,02	1,07	0,01	0,85	0,01	0,98	0,01	0,44	0,01	1,77	0,14	1,78	0,06	1,62	0,03	1,85	0,05	1,00	0,02	1,14	0,04	0,40	0,04	0,30	0,04	1,52	0,03
K_2O	0,02	0,03	0,01	0,01	0,00	0,00	0,00	0,00	0,01	0,00	0,00	0,00	0,00	0,00	0,01	0,00	0,00	0,00	0,00	0,00	0,00	0,00	0,00	0,00	0,00	0,00	0,01	0,01	0,01	0,01
V_2O_3	0,04	0,01	0,03	0,00	0,03	0,00	0,04	0,00	0,04	0,00	0,04	0,01	0,04	0,01	0,04	0,02	0,04	0,01	0,03	0,01	0,03	0,02	0,04	0,02	0,04	0,02	0,04	0,02	0,03	0,03
Total	99,55	0,30	99,44	0,32	99,48	0,47	99,80	0,13	99,03	0,26	98,93	1,16	99,61	0,67	98,97	0,50	99,97	0,33	99,60	0,31	99,49	0,41	99,98	0,05	99,72	2,03	100,56	0,21	100,27	0,17
mg#	88,91	0,45	90,09	0,24	90,18	0,13	91,48	0,10	90,81	0,28	90,87	0,20	89,55	0,69	88,97	0,42	90,32	0,16	89,08	0,25	90,69	0,22	90,82	0,21	92,11	0,17	92,40	0,07	90,36	0,18

Sp																														
Sample	**SZB16**		**SZB44**		**SZB50**		**SZB51**		**SZB52**		**SZB66**		**SZG14**		**SZG23**		**SZG30**		**SZG44**		**FT12**		**FT01P**		**FT08P**		**MSZK1306A**		**MSZK1308**	
n=	**8**	**1σ**	**4**	**1σ**	**4**	**1σ**	**5**	**1σ**	**4**	**1σ**	**4**	**1σ**	**11**	**1σ**	**5**	**1σ**	**1**	**1σ**	**6**	**1σ**	**5**	**1σ**	**2**	**1σ**	**7**	**1σ**	**1**	**1σ**	**4**	**1σ**
SiO_2	0,11	0,02	0,06	0,01	0,07	0,01	0,63	1,30	0,07	0,02	0,12	0,11	0,10	0,03	0,06	0,03	0,06	-	0,07	0,02	0,05	0,02	0,08	0,02	0,03	0,03	0,01	-	0,06	0,02
TiO_2	0,22	0,03	0,10	0,00	0,08	0,03	0,10	0,01	0,10	0,03	0,09	0,03	0,26	0,02	0,20	0,03	0,12	-	0,17	0,02	0,09	0,01	0,35	0,03	0,06	0,01	0,07	-	0,18	0,01
Al_2O_3	57,18	0,50	58,74	0,44	59,15	0,56	31,24	0,29	50,58	0,35	31,87	0,20	58,34	0,34	43,81	1,44	57,00	-	58,17	0,23	57,63	0,54	30,80	0,03	51,08	0,48	36,38	-	54,09	0,34
Cr_2O_3	9,77	0,14	8,30	0,25	7,77	0,34	35,40	0,46	16,72	0,20	31,20	0,73	8,62	0,14	21,63	1,34	10,62	-	8,72	0,21	9,44	0,24	35,92	0,14	15,83	0,39	28,07	-	13,50	0,24
FeO	11,46	0,22	11,58	0,10	11,42	0,18	15,72	0,36	10,79	0,12	18,41	0,76	10,68	0,15	14,71	0,42	10,78	-	11,52	0,13	11,40	0,18	15,42	0,20	12,48	0,64	17,86	-	10,83	0,27
MnO	0,00	0,00	0,00	0,00	0,00	0,00	0,00	0,00	0,00	0,00	0,00	0,00	0,00	0,00	0,00	0,00	0,00	-	0,00	0,00	0,00	0,00	0,00	0,00	0,00	0,00	0,00	-	0,00	0,00
NiO	0,39	0,02	0,38	0,02	0,39	0,02	0,20	0,03	0,33	0,03	0,26	0,03	0,06	0,00	0,08	0,00	0,07	-	0,06	0,00	0,06	0,00	0,14	0,00	0,08	0,00	0,17	-	0,07	0,00
MgO	20,59	0,14	20,16	0,11	20,16	0,06	15,50	0,23	19,61	0,24	15,90	0,67	21,06	0,17	18,08	0,24	20,68	-	20,62	0,11	20,10	0,21	16,26	0,03	19,32	0,54	16,47	-	20,52	0,05
CaO	0,00	0,00	0,01	0,01	0,00	0,00	0,04	0,08	0,01	0,00	0,00	0,00	0,01	0,01	0,00	0,00	0,01	-	0,00	0,00	0,00	0,00	0,00	0,00	0,01	0,01	0,02	-	0,00	0,00
Na_2O	0,01	0,01	0,01	0,01	0,01	0,01	0,06	0,11	0,01	0,01	0,01	0,01	0,01	0,01	0,01	0,02	0,01	-	0,01	0,01	0,00	0,01	0,00	0,00	0,01	0,01	0,02	-	0,01	0,01
K_2O	0,00	0,01	0,00	0,01	0,02	0,02	0,02	0,04	0,01	0,01	0,01	0,01	0,00	0,00	0,00	0,00	0,00	-	0,00	0,00	0,00	0,00	0,00	0,00	0,00	0,00	0,00	-	0,01	0,01
V_2O_3	0,07	0,00	0,06	0,01	0,06	0,00	0,16	0,01	0,08	0,00	0,20	0,00	0,38	0,03	0,33	0,02	0,38	-	0,36	0,03	0,36	0,03	0,27	0,02	0,31	0,03	0,25	-	0,35	0,03
Total	99,80	0,37	99,40	0,12	99,13	0,17	99,06	0,54	98,28	0,20	98,07	0,87	99,52	0,53	98,92	0,36	99,73	-	99,69	0,39	99,13	0,29	99,24	0,31	99,19	0,62	99,33	-	99,63	0,25
mg#	76,21	0,36	75,62	0,12	75,88	0,26	63,73	0,44	76,41	0,37	60,62	1,92	77,85	0,17	68,66	0,85	77,37	-	76,14	0,16	75,86	0,30	65,27	0,33	73,40	1,47	62,18	-	77,16	0,45
cr#	10,28	0,19	8,66	0,29	8,10	0,39	43,18	0,22	18,15	0,22	39,63	0,47	9,02	0,12	24,89	1,78	11,11	-	9,14	0,22	9,90	0,31	43,89	0,07	17,21	0,40	34,11	-	14,34	0,29

Table 2: Major element composition of primary olivines, orthopyroxenes, clinopyroxènes and spinels (in wt. %).

Table3

Click here to download Table: Table 3.doc

Olivine II											Cpx II									Sp II										
Sample	SZB50		SZB51		SZG23		FT12		FT08P		Sample	SZB16		SZB44		SZB50		SZB51		Sample	SZB50		SZB51		SZG23		SZG44		FT12		FT08P	
n=	12	1σ	9	1σ	12	1σ	13	1σ	8	1σ	n=	2	1σ	3	1σ	4	1σ	4	1σ	n=	2	1σ	3	1σ	2	1σ	4	1σ	3	1σ	3	1σ
SiO_2	41,06	0,43	41,51	0,35	41,38	1,10	41,78	0,58	41,62	0,42	SiO_2	52.21	0.03	49.39	2.87	50.56	2.54	51.15	1.26	SiO_2	0.06	0.03	8.88	15.32	0.09	0.04	0.10	0.02	0.08	0.00	1.06	1.69
TiO_2	0,05	0,02	0,03	0,02	0,07	0,11	0,02	0,02	0,03	0,03	TiO_2	0.59	0.07	1.33	0.85	1.00	0.83	0.28	0.07	TiO_2	0.23	0.14	0.15	0.15	0.64	0.02	0.74	0.03	0.27	0.14	0.18	0.19
Al_2O_3	0,05	0,02	0,09	0,15	0,39	1,07	0,06	0,04	0,04	0,03	Al_2O_3	7.67	0.14	8.95	2.91	7.25	2.11	6.99	1.39	Al_2O_3	56.35	2.01	29.91	1.41	38.56	3.96	51.36	4.24	54.34	3.34	48.44	10.45
Cr_2O_3	0,08	0,05	0,10	0,04	0,11	0,05	0,07	0,04	0,11	0,05	Cr_2O_3	0.00	0.00	0.00	0.00	0.00	0.00	0.00	0.00	Cr_2O_3	10.85	2.04	28.48	14.72	25.60	4.58	15.21	4.83	12.31	2.81	18.00	7.36
FeO	8,99	0,51	7,82	0,25	8,27	0,59	8,23	0,30	7,31	0,24	FeO	3.61	0.01	3.05	0.38	3.10	0.10	2.44	0.13	FeO	11.28	1.04	12.57	3.94	14.54	0.66	10.90	0.58	10.63	0.76	11.25	2.47
MnO	0,12	0,03	0,10	0,03	0,12	0,03	0,13	0,03	0,10	0,03	MnO	0.04	0.06	0.10	0.06	0.06	0.02	n.d.	0.03	MnO	n.d.		n.d.		n.d.		n.d.		n.d.		n.d.	
NiO	0,35	0,04	0,34	0,05	0,31	0,05	0,31	0,04	0,42	0,05	NiO	0.00	0.00	0.00	0.00	0.00	0.00	0.00	0.00	NiO	0.42	0.01	0.18	0.07	0.26	0.01	0.36	0.07	0.39	0.02	0.36	0.08
MgO	49,09	0,66	49,37	1,40	48,02	2,86	49,58	0,98	50,11	0,29	MgO	15.32	0.02	14.89	0.91	15.20	1.03	15.33	0.86	MgO	20.81	0.89	14.46	3.89	18.55	1.39	20.35	0.56	21.08	1.03	19.51	2.69
CaO	0,16	0,03	0,36	0,56	0,31	0,47	0,16	0,03	0,24	0,02	CaO	18.35	0.12	20.72	0.48	20.77	0.95	21.59	0.49	CaO	0.02		1.35	2.26	0.05	0.03	0.06	0.03	0.03	0.02	0.46	0.61
Na_2O	0,01	0,01									Na_2O	1.70	0.03	0.94	0.18	0.92	0.12	0.82	0.22	Na_2O	0.00	0.00	1.41	2.00	0.01		0.01	0.01	0.01	0.01	0.04	0.05
K_2O											K_2O	0.00	0.00	0.00	0.01	n.d.	0.01	n.d.	0.02	K_2O	0.02		0.43	0.61	0.00	0.00	0.03		n.d.		0.01	0.01
V_2O_3											V_2O_3	0.00	0.00	0.00	0.00	0.00	0.00	0.00	0.00	V_2O_3	0.10	0.06	0.16	0.00	0.15	0.01	0.20	0.02	0.13	0.06	0.16	0.08
Total	99,91	0,54	99,76	0,82	99,08	2,34	100,34	1,17	99,98	0,55	Total	99.50	0.03	99.38	0.35	98.88	0.79	98.56	0.91	Total	99.82	0.15	97.66	4.24	98.15	0.61	99.15	0.82	99.01	0.51	99.26	0.98
mg#	90,68	0,57	91,84	0,31	91,18	0,66	91,48	0,30	92,44	0,25	mg#	85.60	0.06	87.25	1.34	87.26	0.48	89.76	0.82	mg#	76.67	2.41	67.45	1.51	69.42	2.54	76.89	1.42	77.92	2.06	75.35	6.48
																				cr#	11.45	2.27	36.94	13.53	30.86	6.01	16.64	5.59	13.25	3.29	20.59	10.45

Amp								
Sample	SZG30		FT12		FT08P		MSZK1306 A	
n=	7	σ	1	σ	9	σ	11	σ
SiO_2	42,08	0,79	42,86	-	43,30	0,49	44,40	0,50
TiO_2	2,56	0,07	1,52	-	0,68	0,04	0,32	0,03
Al_2O_3	15,13	0,14	15,13	-	14,70	0,12	13,24	0,14
Cr_2O_3	1,14	0,04	1,00	-	1,25	0,07	1,66	0,08
FeO	4,02	0,03	4,18	-	4,10	0,07	4,14	0,11
MnO	0,02	0,02	0,01	-	0,01	0,02	0.00	0,02
NiO	0,11	0,03	0,15	-	0,13	0,02	0,11	0,03
MgO	17,28	0,33	17,53	-	17,55	0,16	18,08	0,15
CaO	10,55	0,17	10,89	-	11,60	0,14	11,97	0,17
Na_2O	3,38	0,08	3,65	-	2,70	0,04	2,14	0,04
K_2O	0,96	0,04	0,20	-	0,66	0,04	1,10	0,04
V_2O_3	0,07	0,01	0,06	-	0,06	0,01	0,08	0,00
Total	97,45	0,63	97,09	-	96,88	0,75	97,25	0,83
mg#	88,45	0,18	88,20	-	88,41	0,16	88,61	0,23

Table 3: Secondary minerals from veins and melt pockets (ol, cpx, sp) and amphiboles major element compositions (in wt. %).

Table4

Click here to download Table: Table 4.doc

Cpx I																			
Sample	**SZB16**		**SZB44**		**SZB50**		**SZB51**		**SZB52**		**SZB66**		**SZG14**		**SZG23**		**SZG30**		**SZG44**	
n=	**8**	**σ**	**7**	**σ**	**5**	**σ**	**5**	**σ**	**7**	**σ**	**6**	**σ**	**9**	**σ**	**7**	**σ**	**7**	**σ**	**9**	**σ**
Al27	39514	1903	29057	266	29096	346	17205	290	3265	687	16571	437	41315	1290	33800	1324	36597	1011	40524	1344
Ca44	132416	6614	148566	1273	147672	506	149330	1381	19,7	0,4	149337	3395	18,8	0,44	19,1	0,22	19,6	0,3	18,8	0,16
Sc45	57,2	2,54	58,5	0,82	59,2	0,39	81,81	1,12	53	1,64	61,2	1,84	61,8	2,45	69,4	1,68	64,0	1,87	66	1,63
Ti49	3486	177	2236	35,5	2195,39	28,3	317	2,07	1103	17,9	366	10,1	4112	414	2742	549	3561	73,4	4224	136
V51	125	9,98	158	5,36	161	3,32	nd	nd	nd	nd	53,7	24,5	160	4,68	nd	nd	142	4	165	10,5
Cr52	4862	330	3153	38,8	2911	71,7	nd	nd	nd	nd	3381	1143	4982	182	nd	nd	5375	185	5088	140
Cr53	5136	292	3287	65,8	2991	80,9	6841	358	7259	195	5414	164	5103	183	8815	274	5545	183	5234	134
Mn55	771	41,9	698	4,94	695	11,7	643	13,6	714	22,2	645	17	718	32,3	743	14,9	691	14,7	726	28,1
Co59	25,6	1,44	23,5	0,15	22,9	0,55	23,2	0,67	26,3	0,79	24,5	0,67	23,05	1,17	22,9	0,4	22,3	0,61	22,4	0,7
Ni60	409	23,3	367	3,37	358	7,3	370	11,0	433	11,6	410	11,5	358	17,5	366	6,14	350	11,8	336	8,96
Rb85	nd	nd	nd	nd	nd	nd	nd	nd	nd	nd	nd	nd	nd	nd	nd	nd	nd	nd	nd	nd
Sr88	64,3	4,55	nd	nd	67,75	1,16	105,96	0,78	23,12	1,12	62,4	0,98	77,01	2,9	154,64	34,11	71,2	0,95	nd	nd
Y89	18,1	0,85	17,0	0,37	16,88	0,11	3,07	0,05	8,75	0,22	3,02	0,11	18,67	0,53	15,98	0,49	17,07	0,81	18,61	0,31
Zr90	28,0	1,68	30	0,57	29,42	0,14	9,62	0,34	9,4	0,29	8,58	0,31	33,93	1,66	35,99	2,89	27,46	1,14	34,78	1,01
Nb93	0,19	0,09	0,08	0,01	0,08	0,01	0,12	0,02	nd	nd	0,28	0,02	nd	nd	nd	nd	nd	nd	nd	nd
Ba135	nd	nd	nd	nd	nd	nd	nd	nd	nd	nd	nd	nd	nd	nd	nd	nd	nd	nd	nd	nd
Ba137	0,08	0,02	nd	nd	nd	nd	0,08	0,05	0,43	0,67	nd	nd	nd	nd	nd	nd	nd	nd	nd	nd
La139	0,71	0,15	3	0,04	3	0,03	3,43	0,04	0,94	0,03	1,16	0,05	1,3	0,43	7,44	2,37	1,33	0,03	1,28	0,22
Ce140	2,95	0,26	9,61	0,14	9,35	0,18	5,27	0,2	2,71	0,12	2,35	0,05	4,4	1,32	20,88	6,61	4,36	0,14	4,8	0,17
Pr141	0,61	0,04	1,67	0,02	1,64	0,02	0,44	0,02	0,4	0,01	0,31	0,01	0,78	0,19	2,74	0,85	0,74	0,02	0,84	0,05
Nd146	3,96	0,24	8,25	0,65	8,41	0,08	1,43	0,04	1,97	0,04	1,38	0,04	4,66	0,82	11,92	3,36	4,25	0,1	4,89	0,13
Sm147	1,7	0,09	2,34	0,08	2,34	0,04	0,29	0,02	0,62	0,03	0,35	0,01	1,77	0,18	2,73	0,52	1,58	0,04	1,83	0,05
Eu151	0,69	0,04	0,8	0,07	0,81	0,02	0,12	0,01	0,23	0,01	0,13	0,01	0,72	0,04	1	0,15	0,65	0,02	0,71	0,02
Eu153	0,69	0,04	0,81	0,02	0,8	0,02	0,12	0	0,23	0,01	0,14	0	0,72	0,05	1,01	0,15	0,66	0,02	0,71	0,02
Gd157	2,55	0,16	2,77	0,08	2,68	0,03	0,36	0,02	0,97	0,04	0,38	0,03	2,64	0,15	3,03	0,19	2,42	0,11	2,62	0,1
Tb159	0,48	0,02	0,46	0,04	0,46	0,01	0,06	0	0,18	0,01	0,07	0	0,48	0,02	0,49	0,02	0,43	0,02	0,47	0,01
Dy163	3,23	0,14	3,16	0,09	3,11	0,07	0,48	0,03	1,48	0,04	0,5	0,02	3,47	0,12	3,27	0,09	3,11	0,12	3,39	0,09
Ho165	0,7	0,03	0,66	0,02	0,66	0,01	0,12	0	0,34	0,01	0,12	0,01	0,75	0,02	0,63	0,02	0,67	0,03	0,72	0,02
Er166	2,03	0,11	1,92	0,04	1,88	0,03	0,4	0,01	1,04	0,02	0,39	0,01	2,15	0,06	1,7	0,05	1,92	0,08	2,09	0,04
Tm169	0,28	0,02	0,26	0,01	0,26	0,01	0,06	0	0,16	0,01	0,06	0	0,31	0,01	0,23	0,01	0,27	0,01	0,3	0,01
Yb172	1,81	0,09	1,74	0,07	1,71	0,04	0,48	0,03	1,07	0,03	0,44	0,03	2,07	0,04	1,51	0,06	1,79	0,1	2,01	0,06
Lu175	0,26	0,01	0,24	0,01	0,25	0	0,08	0	0,15	0,01	0,07	0	0,29	0,01	0,2	0,01	0,25	0,01	0,29	0,01
Hf178	0,95	0,05	1,01	0,02	1,01	0,03	0,33	0,03	0,26	0,01	0,28	0,01	1,13	0,1	1,03	0,04	0,91	0,03	1,07	0,04
Ta181	nd	nd	nd	nd	0,01	0	0,01	0	0,02	0,01	0,03	0	0,03	0,01	0,01	0,01	0,02	0	nd	nd
Pb208	0,05	0,01	nd	nd	0,3	0,01	0,37	0,02	nd	nd	0,65	0,03	nd	nd	0,28	0,08	0,09	0,02	nd	nd
Th232	0,03	0,01	0,35	0,01	0,35	0,01	0,37	0,01	0,1	0,01	0,07	0,01	0,05	0,01	0,36	0,06	0,05	0	nd	nd
U238	nd	nd	0,08	0,02	0,09	0	0,08	0,01	0,04	0	0,03	0	0,02	0,01	0,06	0,01	0,02	0	nd	nd

Cpx I										
Sample	**FT12**		**FT01P**		**FT08P**		**MSZK1306A**		**MSZK1308**	
n=	**10**	**σ**	**3**	**σ**	**6**	**σ**	**6**	**σ**	**7**	**σ**
Al27	29735	270	22038	1370	18680	1451	13082	518	36909	677
Ca44	152067	1114	137103	1155	161737	12647	168074	596	139918	2328
Sc45	61,3	1,15	56,4	2,18	53,1	3,59	66,3	1,26	63,5	1,27
Ti49	2016	48,3	1348	266	842	74,2	459	11,7	3130	51,1
V51	179	4,91	nd	nd	122	9,9	149	3,84	148	4,94
Cr52	3658	91,1	nd	nd	2982	318	2541	560	6530	245
Cr53	3752	90,6	9920	595	3020	323	2687	602	6864	204
Mn55	674	5,23	688	36,0	617	52	601	14,4	685	14,3
Co59	22,2	0,31	26,1	0,62	21,1	1,94	22,0	0,53	23,4	0,58
Ni60	352	4,05	413	15,6	339	31,2	372	10,5	376	9,58
Rb85	nd	nd	nd	nd	nd	nd	nd	nd	nd	nd
Sr88	109	3,31	88,3	35,5	136	8,27	38,4	0,95	59,8	2,29
Y89	14,6	0,29	6,09	0,73	7,75	0,56	3,45	0,08	15,4	0,31
Zr90	20,6	0,52	16,2	6,29	11,0	1,08	6,49	0,35	23,1	0,42
Nb93	0,21	0,03	1,44	0,32	0,09	0,01	0,12	0,03	0,38	0,01
Ba135	nd	nd	nd	nd	nd	nd	nd	nd	nd	nd
Ba137	nd	nd	0,1	0,03	0,1	0,04	0,04	0,01	nd	nd
La139	13,7	0,41	3,41	1,09	38,5	2,93	2,83	0,06	0,98	0,03
Ce140	36,0	1,13	8,09	2,79	45,4	3,44	6,62	0,35	3,17	0,07
Pr141	4,27	0,15	1,07	0,39	3,68	0,27	0,77	0,07	0,55	0,02
Nd146	15,9	0,5	5,14	1,83	11,5	0,93	2,94	0,24	3,38	0,1
Sm147	2,71	0,07	1,29	0,38	1,66	0,11	0,51	0,05	1,36	0,08
Eu151	0,8	0,03	0,46	0,12	0,44	0,04	0,14	0,01	0,53	0,02
Eu153	0,78	0,02	0,46	0,12	0,43	0,04	0,15	0,02	0,52	0,01
Gd157	2,53	0,1	1,38	0,36	1,37	0,11	0,45	0,03	2,06	0,07
Tb159	0,39	0,02	0,21	0,04	0,21	0,01	0,07	0,01	0,37	0,01
Dy163	2,62	0,11	1,28	0,18	1,37	0,09	0,57	0,04	2,73	0,1
Ho165	0,55	0,02	0,24	0,03	0,29	0,02	0,13	0,01	0,58	0,02
Er166	1,55	0,05	0,63	0,07	0,84	0,05	0,42	0,02	1,66	0,05
Tm169	0,23	0,01	0,08	0,01	0,13	0,01	0,07	0	0,23	0,01
Yb172	1,47	0,06	0,51	0,03	0,86	0,06	0,51	0,02	1,49	0,06
Lu175	0,21	0,01	0,07	0	0,13	0,01	0,07	0	0,21	0,01
Hf178	0,77	0,04	0,49	0,12	0,23	0,03	0,19	0,02	0,79	0,03
Ta181	0,02	0	0,16	0,07	0,02	0	0,02	0	0,03	0
Pb208	1,58	0,08	0,06	0,02	5,42	0,57	0,17	0,02	nd	nd
Th232	2,53	0,18	0,32	0,08	6,71	0,76	0,21	0,02	0,03	0,01
U238	0,36	0,03	0,07	0,01	1,77	0,18	0,04	0,01	nd	Nd

Amphibole				
Sample	**FT08P**		**MSZK1306A**	
N=	**5**	**σ**	**6**	**σ**
Al27	68264	785	59474	965
P31	nd	nd	nd	nd
Ca44	71470	0	71470	0
Sc45	58,3	1,27	82,6	1,88
Ti49	3607	83,2	1826	28,3
V51	193	17,8	102	52,18
Cr52	6859	427	4545	1802
Cr53	7324	195	9683	236
Mn55	370	8,53	323	3,03
Co59	34,2	1,29	32,7	0,42
Ni60	759	25,6	781	13,9
Rb85	16,7	1,53	12,3	1,22
Sr88	492	18,8	112	2,82
Y89	16,1	0,35	7,97	0,27
Zr90	20,3	0,45	15,6	0,19
Nb93	10,7	0,33	14,1	0,21
Ba135	912	44,0	235	24,4
Ba137	915	43,3	234	25,4
La139	72,1	2,44	6,69	0,21
Ce140	83,4	3,17	16,0	0,26
Pr141	6,68	0,27	1,89	0,09
Pr141	nd	nd	nd	nd
Nd146	20,8	0,63	7,45	0,52
Sm147	3,14	0,15	1,21	0,08
Eu151	0,88	0,05	0,35	0,01
Eu153	0,85	0,02	0,34	0,01
Gd157	2,77	0,11	1,08	0,05
Tb159	0,4	0,01	0,16	0
Dy163	2,77	0,09	1,25	0,05
Ho165	0,59	0,03	0,31	0,01
Er166	1,75	0,02	0,96	0,04
Tm169	0,25	0,01	0,15	0,01
Yb172	1,64	0,07	1,08	0,04
Lu175	0,25	0,01	0,16	0,01
Hf178	0,41	0,03	0,42	0,02
Ta181	0,34	0,02	0,77	0,04
Pb208	28,4	1,25	0,61	0,02
Th232	14,5	0,5	0,62	0,04
U238	3,16	0,13	0,1	0,01

Table 4: Primary Cpx and amphiboles trace element compositions (in ppm).

Table5

Click here to download Table: Table 5.doc

Glass																				
	SZB16			SZB44			SZB50			SZB51			SZB51			SZB52			SZB66		
	Vein			MP			MP			MP			Vein			Vein			Vein		
	8	Min	Max	10	Min	Max	4	Min	Max	3	Min	Max	4	Min	Max	6	Min	Max	6	Min	Max
SiO_2	56,55	55,82	57,60	54,16	53,39	54,81	55,43	55,28	55,87	56,63	56,63	56,63	61,89	60,53	62,71	57,87	56,52	59,02	60,86	59,55	61,50
TiO_2	1,57	1,46	1,69	1,72	1,67	1,84	1,71	1,62	1,73	0,43	0,43	0,43	0,14	0,07	0,19	0,75	0,52	0,99	1,29	1,21	1,41
Al_2O_3	19,15	18,82	19,51	20,79	20,20	21,28	20,60	20,52	20,86	22,55	22,55	22,55	18,57	18,54	18,66	20,37	19,96	20,95	18,04	18,02	18,11
FeO	3,85	3,28	4,34	3,99	3,69	4,49	3,82	3,67	3,88	2,89	2,89	2,89	2,88	2,80	3,01	3,11	2,97	3,28	3,06	2,99	3,14
MnO	0,06	0,01	0,09	0,08	0,05	0,11	0,06	0,05	0,06	0,07	0,07	0,07	0,04	0,00	0,07	0,07	0,01	0,13	0,08	0,05	0,12
MgO	3,57	3,49	3,73	4,59	4,29	4,86	4,33	4,20	4,38	3,23	3,23	3,23	2,56	2,46	2,70	3,37	3,16	3,49	3,08	2,91	3,30
CaO	7,88	7,47	8,25	9,89	9,55	10,08	9,19	8,34	9,47	7,66	7,66	7,66	4,82	4,50	5,45	7,79	7,64	7,90	5,88	5,70	6,12
Na_2O	4,12	3,97	4,21	4,05	4,03	4,10	4,32	4,16	4,38	5,50	5,50	5,50	5,58	5,48	5,66	4,13	3,92	4,27	4,70	4,42	4,82
K_2O	1,71	1,59	1,84	0,08	0,05	0,09	0,05	0,04	0,08	1,76	1,76	1,76	2,33	2,19	2,42	1,96	1,87	2,15	2,81	2,71	2,94
P_2O_5	0,45	0,38	0,52	0,05	0,01	0,07	0,01	0,01	0,03	0,24	0,24	0,24	1,10	0,98	1,15	0,50	0,48	0,54	0,94	0,92	0,94
Total	99,04	98,39	99,39	99,54	98,87	100,24	99,65	98,98	99,87	101,07	101,07	101,07	100,14	99,38	100,99	100,05	98,53	101,41	100,91	99,83	101,53
Mg#	62,35	59,58	65,48	67,25	64,57	68,71	66,89	66,81	67,12	66,58	66,58	66,58	61,33	60,57	62,69	65,83	64,99	66,39	64,14	63,13	65,98

	SZG14	SZG23				SZG44			FT12			FT01P			FT08P		
	Vein	SMI	MP			MP			MP			Vein			MP		
	3	Min	6	Min	Max	8	Min	Max	9	Min	Max	8	Min	Max	6	Min	Max
SiO_2	54,97	54,20	56,33	55,41	57,17	51,71	50,81	51,93	54,83	53,73	55,83	57,79	56,18	59,58	52,89	51,35	56,17
TiO_2	1,74	1,74	1,52	1,27	1,88	2,72	2,45	3,21	1,64	1,60	1,69	1,76	1,58	2,03	0,80	0,72	0,93
Al_2O_3	20,63	22,89	20,16	19,46	20,87	20,40	19,58	21,15	20,43	19,55	21,06	17,56	16,99	18,37	22,90	21,62	23,75
FeO	3,47	3,34	3,60	3,42	4,07	3,82	3,62	4,15	3,62	3,01	4,89	2,67	2,47	2,94	3,67	3,02	4,25
MnO	0,11	0,01	0,08	0,00	0,14	0,08	0,04	0,12	0,05	0,03	0,10	0,04	-0,01	0,08	0,09	0,06	0,11
MgO	4,21	2,32	3,88	3,15	4,39	4,76	4,51	5,00	3,61	3,37	4,13	2,54	2,40	2,66	3,19	2,83	3,41
CaO	7,50	2,02	8,02	7,72	8,19	8,91	8,66	9,40	9,83	9,50	10,45	5,80	5,54	6,50	9,41	7,99	12,47
Na_2O	5,10	7,31	4,93	4,80	5,09	5,17	4,79	5,45	5,15	4,65	5,55	4,82	4,59	5,20	5,25	4,53	5,81
K_2O	1,85	5,26	0,90	0,57	1,19	0,63	0,40	0,77	0,26	0,21	0,33	4,55	3,18	5,87	0,95	0,34	1,38
P_2O_5	0,22	0,12	0,08	0,04	0,12	0,05	0,04	0,06	0,05	0,00	0,09	0,48	0,45	0,54	0,09	0,06	0,11
Total	99,92	99,39	99,58	99,02	100,26	98,30	97,83	98,81	99,56	99,06	100,09	98,15	97,60	98,76	99,65	98,92	100,91
Mg#	68,35	55,30	65,49	62,14	68,30	68,91	66,95	71,08	62,59	55,57	67,52	62,91	60,38	65,24	60,94	58,11	63,99

Table 5: Major element composition for glass in melt veins, melt pockets (MP) and silicate melt inclusions (SMI) (in wt. %).

Table6

Click here to download Table: Table 6.doc

Sample	SZB16		SZB44		SZB50		SZB51		SZB51		SZB52		SZB66	
Area	vein		MP		MP		MP		vein		vein		vein	
n=	8	σ	10	σ	4	σ	3	σ	4	σ	6	σ	6	σ
Al27	101040,49	1801,77	109676,54	1926,10	109303,43	872,20	119310,66	30,55	98308,24	300,94	107799,47	1762,47	95459,12	213,46
P31	1919,30	221,93	nd	nd	198,27	38,58	484,84	331,48	5565,36	1759,09	2104,08	114,06	4403,98	269,55
Ca44	55865,74	2544,66	109509,87	89709,17	65041,53	3400,12	294332,43	234191,99	39333,34	8606,68	53587,94	1822,67	40433,12	1783,61
Sc45	24,68	1,62	84,03	95,15	38,72	0,51	312,72	267,09	35,82	31,15	19,66	1,58	24,96	0,85
Ti49	10377,10	800,97	13640,90	5207,73	11042,95	338,57	4387,56	1514,70	1045,92	120,49	5367,87	546,38	9828,74	331,54
V51	183,45	17,29	370,93	217,85	213,71	13,45	428,35	289,10	112,91	45,77	110,80	3,86	159,98	4,87
Cr52	157,71	81,26	4547,71	8431,73	117,29	87,04	16977,90	12479,66	865,04	1392,96	251,48	300,36	103,46	16,08
Cr53	134,38	35,97	4783,44	8918,07	113,78	85,97	24251,49	22983,23	873,94	1378,29	262,08	324,38	107,17	17,17
Mn55	656,53	67,49	715,39	216,35	741,21	266,20	958,82	484,17	5717,65	9279,33	577,32	230,70	469,73	41,04
Co59	19,54	5,99	22,35	10,31	31,32	28,92	45,81	26,43	791,75	1347,95	25,33	28,65	10,09	2,06
Ni60	154,12	106,84	206,29	280,27	366,49	561,08	727,31	679,09	2172,06	625,64	297,97	570,17	43,75	34,36
Rb85	39,89	3,28	nd	nd	1,05	0,28	17,96	14,61	80,87	15,84	44,47	3,00	69,94	5,60
Sr88	557,77	29,91	205,35	74,44	237,71	9,28	486,64	183,18	1034,42	21,91	541,32	11,74	866,23	57,64
Y89	16,46	0,80	34,62	22,17	22,69	1,15	13,69	6,61	8,08	0,75	12,33	0,27	18,58	0,75
Zr90	139,74	11,47	35,61	3,29	34,49	2,29	71,45	15,15	378,02	21,36	134,38	3,21	259,74	14,04
Nb93	51,62	3,62	5,14	2,45	6,74	0,63	23,33	17,39	92,80	4,52	51,77	1,06	89,18	3,26
Cs133	0,49	0,06	nd	nd	0,05	0,01	nd	nd	1,99	0,33	0,59	0,05	0,99	0,10
Ba135	524,37	29,69	95,32	76,02	124,99	71,45	209,99	167,51	791,48	48,44	635,20	36,62	833,22	20,00
Ba137	526,16	29,32	95,66	76,93	124,30	69,88	211,34	166,13	791,05	25,30	632,61	34,98	830,98	15,27
La139	27,98	2,52	3,81	1,18	4,72	0,46	16,68	7,14	72,55	4,02	30,41	0,74	58,58	3,86
Ce140	53,10	4,52	12,46	2,00	12,83	0,42	27,71	6,85	112,40	4,12	54,64	1,11	100,46	2,32
Pr141	5,84	0,52	2,24	0,27	2,13	0,05	2,57	0,16	9,17	0,54	5,64	0,14	11,07	0,79
Nd146	22,58	2,51	12,41	3,26	11,33	0,30	8,80	1,18	25,30	4,03	20,64	0,99	39,95	2,40
Sm147	4,08	0,35	3,89	1,87	2,79	0,14	1,57	0,44	3,06	0,69	3,23	0,28	6,56	0,38
Eu151	1,34	0,08	1,39	0,71	0,99	0,10	0,60	0,15	0,89	0,30	0,99	0,10	1,97	0,12
Eu153	1,33	0,13	1,36	0,68	1,05	0,07	0,59	0,18	0,87	0,16	0,99	0,09	2,00	0,13
Gd157	3,73	0,40	5,11	3,14	3,26	0,23	1,78	0,73	nd	nd	2,67	0,22	4,99	0,29
Tb159	0,53	0,04	0,87	0,58	0,59	0,04	0,30	0,13	nd	nd	0,34	0,04	0,66	0,03
Dy163	3,28	0,24	6,41	4,25	4,01	0,20	2,13	0,96	nd	nd	2,26	0,12	3,74	0,27
Ho165	0,62	0,04	1,32	0,86	0,83	0,09	0,52	0,25	0,30	0,09	0,44	0,03	0,69	0,04
Er166	1,72	0,11	3,84	2,44	2,50	0,19	1,57	0,77	0,78	0,12	1,32	0,09	1,87	0,13
Tm169	0,25	0,02	0,55	0,35	0,35	0,02	0,26	0,14	0,16	0,09	0,18	0,02	0,26	0,02
Yb172	1,71	0,13	3,61	2,17	2,43	0,13	1,99	0,87	nd	nd	1,32	0,06	1,75	0,13
Lu175	0,25	0,02	0,49	0,25	0,36	0,01	0,29	0,12	0,18	0,07	0,19	0,01	0,25	0,01
Hf178	3,01	0,31	1,21	0,38	0,98	0,04	1,93	0,35	5,40	1,08	2,65	0,06	5,05	0,38
Ta181	3,03	0,29	0,22	0,09	0,24	0,03	1,19	0,80	6,08	0,47	3,03	0,17	5,39	0,27
Pb208	2,99	0,75	nd	nd	1,26	0,13	1,05	0,83	nd	nd	1,31	0,14	6,45	0,49
Th232	3,77	0,45	0,37	0,17	0,47	0,03	2,31	1,69	16,68	2,46	4,39	0,23	8,94	0,53
U238	1,15	0,15	nd	nd	0,14	0,03	0,58	0,50	5,12	0,54	1,32	0,06	2,59	0,17

Sample	SZG14		SZG14		SZG23		SZG44		FT12		FT01P		FT08P	
Area	vein		SMI		MP		MP		MP		vein		MP	
n=	1	σ	2	σ	6	σ	8	σ	9	σ	8	σ	6	σ
Al27	109184,34	-	120748,48	561,36	106873,28	4107,02	92149,11	27353,80	96488,23	28673,88	92956,22	2433,56	109978,23	26805,35
P31	1325,29	-	695,06	116,52	395,80	137,63	228,64	74,04	nd	nd	nd	nd	nd	nd
Ca44	48857,56	-	25493,42	347,92	55263,25	3220,70	50025,66	16068,89	51124,42	15685,12	39010,05	6080,18	87336,26	34620,34
Sc45	17,60	-	16,16	0,88	35,98	5,04	24,81	9,24	28,15	8,78	16,40	2,21	48,69	53,13
Ti49	11032,17	-	10232,71	2984,16	10372,61	748,18	15903,28	5672,20	9276,16	2734,51	12077,85	1369,54	5420,33	396,15
V51	108,41	-	106,48	2,80	247,47	60,32	228,88	84,38	231,67	74,98	159,65	16,94	311,34	111,38
Cr52	69,51	-	251,93	180,20	3351,20	5110,57	87,50	32,26	775,32	1873,72	70,50	17,10	2023,04	3415,28
Cr53	85,82	-	270,75	200,30	3549,59	5406,26	84,03	33,18	796,64	1925,38	73,07	16,51	2896,19	5262,64
Mn55	531,03	-	446,90	6,08	973,95	984,09	496,40	157,47	536,41	139,93	375,15	66,66	530,91	157,25
Co59	12,84	-	17,12	2,41	69,37	125,36	12,38	4,18	33,77	36,52	11,34	4,36	24,84	24,18
Ni60	37,19	-	53,88	14,28	1000,93	2196,28	39,20	18,03	712,91	1544,87	82,33	70,76	318,39	470,67
Rb85	26,33	-	35,87	6,05	6,28	1,99	4,52	2,06	5,56	1,48	63,00	4,46	18,90	8,82
Sr88	485,15	-	570,38	128,38	609,64	112,98	278,51	77,77	364,70	108,65	601,18	81,48	1067,74	455,20
Y89	15,51	-	11,04	0,31	18,52	2,94	18,76	6,13	18,83	5,68	13,46	1,61	22,92	2,97
Zr90	99,41	-	111,08	5,51	69,92	22,61	40,34	12,20	25,84	7,49	153,22	11,02	34,31	5,89
Nb93	45,24	-	54,40	9,67	23,89	9,47	11,24	3,96	23,33	6,92	59,35	6,18	24,64	10,91
Cs133	0,27	-	0,25	0,06	0,11	0,06	0,03	0,02	nd	nd	nd	nd	nd	nd
Ba135	380,70	-	414,13	117,80	187,31	39,59	60,52	34,04	322,11	96,39	603,80	30,84	2696,51	1232,56
Ba137	388,04	-	434,17	137,19	188,01	37,66	61,45	34,23	321,29	96,49	604,99	35,11	2691,62	1232,25
La139	9,37	-	6,71	1,56	17,56	6,21	2,32	0,70	21,52	6,47	33,15	4,81	151,07	58,82
Ce140	15,95	-	14,12	3,26	47,19	15,60	7,41	2,19	53,38	15,90	59,45	8,17	163,69	51,63
Pr141	1,67	-	1,36	0,09	5,68	1,47	1,16	0,35	6,11	1,85	6,44	0,78	12,21	3,13
Nd146	6,78	-	5,90	0,37	23,83	6,72	6,28	1,92	22,41	6,82	24,73	3,38	35,98	5,73
Sm147	1,81	-	1,57	0,13	4,60	1,32	2,02	0,66	3,58	1,09	4,27	0,79	4,72	0,35
Eu151	0,68	-	0,66	0,22	1,54	0,39	0,79	0,26	1,07	0,33	1,48	0,37	1,38	0,12
Eu153	0,78	-	0,63	0,16	1,58	0,45	0,78	0,25	1,06	0,32	1,53	0,22	1,40	0,13
Gd157	2,00	-	2,24	0,26	4,34	1,02	2,73	0,93	3,17	0,98	3,55	0,74	3,86	0,71
Tb159	0,40	-	0,33	0,16	0,58	0,14	0,46	0,14	0,48	0,15	0,50	0,08	0,58	0,10
Dy163	2,92	-	1,88	0,09	3,67	0,77	3,25	1,08	3,26	1,01	2,91	0,37	3,88	0,88
Ho165	0,57	-	0,44	0,04	0,68	0,11	0,70	0,23	0,69	0,21	0,54	0,12	0,82	0,15
Er166	1,43	-	1,19	0,15	1,85	0,23	2,05	0,65	2,01	0,61	1,33	0,16	2,54	0,38
Tm169	0,16	-	0,20	0,01	0,24	0,03	0,29	0,09	0,30	0,10	0,18	0,03	0,39	0,07
Yb172	1,51	-	0,99	0,11	1,60	0,26	2,01	0,66	2,14	0,67	1,18	0,23	2,72	0,28
Lu175	0,29	-	0,16	0,04	0,22	0,04	0,29	0,09	0,30	0,09	0,17	0,04	0,38	0,07
Hf178	2,11	-	2,25	0,31	1,23	0,33	1,01	0,33	0,83	0,25	3,52	0,36	0,61	0,10
Ta181	2,05	-	1,94	0,54	0,56	0,37	0,54	0,19	0,58	0,18	3,51	0,27	0,82	0,33
Pb208	0,69	-	1,03	0,47	5,36	1,44	0,27	0,18	12,56	3,61	6,95	2,87	57,38	27,54
Th232	1,55	-	0,65	0,33	0,40	0,03	0,05	0,01	4,43	1,30	4,84	0,64	32,23	14,03
U238	nd	-	nd	nd	nd	nd	nd	nd	0,60	0,19	1,43	0,21	7,11	3,07

Table 6: Trace element compositions for glass in in melt veins (GB), melt pockets (MP) and silicate melt inclusions (SMI) (in ppm).

Table7

Click here to download Table: Table 7.doc

SZB50							SZG23							FT12						
	Ol-II	Cpx-II	Sp-II	Glass	MP compo	SZT1111		Ol-II	Cpx-II	Sp-II	Glass	MP compo	FT08P		Ol-II	Cpx-II	Sp-II	Glass	MP compo	FT08P
Modal	**0,13**	**0,34**	**0,17**	**0,36**			**Modal**	**0,12**	**0,5**	**0,13**	**0,26**			**Modal**	**0,44**	**0,19**	**0,05**	**0,33**		
Na_2O	0,01	1,07	0,00	4,16	**1,86**	2,90	**Na_2O**	0,07	1,00	0,01	4,93	**1,79**	2,72	**Na_2O**	0,01	0,77	0,01	5,15	**1,85**	2,72
MgO	49,09	15,65	20,81	4,20	**16,75**	18,07	**MgO**	48,02	13,28	18,55	3,88	**15,82**	17,60	**MgO**	49,58	14,58	21,08	3,61	**26,83**	17,60
SiO_2	41,06	52,84	0,06	55,87	**43,43**	42,46	**SiO_2**	41,38	46,63	0,09	56,33	**42,94**	43,18	**SiO_2**	41,78	47,83	0,08	54,83	**45,57**	43,18
Al_2O_3	0,05	5,76	56,35	20,86	**19,05**	15,28	**Al_2O_3**	0,39	8,49	38,56	20,16	**14,55**	14,75	**Al_2O_3**	0,06	9,32	54,34	20,43	**11,26**	14,75
K_2O	0,02	0,01	0,02	0,08	**0,04**	0,36	**K_2O**	0,04	0,01	0,00	0,90	**0,24**	0,63	**K_2O**	0,01	0,03	0,00	0,26	**0,10**	0,63
CaO	0,16	21,06	0,02	8,34	**10,19**	11,58	**CaO**	0,31	19,97	0,05	8,02	**12,11**	11,67	**CaO**	0,16	20,05	0,03	9,83	**7,13**	11,67
TiO_2	0,05	0,43	0,23	3,67	**1,51**	1,20	**TiO_2**	0,07	1,37	0,64	3,60	**1,71**	0,71	**TiO_2**	0,02	1,77	0,27	3,62	**1,55**	0,71
FeO	8,99	3,20	11,28	1,62	**4,76**	4,09	**FeO**	8,27	2,98	14,54	1,52	**4,77**	4,11	**FeO**	8,23	3,14	10,63	1,64	**5,29**	4,11
P_2O_5	0,02	0,04	n.d	0,03	**0,03**	n.d	**P_2O_5**	0,04	0,01	0,01	0,08	**0,03**	0,04	**P_2O_5**	0,04	0,06	0,06	0,05	**0,05**	0,04
MnO	0,12	0,04	n.d	0,05	**0,05**	0,06	**MnO**	0,12	n.d	0,00	0,08	**0,04**	0,01	**MnO**	0,13	0,04	0,00	0,05	**0,08**	0,01
Cr_2O_3	0,08	n.d	10,85	n.d	**1,85**	n.d	**Cr_2O_3**	0,11	3,80	25,60	n.d	**5,24**	1,29	**Cr_2O_3**	n.d	2,52	12,31	n.d	**1,09**	1,29
Total	99,91	100,85	99,82	98,98	**99,88**	97,55	**Total**	99,08	97,58	98,15	99,58	**99,33**	97,02	**Total**	100,34	100,40	99,01	99,56	**101,03**	97,02

Table 7: Bulk melt pocket compositions based on mass balance calculation from modal and chemical compositions of phases. Comparison with pargasite amphibole compositions (SZT111 and FT08P).

Table8
Click here to download Table: Table 8.doc

	Rock type	T primary (°C)	Estimated P (GPa)	T cpxII-glass (°C)	ΔT (°C)	P cpxII-glass (GPa)
SZB16	Lhz	1135	1.50			
SZB44	Lhz	992	1.28	1250	258	0.8
SZB50	Lhz	1007	1.14	1245	238	0.7
SZB51	Lhz	1039	1.27	1211	172	0.7
SZB52	Lhz	1128	1.59			
SZB66	Lhz	1029	1.36			
SZG14	Lhz	1086	1.30			
SZG23	Lhz	1041	1.30	1228	187	0.7
SZG30	Lhz	1052	1.25			
SZG44	Lhz	1086	1.17	1267	181	0.9
FT12	Lhz	968	1.15	1207	239	0.6
FT01P	Hbz	1137	1.63			
FT08P	Hbz	852	1.07	1222	370	0.6
MSZK1306A	Lhz	861	1.07			
MSZK1308	Lhz	1080	1.39			

Table 8: Minimum T and P of melt pocket formation in the lithospheric mantle beneath the BBHVF. T for the primary mantle mineral assemblage calculated after Brey & Kohler (1990); Estimated P from T equilibrium and Kovacs et al. (2012) geotherm; dT = temperature difference between the mantle minerals and melt pocket phases